

REPUBLIQUE ALGERIENNE DEMOCRATIQUE ET POPULAIRE
MINISTERS DE L'ENSEIGNEMENT SUPERIEUR ET DE LA RECHERCHE
SCIENTIFIQUE

UNIVERSITE FRERES MENTOURI-CONSTANTINE 1
FACULTE DES SCIENCES EXACTES
DEPARTEMENT DE CHIMIE

N° d'ordre
Série

THESE

PRESENTEE EN VUE DE L'OBTENTION DE DIPLOME DE

DOCTORAT EN SCIENCES EN CHIMIE

INTITULEE

.....
**Photodégradation d'un polluant organique sous la lumière solaire
simulée, par un processus type photo-Fenton hétérogène: cas de
photodégradation du 2-mercaptobenzothiazole en présence d'une
poudre argileuse naturelle locale**

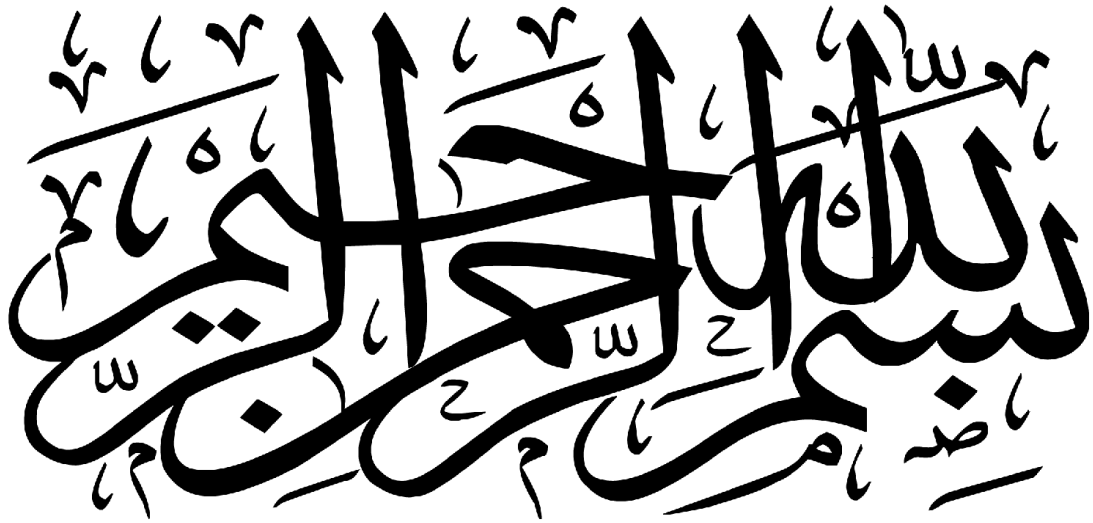
**Simulated sunlight photodegradation of an organic pollutant by
heterogeneous photo-Fenton-like processes: case of
2-mercaptobenzothiazole using a local natural clay powder**

.....
PREPAREE PAR: Zakaria REDOUANE-SALAH

DEVANT LE JURY :

Abdennour ZERTAL	Université Frères Mentouri-Constantine 1	Professeur	Président
Moulay Abderrahmane MALOUKI	Centre Universitaire Amine Elokhal El Hadj Moussa Eg Akhamouk-Tamanrasset	Professeur	Rapporteur
Abdelaziz BOULKAMH	Université Frères Mentouri-Constantine 1	Professeur	Examineur
Sabrina HALLADJA	Université 20 Aout 1955-Skikda	MCA	Examinatrice
Mahdi CHIHA	Université 20 Aout 1955-Skikda	MCA	Examineur

SOUTENANUE LE: 10 Juillet 2018



In the name of Allah, Most Gracious, Most Merciful.

"Say: He is Allah,

The One;

Allah, the Eternal, Absolute;

He begetteth not,

Nor is he begotten;

And there is none

Like unto Him."

From: The Holy Quran,

Sura Al-Ikhlās, or the Purity (of Faith)

DEDICATION

To my Mother and Father

To my brother and sisters

To my wife and my son Younes

*All of you deserve a special mention for your inestimable support
and prayers.*

ACKNOWLEDGMENTS

First of all, I praise **God**, the almighty, merciful and passionate, for providing me this opportunity and granting me the capability to proceed successfully.

This study was carried out partly in the laboratory of “**Laboratoire des Techniques Innovantes de Preservation de L’environnement (LTIPE)**” at the University of Constantine 1 in Algeria. I would like to express my gratitude to the professor **Abdennour ZERTAL**, by accepting me to work in his laboratory. The rest of the work was done at the laboratory of “**Chemical Reactivity & Photoreactivity**” at the University of A Coruña in Spain, directed by Professor **Moisés Canle López**.

I would like to express my profound and sincere gratitude to the following for their contributions and assistance:

Abdennour ZERTAL professor at the University of Constantine 1 and head of our research team for the honor that he did to me by accepting to preside the jury of this thesis.

Professor **Moisés Canle López**. I sincerely wish to thank him for his gracious collaboration and for the support and confidence he has given me by welcoming me to his laboratory.

Moulay Abderrahman MALOUKI, my supervisor and professor at the University of Constantine 1 and actually at the University Center of Tamanrasset, for advising and assisting the project.

The reviewers of this thesis, Prof: **Abdelaziz BOULKAMH**, **Sabrina HALLADJA** and **Mahdi CHIHA** for accepting to read and evaluate this work.

My colleagues, **Khennaoui BADIS**, **Mammeri YAZID**, **Salah-Eddine LEMALLEM** and **Abd-Elmoula BOUMAZA** for their assistance, help and friendship.

I also wish to thank **Houria BOUKHATEM** for her assistance during my research internship in Spain and **Fouzia ZEHANI** for helping me in the interpretation of XRD spectrum.

Finally, I would like to thank everybody who was important to the successful realization of this thesis, as well as expressing my apology that I could not mention personally one by one.

Zakaria REDOUANE-SALAH ...

List of Symbols

A: Absorbance

AOP: Advanced Oxidation Processes

BET: Brunauer–Emmett–Teller

BJH: Barrett-Joyner-Halenda

BT: Benzothiazole

CA: Citric Acid

C₀: Initial Concentration

DRS: Diffuse Reflectance Spectroscopy

EDS: Energy-dispersive X-ray spectroscopy

HPLC: High Performance Liquid Chromatography

H₂O₂: Hydrogen peroxyde

IR: Infrared Spectroscopy

OA: Oxalic acid

MS: Mass Spectrometry

SEM: Scanning electron microscopy

TGA: Thermal gravimetric analysis

TDA: Topological data analysis

TOC: total organic carbon

UV-Vis: Ultraviolet-visible Spectroscopy

XRD: X-ray diffraction

XRF: X-ray fluorescence

2-MBT: 2-mercaptobenzothiazole

List of Figures

Figure I. 1: Chemical structures of some benzothiazoles.	22
Figure I. 2: Equilibrium of different forms of MBT.	29
Figure I. 3: Some characteristics of Hydroxyl radicals.	47
Figure I. 4: Main advanced oxidation process.	49
Figure I. 5: Suitability of water treatment technologies according to COD content [85].	50
Figure II.1: Nahita Centrifuge and Filter holder used to separate NCP from MBT solutions. ..	67
Figure II.2: quartz photoreactor used in the lab equipped with UV lamp 254 nm and its emission spectrum.	68
Figure II.3: Pyrex glass photoreactor used in the lab equipped with Vis lamp at 366 nm.	69
Figure II.4: Emission spectrum of the Vis lamp at 366nm.	69
Figure II.5: Transmission spectrum of the Quartz and Glass tubes.	70
Figure II.6: UV-Vis Spectrophotometer used in this study.	70
Figure II.7: HPLC instrument used in this study.	71
Figure II.8: NCP used in this study.	72
Figure II.9: UV-Visible diffuse reflectance spectrophotometer used in the study.	73
Figure III.1: UV-Vis spectrum of aqueous $5.0 \cdot 10^{-5}$ M MBT, natural pH.	77
Figure III.2: Evolution of UV-Vis spectrum of MBT in acidic and basic medium.	77
Figure III.3: Tautomerism thiol-thione of MBT.	78
Figure III.4: SEM image of a randomly taken sample of the NCP.	79
Figure III.5: EDS for a randomly taken portion of the NCP.	80
Figure III.6: UV-Vis diffuse reflectance spectrum of NCP.	83
Figure III.7: X-ray diffractogram of the natural clay powder.	83
Figure III. 8 : Effect of contact time on MBT adsorption onto NCP [MBT]= $5.0 \cdot 10^{-5}$ M, $0.5 \text{ g} \cdot \text{L}^{-1}$ NCP, T = 298 K.	84
Figure III.9: Effect of initial MBT concentration on its adsorption capacity.	85
Figure III.10: Effect of agitation speed (rpm) on the adsorption capacity of MBT.	86
Figure III.11: Effect of natural clay dose on MBT retention.	87
Figure III.12: Effect of initial pH on the adsorption of MBT by NCP.	88
Figure III.13: The Langmuir isotherm of MBT adsorption on the NCP.	90
Figure III.14: Freundlich isotherm of MBT adsorption on clay.	91
Figure III.15: First order adsorption kinetics for the adsorption of MBT on NCP.	92
Figure III.16: Second order adsorption kinetics for the adsorption of MBT on NCP.	93
Figure III.17: Effect of initial MBT concentration on its degradation by heterogeneous Fenton process.	95
Figure III.18: Kinetic study of the degradation of MBT by heterogeneous Fenton process.	96
Figure III.19: Effect of the initial concentration on the apparent degradation constant of MBT.	97
Figure III.20: Influence of $[\text{H}_2\text{O}_2]$ on the degradation efficiency of $5.0 \cdot 10^{-5}$ M MBT.	98
Figure III.21: Effect of initial pH on the degradation of 5.10^{-5} M MBT.	99
Figure III.22: Determination of equilibrium times for each NCP dose.	99

Figure III.23: Effect of NCP dose on the degradation efficiency of $5 \cdot 10^{-5}$ M MBT by heterogeneous Fenton process.....	100
Figure III.24: Degradation of MBT under different conditions. $[MBT] = 5.0 \cdot 10^{-5}$ M, $[H_2O_2]_0 = 1.0 \cdot 10^{-3}$ M, $0.5 \text{ g} \cdot \text{L}^{-1}$ NCP, natural pH, $T = 298 \text{ K}$	101
Figure III.25: Effect of tert-BuOH on the rate of degradation of aqueous MBT. $[MBT] = 5.0 \cdot 10^{-5}$ M, $[H_2O_2]_0 = 1.0 \cdot 10^{-3}$ M, $0.5 \text{ g} \cdot \text{L}^{-1}$ NCP upon UVA/Vis irradiation, natural pH, $T = 298.0 \text{ K}$	103
Figure III.26: Effect of pH on the heterogeneous photodegradation of aqueous MBT. $[MBT] = 5.0 \cdot 10^{-5}$ M, $[H_2O_2]_0 = 1.0 \cdot 10^{-3}$ M, $0.5 \text{ g} \cdot \text{L}^{-1}$ NCP upon UVA/Vis irradiation. $T = 298.0 \text{ K}$	105
Figure III.27: Effect of MBT concentration on its photo-Fenton heterogeneous degradation. $[MBT] = (2,5-7,5) \cdot 10^{-5}$ M, $[H_2O_2] = 1.0 \cdot 10^{-3}$ M, $0.5 \text{ g} \cdot \text{L}^{-1}$ upon UVA/Vis irradiation, natural pH, $T = 298.0 \text{ K}$	105
Figure III.28: Effect of H_2O_2 on the heterogeneous photo-Fenton degradation of aqueous MBT. $[MBT] = 5.0 \cdot 10^{-5}$ M, $0.5 \text{ g} \cdot \text{L}^{-1}$ NCP upon UVA/Vis irradiation, natural pH, $T = 298 \text{ K}$	106
Figure III.29: Effect of the load of NCP on the rate of heterogeneous photo-Fenton degradation of MBT. $[MBT] = 5.0 \cdot 10^{-5}$ M, $[H_2O_2] = 1.0 \cdot 10^{-3}$ M, UVA/Vis irradiation, natural pH, $T = 298 \text{ K}$. Inset: dependence k_{obs} vs. $[NCP]$	107
Figure III.30: Kinetic study for the degradation of MBT by heterogeneous photo-Fenton process.....	108
Figure III.31: Effect of the concentration of dissolved O_2 on the rate of degradation of MBT by heterogeneous photo-Fenton process. $[MBT] = 5.0 \cdot 10^{-5}$ M, $[NCP] = 0.5 \text{ g} \cdot \text{L}^{-1}$ upon UVA/Vis irradiation, $[H_2O_2] = 1.0 \cdot 10^{-3}$ M, natural pH, $T = 298 \text{ K}$	109
Figure III.32: Effect of oxalic acid and citric acid on the heterogeneous photo-Fenton degradation of aqueous MBT. $[MBT] = 5.0 \cdot 10^{-5}$ M, NCP $0.5 \text{ g} \cdot \text{L}^{-1}$ upon UVA/Vis irradiation, $[H_2O_2] = 1.0 \cdot 10^{-3}$ M, $pH_0 = 6.8$, $T = 298 \text{ K}$	110

List of Schemes

Scheme I.1: Postulated microaerobic degradation pathway of MBT by isolated strain <i>Alcaligenas</i> sp.MH 146 strain CSMB1. [8].	34
Scheme I.2: Proposed metabolic pathway of MBT in <i>R. rhodochrous</i> OBT18 [77].	36
Scheme I.3: Proposed pathway of direct photolysis of MBT at 313 nm proposed by Malouki <i>et al</i> [15].	37
Scheme I.4: Photolytic pathway of direct photolysis of MBT proposed by Zajíčková <i>et al</i> [78].	38
Scheme I.5: The proposed mechanism for MBT photodegradation, Maria Serdechnova <i>et al</i> [79].	39
Scheme I.6: Degradation mechanism of MBT in the presence of DTA under irradiation at 365 nm [6].	40
Scheme I.7: Direct photolysis of MBT in organic solution [80].	41
Scheme I.8: Proposal pathway of the MBT photocatalytic degradation [5].	43
Scheme III.1: Proposed mechanism of photodegradation of MBT in the presence of NCP under simulated sunlight irradiation at 366 nm. (Between brackets: hypothesized, undetected structure).	116

List of tables

Table I.1: General properties of Benzothiazoles [28].	23
Table I.2: Summary of AOPs used for the removal/degradation of benzothiazole's compounds.	26
Table I.3: Oxidation potential of most commonly used oxidizers in water [88].	47
Table I.4: Type and classification of AOP.	49
Table I.5: Varieties of Fenton reactions.	63
Table II.1: Chemicals products used in the study and their origins.	65
Table III.1: Physico-chemical properties of MBT.	76
Table III.2: Spectroscopic properties of MBT in aqueous solution ($5 \cdot 10^{-5} \text{M}$).	78
Table III.3: EDS analysis of NCP.	80
Table III.4: BET analysis of the NCP.	81
Table III.5: Chemical composition % of NCP obtained by XRF.	82
Table III.6: Summary of the Freundlich and Langmuir constants.	91
Table III.7: Pseudo first-order and pseudo second-order adsorption kinetic parameters for MBT adsorption onto NCP.	93
Table III. 8 : Effect of initial MBT concentration on the rate constant, half time of the reaction and correlation coefficient.	96
Table III.9: Rate constants obtained for the degradation of MBT under different conditions.	102
Table III.10: Effect of H_2O_2 on the rate constant for heterogeneous photo-Fenton degradation of aqueous MBT. $[\text{MBT}] = 5 \cdot 10^{-5} \text{ M}$, $[\text{NCP}] = 0.5 \text{ g} \cdot \text{L}^{-1}$ upon UVA/Vis irradiation, natural pH, $T = 298.0 \text{ K}$.	106
Table III.11: Effect of the load of NCP on the rate constant for the heterogeneous photo-Fenton degradation of aqueous MBT. $[\text{MBT}] = 5.0 \cdot 10^{-5} \text{ M}$, $[\text{H}_2\text{O}_2] = 1.0 \cdot 10^{-3} \text{ M}$, UVA/Vis irradiation, natural pH, $T = 298 \text{ K}$.	108
Table III.12: Effect of the partial pressure of O_2 on the rate constant for the heterogeneous photo-Fenton degradation of aqueous $5.0 \cdot 10^{-5} \text{ M}$ MBT, $[\text{NCP}] = 0.5 \text{ g} \cdot \text{L}^{-1}$ upon UVA/Vis irradiation, $[\text{H}_2\text{O}_2] = 1.0 \cdot 10^{-3} \text{ M}$, natural pH, $T = 298.0 \text{ K}$.	109
Table III.13: effect of different operational parameters on TOC removal from MBT solutions. $[\text{MBT}]_0 = 7.75 \text{ mg} \cdot \text{L}^{-1}$, $[\text{H}_2\text{O}_2]_0 = 1.0 \cdot 10^{-3} \text{ M}$, $[\text{NCP}] = 0.5 \text{ g} \cdot \text{L}^{-1}$, $T = 298.0 \text{ K}$.	112
Table III.14: Identified photoproducts and comparison with others reported in the literature.	113

Table of Content

TABLE OF CONTENT

List of Figures	7
List of Schemes	9
List of tables.....	10
TABLE OF CONTENT	12
INTRODUCTION.....	17
I. Literature survey.....	21
PART A: BENZOTHAZOLES AND 2-MERCAPTOBENZOTHAZOLE.....	22
I.1 BENZOTHAZOLES	22
I.1.1 Benzothiazoles applications.....	23
I.1.2 Provenance.....	24
I.1.3 Benzothiazoles toxicity.....	25
I.1.4 Benzothiazoles degradation	25
I.2. 2-MERCAPTOBENZOTHAZOLE (MBT).....	29
I.2.1 MBT synthesis	29
I.2.2 MBT Toxicity	31
I.2.3 MBT in Environment.....	32
I.2.4 MBT Biodegradation	33
I.2.5 MBT photodegradation.....	37
I.2.5.1 Direct photolysis	37
I.2.5.2 Homogeneous photodegradation.....	39
a. Using DTA	39
b. Ozonation	41
I.2.5.3 Heterogeneous photodegradation.....	42
PART B: ADVANCED OXIDATION PROCESSES	46
I.1 CONCEPT AND FUNDAMENTALS	46
I.1.1 Hydroxyl radicals.....	46
I.1.2 Mechanism.....	48
I.2 CLASSIFICATION OF AOPs	48
I.2.1 UV PHOTOLYSIS and UV/H ₂ O ₂ PROCESSES	51
I.2.1.1 Advantages.....	53
I.2.1.2 Disadvantages	53
I.2.2 HOMOGENEOUS FENTON AND PHOTO-FENTON PROCESS.....	54

I.2.2.1 Fenton process: $\text{Fe}^{2+}(\text{Fe}^{3+})/\text{H}_2\text{O}_2$	54
I.2.2.2 Photo-Fenton process ($\text{Fe}^{2+}(\text{Fe}^{3+})/\text{H}_2\text{O}_2/\text{UV}$).....	55
I.3 PARAMETERS AFFECTING FENTON AND PHOTO-FENTON PROCESSES.....	58
I.3.1 The effect of pH.....	58
I.3.2 Effect of H_2O_2 concentration	58
I.3.3 Effect of the initial iron concentration	59
I.3.4 Effect of $[\text{Fe}^{2+}]/[\text{H}_2\text{O}_2]$ ratio.....	59
I.3.5 Advantages	60
I.3.6 Disadvantages	60
I.4 HETEROGENEOUS FENTON AND PHOTO-FENTON PROCESS	61
I.5 Developments of the Fenton Reaction.....	62
II. Experimental.....	65
II.1 Chemicals	65
II.2 Experimental procedure.....	66
II.2.1 Adsorption study.....	66
II.2.2 Heterogeneous degradation and photodegradation study	67
II.3 Irradiation systems.....	68
II.3.1 irradiation at 254 nm.....	68
II.3.2 Irradiation at 366 nm	68
II.4 Analytical techniques	70
II.4.1 UV-Visible absorption analysis.....	70
II.4.2 HPLC analysis	71
II.4.3 HPLC-MS analysis	71
II.5 Kinetic treatment	71
II.6 Characterisation analyses	72
II.6.1 SEM-EDS analysis	72
II.6.2 BET analysis.....	73
II.6.3 UV-Vis DRS analysis.....	73
II.6.4 x-ray fluorescence spectroscopy (XRF)	73
II.6.5 x-ray diffraction spectroscopy (XRD).....	73
III. RESULTS AND DISCUSSION	76
III.1. Contaminant properties	76
III.1.1. Physico-chemical properties.....	76
III.1.2 Spectroscopic properties	76
III.2 CHARACTERISATION STUDY OF THE NATURAL CLAY.....	79

III.2.1 SEM-EDS analysis.....	79
III.2.2 BET analysis	80
III.2.3 XRF Analysis	82
III.2.4 UV-Vis DRS Analysis	82
III.2.5 XRD Analysis	83
III.3 ADSORPTION STUDY	84
III.3.1 MBT adsorption onto NCP (effect of contact time).....	84
III.3.2 Effect of operational parameters	84
III.3.2.1 Effect of initial MBT concentration	84
III.3.2.2 Effect of agitation speed.....	85
III.3.2.3 Effect of natural clay dose.....	87
III.3.2.4 Effect of initial pH.....	88
III.4 ADSORPTION ISOTHERMS.....	89
III.4.1 Langmuir isotherm	89
III.4.2 Freundlich isotherm.....	90
III.5 ADSORPTION KINETICS OF MBT.....	92
III.5.1 Pseudo-First-order kinetic	92
III.5.2 Pseudo-Second-order kinetic.....	93
III.6 DEGRADATION STUDY	94
III.6.1 Heterogeneous Fenton System :(MBT/H ₂ O ₂ /NCP)	94
III.6.1.1 Thermal effect of Natural Clay and H ₂ O ₂	94
III.6.1.2 Influence of operational parameters	94
a. Effect of initial MBT concentration	94
b. Effect of initial concentration of hydrogen peroxide	97
c. Effect of pH.....	98
d. Effect of clay dose.....	99
III.6.2 PHOTO-FENTON SYSTEM (MBT/H ₂ O ₂ /Clay/UV).....	101
III.6.2.1 Degradation of MBT under different conditions.....	101
III.6.2.2 Role of the hydroxyl radical.....	102
III.6.2.3 Effect of operational parameters	104
a. Effect of pH.....	104
b. Effect of MBT concentration	105
c. Effect of H ₂ O ₂ concentration.....	106
d. Effect of the load of NCP.....	107

e. Effect of oxygen	108
f. Effect of oxalic and citric acids.....	110
III.6.2.4 MINERALIZATION EFFICIENCY	112
III.6.2.5 Identification of intermediates and reaction mechanism.....	113
➤ Degradation mechanism.....	116
IV. GENERAL CONCLUSION	117
V. ANNEXES	119
VI. REFERENCES	122
PUBLISHED PAPER	142
Curriculum Vitae.....	154
Summary	158
ملخص.....	160
Résumé.....	162

Introduction

INTRODUCTION

In the twenty-first century, environmental protection has become a major issue, The UN reminds in its latest GEO-4 report, that its degradation "undermines development and threatens future progress in development ..." and "threatens all aspects of human well-being, it was demonstrated that the degradation of the environment is linked to human health problems, including certain types of cancers, vector-borne diseases, more and more of zoonoses, nutritional deficiencies and respiratory assignments.

The UN considered preservation of the environment as "crucial for the success of other objectives stated in the declaration of the Millennium Summit" [1].

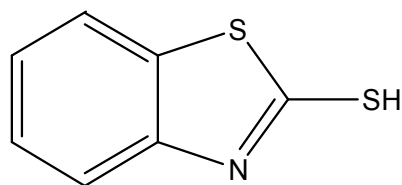
Our environment today is polluted (degraded) by chemicals widely used in everyday life and in industrial applications; agricultural, health, etc.

More than 60 million organic and inorganic substances have been listed in the Register of the American Chemical Society, the most up to date database and most comprehensive chemicals worldwide. Every day, 12,000 new chemicals entering the market. In this universe constantly expanding, many of them enter the soil, air, rivers and the sea [1].

Of these complex chemical, Benzothiazoles are considered as emerging contaminants, and pose an environmental concern when they released into watercourses [2].

In this work, we focused our study on one of the most important member of benzothiazole's family, yet little studied its presence in aqueous media, and its transfer capacity in soil and groundwater(2-mercaptobenzothiazole MBT) [3].

MBT is an odorous, toxic and poorly biodegradable chemical [4]. It has been detected in wastewater effluents, sewage treatment plants, road drainage and surface waters [5]. A number of studies have confirmed that MBT shows toxic effect on aquatic organisms, and is an allergen and potentially mutagen for human [4], with a non-negligible impact of MBT on environment [6].



2-mercaptobenzothiazole (MBT)

Studies on the biodegradation behavior of MBT have suggested that it is recalcitrant to biodegradation, has toxic effects on bacteria, and its presence inhibits biodegradation of other compounds, including some of its own degradation products [7, 8].

The photocatalytic degradation of MBT in aqueous solution using: La^{3+} - TiO_2 , Ce^{3+} - TiO_2 and $\gamma\text{-Fe}_2\text{O}_3/\text{Oxalate}$ under UV irradiation has been reported by Li *et al* [9, 10] and Wang *et al*, [11] respectively. The effect of iron oxides and oxalate on the photodegradation of MBT has been studied by Chengshuai Liu *et al.*[12] The oxidative degradation of MBT at the interface of $\beta\text{-MnO}_2$ and water was reported by Fangbai Li *et al.*[13]. Andreozzi *et al* [14] reported on the oxidation of MBT in aqueous solution using $\text{H}_2\text{O}_2/\text{UV}$ and Fe^{3+} -photoassisted Fenton techniques, in the pH range 3.0 - 8.0.

Malouki *et al* [15] found that the deprotonated form of MBT is 10 times more reactive than its molecular form toward direct photolysis at 313 nm. MBT was photoconverted into benzothiazole (BT) and 2-hydroxybenzothiazole (2-HOBT) when irradiated in aerated medium, with a photoconversion yield of 0.02. Moreover, the authors compared the disappearance of MBT in Milli-Q water at pH=8 and lake water, finding that the disappearance of MBT was 4 times faster in natural water, showing the synergistic effect of the matrix, that significantly contributed to the phototransformation of MBT.[15, 16]

Derco *et al* [4] investigated the feasibility of ozonation on the removal of $200 \text{ mg}\cdot\text{L}^{-1}$ MBT from model wastewater of rubber industry.

Recently, Allaoui *et al* [6] studied the homogeneous photochemical degradation of MBT in the presence of decatungstate anion (DTA) in aqueous solution, observing an increase of photodegradation by a factor of 6 in the presence of DTA, as compared to direct photolysis.

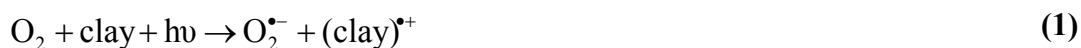
Considering the persistence of MBT in the environment, its confirmed toxicity and low biodegradability, we concentrated our study on the ability of simulated sunlight to

degrade it, in the presence of natural clay as a source of iron, and hydrogen peroxide as oxydant.

This type of reaction is known as heterogeneous photo-Fenton process, which has demonstrated remarkable performance in the treatment of wastewater containing toxic or non-biodegradable organic compounds [17].

The core of the process is the production of hydroxyl radical (HO^\bullet) by interaction between iron species and UV light. This radical species is well-known as highly effective and unselective in the degradation of persistent organic pollutants [18-21].

Further, UVA irradiation of clays may also yield different reactive oxygen species (ROS), as in eqs. (1)-(5)[22].



The different generated ROS, and specially HO^\bullet , the strongest oxidant possibly found in aqueous environment ($E^\circ(\text{HO}^\bullet, \text{H}^+/\text{H}_2\text{O})=2.73 \text{ eV vs. NHE}$),[23] are highly oxidative and may react with essentially any persistent organic pollutant, due to their high oxidation potential.

Clays are abundant fine grained components of geological materials, produced by the weathering and disintegration of granite and feldspathic rocks [24]. These anhydrous complex compounds are composed of alumina (Al_2O_3) and silica (SiO_2). Clays usually have diameters ranging from a few microns to a few hundredths of a micron, and tend to show large surface areas and adsorption capacities. They contain varied amounts of impurities of iron, organic matters and residual minerals [25,26].

Recently, clays have been reported to be good candidate as catalysts support because they are natural, abundant, cost-effective, available for wide pH range, environmentally benign as well as have high catalytic activity and stability.

Homogeneous photo-Fenton has been widely investigated as an innovative for environmental applications such as detoxification processes in water. Nevertheless, and to the best of our knowledge detailed studies on UV/H₂O₂/clay processes using natural clays as heterogeneous photocatalysts for especially the degradation of MBT have not been reported before.

The main objective of this thesis is to investigate the potential efficiency of heterogeneous photo-Fenton process for the removal of MBT from aqueous media using a local abundant cheap material as a photocatalyst in the presence of hydrogen peroxide under simulated sunlight irradiation.

This thesis was composed by a general introduction followed by three main chapters and was completed by conclusions and a list of references used for the writing of this work.

The first chapter presented a dense literature review on benzothiazole's family, with a special focus on MBT; its provenance, its toxicity, and its degradation by different chemical, photochemical and biological techniques. Moreover, the main findings and related mechanisms of degradation were exposed. Another part of this chapter focused on the principal Advanced Oxidation Processes (AOPs) used in the treatment of contaminated wastewater including homogeneous and heterogeneous photo-Fenton processes.

The second chapter exposed the material and methods used to accomplish the experimental part such as reagents, irradiations devices and experimental techniques.

The last chapter was dedicated to present the main findings on MBT adsorption, degradation and especially its photo-degradation by heterogeneous photo-Fenton process.

I

Literature Survey

PART A: BENZOTHAZOLES AND 2-MERCAPTOBENZOTHAZOLE

I.1 BENZOTHAZOLES

Benzothiazoles are heterocyclic xenobiotic compounds; considered as emerging contaminants [27] their basic chemical structure consists of a benzene ring fused with a five-membered thiazole ring including nitrogen and sulfur atoms. The chemical structures of some benzothiazoles are illustrated in Fig.I.1.

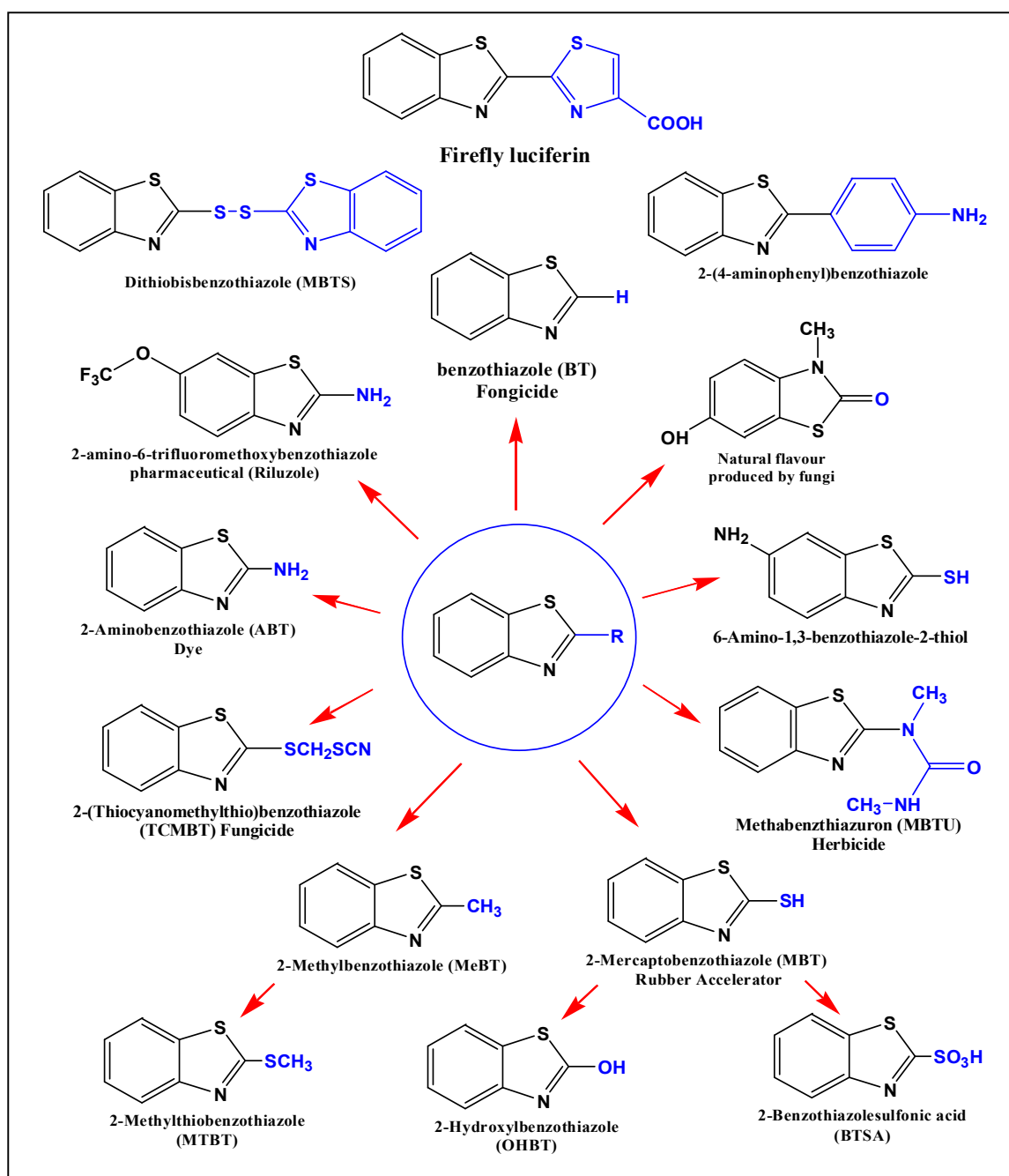


Figure I. 1: Chemical structures of some benzothiazoles.

The majority of benzothiazole are solids at room temperature with the exception of benzothiazole (BT), which is liquid.

Table.I.1 shows that BT possesses the highest solubility (4300 mg/L), this is probably due to its high polarity and the fact that it is a liquid at room temperature. BT is also considered as volatile with a vapor pressure 0.0143 mm Hg (25°C).

OHBT has a good solubility of 2354 mg/L in water. MBT, MTBT and TCMTB are moderately soluble with solubilities of 120 mg/L, 125 mg/L and 125 mg/L respectively. These values of solubility and their respective vapor pressure (0.000464, 0.00026, and $3.12 \cdot 10^{-7}$ mm Hg) show that these benzothiazoles are considered as not volatile from aqueous solutions (or volatile with difficulty).

Table I.1: General properties of Benzothiazoles [28].

	Solubility (mg/L)	Saturated vapor pressure (mmHg at 25°)	pK _{ow}
BT	4300	$1,43 \cdot 10^{-2}$	2,17
MBT	120	$4,64 \cdot 10^{-4}$	2,86
TCMBT	125	$3,12 \cdot 10^{-7}$	3,22
MBTS	10	$2,54 \cdot 10^{-10}$	4,66
MTBT	125	$2,60 \cdot 10^{-4}$	3,12
ABT	310,3	n.d.	2,00

pK_{ow}: partition's coefficient octanol/water

1.1.1 Benzothiazoles applications

Benzothiazoles are rarely natural products; (except BT and MeBT in tea leaves [29] and MBT in cranberry [30]). They are synthesized on a large scale industrial level, and have found many applications such as:

- Pesticides and herbicides: Methabenzthiazuron (MBTU) is used as herbicide in winter corn crops, and is an active ingredient of two commercially available formula Tribunil ® and Ormet ®.
- In the manufacture of dye: 2-Aminobenzothiazole (ABT) is used in the manufacture of some disperse azo dye [31].
- Biocorrosion inhibitors in cooling systems.

- Ingredients in antifreezing agents for automobiles.
- Industrial chemicals in the leather and wood industries.
- Medical research, agriculture and materials sciences. For example: Riluzole (2-amino-6-trifluoromethoxybenzothiazole) marketed by Sanofii-Aventis, is a benzothiazole based drug that is used to treat amyotrophic lateral sclerosis (ALS).

Other derivatives of benzothiazole have been recently developed for their biological activities as inhibitor of topoisomerase II [32] or anti-malaria agents [33], some derivatives having similar activities as the reference compounds.

Benzothiazole are often used also, as herbicides and fungicides, as anti-fungal drug, as slimicides in the paper and pulp industry, and mainly as vulcanization accelerators in rubber production such as MBT [34].

I.1.2 Provenance

Benzothiazole are widely distributed in the environment and have been detected in industrial wastewater, as well as in soils, estuarine sediments, and superficial water [35]. They enter the environment from a variety of sources such as the leaching of rubber products, fine particles of automobile tires, and antifreeze.

In fact, only few data are available about the quantity of benzothiazoles produced each year that can be found in the environment (surface and ground waters) but also in urban wastewater treatment plants. Some data are related to benzothiazoles used for gums and tires (such as MBT). The available data are not up to date, for instance in the 1980's, the total production of MBT in Europe was estimated to 38 000 tons [36]. In 1985, this production was about 25 000 tons in the USA and the American Environment Protection Agency (www.epa.gov) estimated that about 500 tons were released in nature.

In addition to the production units of these industrial compounds, the wash out of manufactured products (rubber gloves, syringes, tires...) can be a source of indirect contamination. Only few studies report quantitative estimation of the exact amount of benzothiazoles in waters because complex analytical tools are required. Only LC-MS techniques recently adapted by the team of Reemstma [37] allowed analyzing the main benzothiazole derivatives in wastewater treatment plants, in surface waters, in domestic wastewaters and in waters issued from motorway wash-out.

I.1.3 Benzothiazoles toxicity

Benzothiazoles pose an environmental concern when released into watercourses [2]. These compounds inhibit microorganisms activity in conventional biological wastewater treatment systems and most of them are not readily biodegradable [34, 38]. Moreover, these compounds can be absorbed into cell membranes, leading to bioaccumulation. Unfortunately, conventional biological wastewater treatment cannot effectively remove such contaminants, since they are resistant to biodegradation [34].

I.1.4 Benzothiazoles degradation

Several published studies reported the degradation of the benzothiazole compounds by different AOPs as presented explicitly in Table.I.2 advanced by M. Antonopoulou *et al* (2014). Important details are provided on the features and experimental conditions applied for each treatment process as well as on the observed kinetics and degradation degrees. Various AOPs were examined for MBT degradation in aqueous solution with a wide range of initial concentration in laboratory scale.

Table I.2: Summary of AOPs used for the removal/degradation of benzothiazole's compounds.

C_0	Matrix-scale	AOP features	Kinetic data	Reference
2-mercaptobenzothiazole (MBT)				
600 $\mu\text{mol L}^{-1}$	Pure water, Treated tannery wastewater Lab scale	O_3 pH =7	~100% removal in 6 min in both matrixes	Fiehn et al., 1998 [39].
1.10 ⁻⁵ mol L ⁻¹	Bi-distilled water Lab scale	$\text{H}_2\text{O}_2/\text{UV}$ (UV 17 W low pressure (LP) lamp, $\lambda = 254 \text{ nm}$) $[\text{H}_2\text{O}_2]=3\text{-}6.10^{-3} \text{ mol L}^{-1}$, pH=3, 5, 8	$k_{\text{OH}} = 4.27 \pm 0.038 \times 10^9 \text{ L. mol}^{-1} \cdot \text{s}^{-1}$	Andreozzi et al., 2001 [14].
1.10 ⁻⁵ mol L ⁻¹	Bi-distilled water Lab scale	$\text{Fe}^{3+}/\text{H}_2\text{O}_2/\text{UV}$ (UV 125 W high pressure (HP) Hg lamp, 305-366 nm) $[\text{H}_2\text{O}_2]=1.10^{-3} \text{ mol L}^{-1}$ $[\text{Fe(III)}]_0 = 3.10^{-6} \text{ mol L}^{-1}$, pH= 2-4	>80% degradation in ~15-35 min Depending on pH value Max. removal in range pH 2.7-3.2	Andreozzi et al., 2001 [14].
0.28 mM	Water Lab scale	Suspended $\text{Nd}^{3+}\text{-TiO}_2/\text{UV}$ (8 W medium pressure (MP) Hg lamp, $\lambda_{\text{max}}=365 \text{ nm}$) $[1.2 \text{ Nd}^{3+}\text{-TiO}_2]=1000 \text{ mg L}^{-1}$, pH= 6.46	$K_{\text{app}}=0.1795 \text{ min}^{-1}$ 59.2% DOC reduction in 80 min	Li et al., 2006 [5].
0.13 mM	Distilled water, Lab scale	Suspended $\text{Nd-TiO}_2/\text{Vis}$ (110 W HP sodium lamp, 400-800 nm) $[0,7 \text{ Nd}^{3+}\text{-TiO}_2] = 1000 \text{ mg L}^{-1}$	$K_{\text{ap}}=0.0616 \text{ min}^{-1}$ $k_r = 10.6 \times 10^{-6} \text{ mol}^{-1} \text{ min}^{-1}$ 48% DOC reduction in 100 min	Li et al., 2005a [40].
0.28 mM 0.13 mM	Water, Lab scale	Suspended $\text{Ce}^{3+}\text{-TiO}_2/\text{UV}$ (8 W UVA lamp, $\lambda_{\text{max}}=365 \text{ nm}$) $[1,2 \text{ Ce-TiO}_2]=1000 \text{ mg L}^{-1}$ Suspended $\text{Ce}^{3+}\text{-TiO}_2/\text{Vis}$ light (110 W HP sodium lamp, 400-800 nm), $[0.7 \text{ Ce-TiO}_2]=1000 \text{ mg L}^{-1}$	~100% in 40 min ~98% removal in 100min	Li et al., 2005b [10].
0.278 mmol L ⁻¹	Water Lab scale	Suspended $\text{La}^{3+}\text{-TiO}_2/\text{UV}$ (8 W MP Hg lamp, $\lambda_{\text{max}}=365 \text{ nm}$) $[1.2 \text{ La-TiO}_2]=1000 \text{ mg L}^{-1}$	$k_{\text{app}}= 0.1653 \text{ min}^{-1}$ $k_r = 2.5918 \times 10^{-5} \text{ mol L}^{-1} \text{ min}^{-1}$ 61.1% DOC reduction in 80 min	Li et al., 2004 [9].

1mM	Pure Water Lab scale	Suspended TiO ₂ /UV (400 W HP Hg lamp), [TiO ₂]=50 mg/15 mL O ₂ flux=1 mL min ⁻¹ , pH=9	98% degradation in 8 h	Habibi et al., 2001a [41].
1. 10 ⁻⁴ M	Water Lab scale	Na ₄ W ₁₀ O ₃₂ /UV (125 W HP Hg lamp, λ=365 nm) [W ₁₀ O ₃₂ ⁴⁻]=2.10 ⁻⁴ M, pH=4.4 Aerated conditions O ₂ saturated conditions Deoxygenated conditions	k _{app} =0.25 h ⁻¹ , t _{1/2} =2.8 h, 90% degradation in 8 h k _{app} = 0.47 h ⁻¹ , t _{1/2} =1.5 h, 100% degradation in 8 h ~50% inhibition	Allaoui et al., 2010 [6].
10mg.L ⁻¹	Deionised Water Lab scale	γ-Fe ₂ O ₃ / oxalate / UV (UVA lamps, λ _{main} =365 nm, 8 W black light lamp) [γ-Fe ₂ O ₃]=0.4 g L ⁻¹ , C _{ox} ⁰ =0.8 mM, I=1800 mW/cm ²	96.7% removal in 45 min k _{app} = 8,98x10 ⁻² min ⁻¹	Wang et al., 2008 [11].
10mg.L ⁻¹	Water Lab scale	γ-Fe ₂ O ₃ /oxalate/UV (8 W black light lamp λ _{max} =365 nm) [I.O.]=0.4 g L ⁻¹ , C _{ox.ac.} =1mM UV (365 nm)/0.4 g L ⁻¹ I.O.-420	41-89.5% degradation in 90 min k _{app.} = 0.75.10 ⁻² -2.74.10 ⁻² min ⁻¹ 12% degradation in 90 min	Liu et al., 2006 [12].
Benzothiazole (BT)				
1.10 ⁻⁵ -5.10 ⁻⁵ mol L ⁻¹ 10 ⁻⁵ mol L ⁻¹	Bi-distilled water Lab scale	H ₂ O ₂ /UV (UV 17 W LP lamp, λ=254 nm) [H ₂ O ₂]=5.10 ⁻³ mol L ⁻¹ , pH=4/4 H ₂ O ₂ /UV (UV 17 W LP lamp, λ=254 nm) [H ₂ O ₂]=2-5.10 ⁻³ mol L ⁻¹ , pH=4, 6,8	> 95% degradation in 80-170 min A decrease in the degradation rate was observed, increasing the [BT] ₀ k _{OH} = 3.85±0.033 L ⁻¹ mol ⁻¹ s ⁻¹	Andreozzi et al., 2001 [14].
1.10 ⁻⁵ mol L ⁻¹	Bi-distilled water Lab scale	Fe ³⁺ /H ₂ O ₂ /UV (UV 125 HP Hg lamp, 305-366 nm) [H ₂ O ₂]=1.10 ⁻³ mol L ⁻¹ [Fe(III)] ₀ =3.10 ⁻⁶ mol L ⁻¹ , pH=2-4 Fe ³⁺ /H ₂ O ₂ /UV (125 HP Hg Lamp, 305-366 nm) [H ₂ O ₂]=2.5.10 ⁻⁴ -2.10 ⁻³ mol L ⁻¹ [Fe(III)] ₀ =1-3.10 ⁻⁶ mol L ⁻¹ , pH=2.7	> 90% degradation in ~15-45 min Depending on pH value Max. removal in range pH 2.7-3.2 Increase of the system reactivity with increasing [Fe ³⁺]. Maximum is recorded with changing [H ₂ O ₂]	Andreozzi et al., 2001 [14].

2-hydroxybenzothiazole (OHBT)				
$5 \cdot 10^{-6} \text{ mol L}^{-1}$	Bi-distilled water Lab scale	$\text{H}_2\text{O}_2/\text{UV}$ (UV 17 W LP lamp, 254 nm) $[\text{H}_2\text{O}_2]=2\text{-}8 \cdot 10^{-3} \text{ mol L}^{-1}$, pH=3-8	$k_{\text{OH}}=3.97 \pm 0.022 \times 10^9 \text{ L mol}^{-1} \text{ s}^{-1}$	Andreozzi et al., 2001 [14].
$1 \cdot 10^{-5} \text{ mol L}^{-1}$	Bi-distilled water Lab scale	$\text{Fe}^{3+}/\text{H}_2\text{O}_2/\text{UV}$ (UV 125 W HP Hg lamp, 305-366 nm) $[\text{H}_2\text{O}_2]=1 \cdot 10^{-3} \text{ mol L}^{-1}$, $[\text{Fe(III)}]_0=3 \cdot 10^{-6} \text{ mol dm}^{-3}$, pH=2.7-4	>~90% degradation in ~25 min (pH=2.7, 3.2) ~80% degradation in ~55-65 min (pH=2, 4)	Andreozzi et al., 2001 [14].

1.2. 2-MERCAPTOBENZOTHAZOLE (MBT)

2-mercaptobenzothiazole or benzothiazolethiol (MBT) is one of the most important members of benzothiazole's family [3]. This xenobiotic compound, is a synthetic product exist as sodium, potassium and zinc salts, and its salts are used as pesticides or fungicides, MBT as an important chemical additives, is mainly used as a vulcanization accelerator in tire industry [15], and widely used in synthesis of antibiotic and rubber [2], but also has other uses notably as preservative or as anticorrosion agent of metals such as copper [3,4], zinc or silver [5].

In the past, MBT has been used in the gold-mining industry to "float" the gold from ore residue as part of the extraction process (Wikipedia).

MBT is a condensed heterocyclic compound with a molecular weight of 167 amu (Fig.I.2). Its Structure is composed by a mercapto exocyclic group possessing a labile hydrogen atom and it can exist in three forms (deprotonated and two molecular forms tautomers) which have yellow colored crystals with pungent odor and are soluble in water.

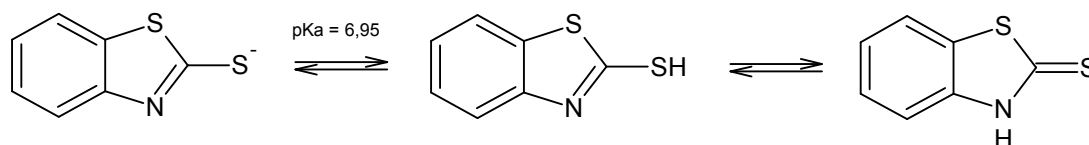


Figure I. 2: Equilibrium of different forms of MBT.

The solubility of 2-mercaptobenzothiazole in non-polar organic solvent is relatively less.

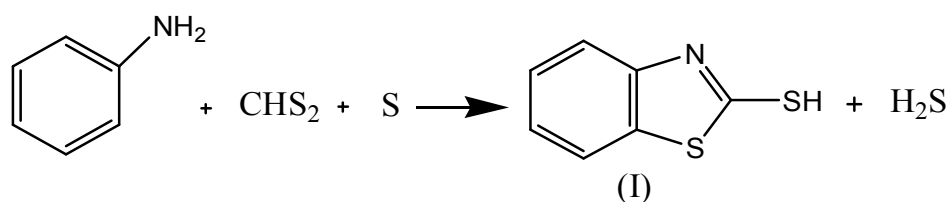
1.2.1 MBT synthesis

A number of methods for the synthesis of 2-mercaptobenzothiazoles (MBTs) have been reported. Among them, classical approaches involve the reaction of thiocarbanilide with sulfur or the interaction of o-aminothiophenol with carbon disulfide under high pressure [47–50]. Several groups reported synthesis of MBTs by the nucleophilic aromatic substitution reaction of a potassium/sodium o-ethyl dithiocarbonate with o-haloanilines followed by a subsequent cyclization [51–56]. Recently, two efficient approaches from 2-haloaniline precursors were applied for the synthesis of MBTs. The first approach [57] involves a copper-catalyzed condensation reaction of the 2-iodoaniline with thiols

in the presence of potassium carbonate. The second [58] involves the reaction of the o-haloanilines with carbon disulfide in the presence of 1,8-diazabicyclo[5.4.0]undec-7-ene (DBU).

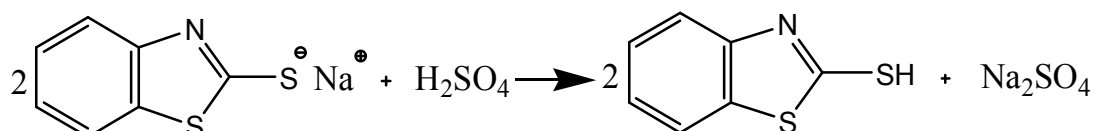
According to the reactions reported by DE Wever *et al* [34] the synthesis of MBT could occur in two steps;

In a first step, the heterocyclic five-membered ring in MBT is formed through the condensation of aniline and carbon disulfide, in a redox reaction with S as electron acceptor. As shown in following first reaction.



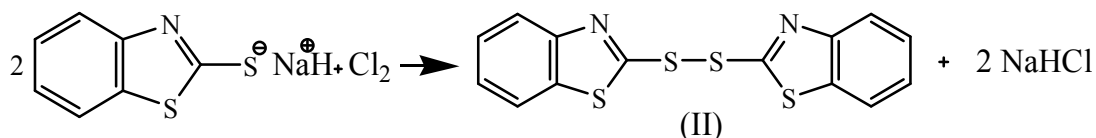
Reaction I.1

Extraction of the obtained organic phase with an aqueous NaOH solution yields a concentrated NaMBT solution, from which several compounds can be precipitated. After acidification (reaction I.2), pure MBT is obtained and a salt-rich water phase with a residual MBT concentration below saturation level.



Reaction I.2

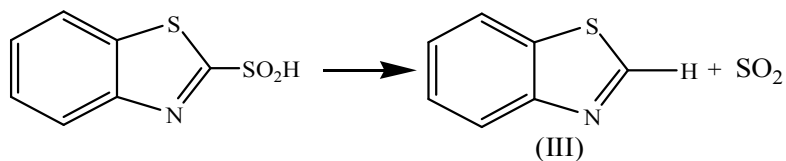
Oxidation with Cl₂ yields the insoluble DM (reaction I.3) or sulfenamides when amines are also present.



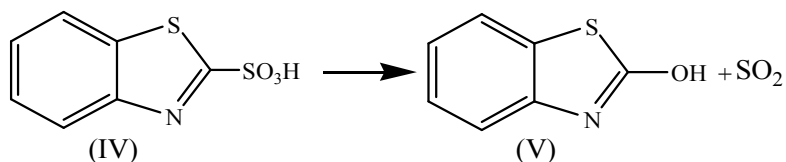
Reaction I.3

Hydrolysis of DM and the sulfenamides and some oxidative reactions produce oxidation products of MBT, namely the sulfenic, sulfinic and sulfonic acids. Dissociation of the sulfinic acid leads to the presence of benzothiazole (BT)

(reaction I.4), whereas 2-hydroxybenzothiazole (OBT) originates from the sulfonic acid (reaction I.5).



Reaction I.4



Reaction I.5

The industrial manufacture of MBT thus gives rise to a salt-rich wastewater which contains four benzothiazoles in particular: MBT (I), BT (III), BTSO₃ (IV) and OBT (V). DM (II) may occur as oxidation product of MBT.

I.2.2 MBT Toxicity

The presence of MBT in many compartments and its high toxicity are the basis of many studies to evaluate both its environmental fate and toxicity for long terms, and in the other hand to provide a process capable to eliminating it completely.

Its toxicity towards microorganisms [7,34,59-60] and its allergenicity resulting in serious dermatoses [61], and its potential mutagenic effects [7], make its presence in the environment a matter of great concern.

Recent studies have identified it as a potential human carcinogen [62]. In 2016, it was identified by the World Health Organization as a human carcinogen.[63] It causes allergic contact dermatitis [64]. The derivative morpholinylmercaptobenzothiazole is a reported allergen in protective gloves, including latex, nitrile, and neoprene gloves. [63]

It becomes air-borne as a result of wear on car tires, and is able to be inhaled [64].

Several epidemiologic studies have reported that workers in the rubber industry have an increased risk of cancer [65-67]. The laboratory and epidemiological studies suggest

that MBT acts as a carcinogen in mammals [68] and thus it becomes important to study the photochemical and biological activity of MBT.

De Wever *et al.* [7] Have reported the toxicity of 2-mercaptobenzothiazole towards bacterial growth and respiration. The studies suggest that rats chronically exposed to MBT show increase in various type of tumors, such as adrenal gland, pituitary gland, liver and renal pelvis tumors. A comprehensive review of the epidemiological and toxicological dataset for MBT indicates that the induction of renal pelvis transitional cell tumors is the most sensitive and relevant health effects. The total allowable concentration (TAC) and single product allowable concentration (SPAC) has been based on these studies [68].

In general, it has been shown that the compounds of the family of benzothiazoles, including MBT, prove dangerous for microorganisms and humans.

1.2.3 MBT in Environment

MBT is a toxic and poorly biodegradable chemical [4,69] has been detected in wastewater effluents from rubber additive manufactures, river water, sewage treatment plants, roads dusts and especially in surface water [5]. and can come into contact with potable water. This clearly confirms the eventual pollution of environmental compartments. Moreover, many previous studies have confirmed that MBT is a strong pollutant of aquatic organisms, allergen and potentially mutagen for human [4]. That means a non-negligible impact of MBT on environment and on human health.

2-Mercaptobenzothiazole (MBT) is an important industrial chemical with an annual production of approximately 40,000 tons in Europe [70] and According to EPA Toxic Release Inventory in 2010, total on-site and off-site disposals of MBT in USA was 190575.42 lb, of which chemical industry released 6071 lb and plastic/rubber industry released 60749.6 lb.

Unfortunately we didn't find relevant data about the production of MBT in Algeria or in Africa in general.

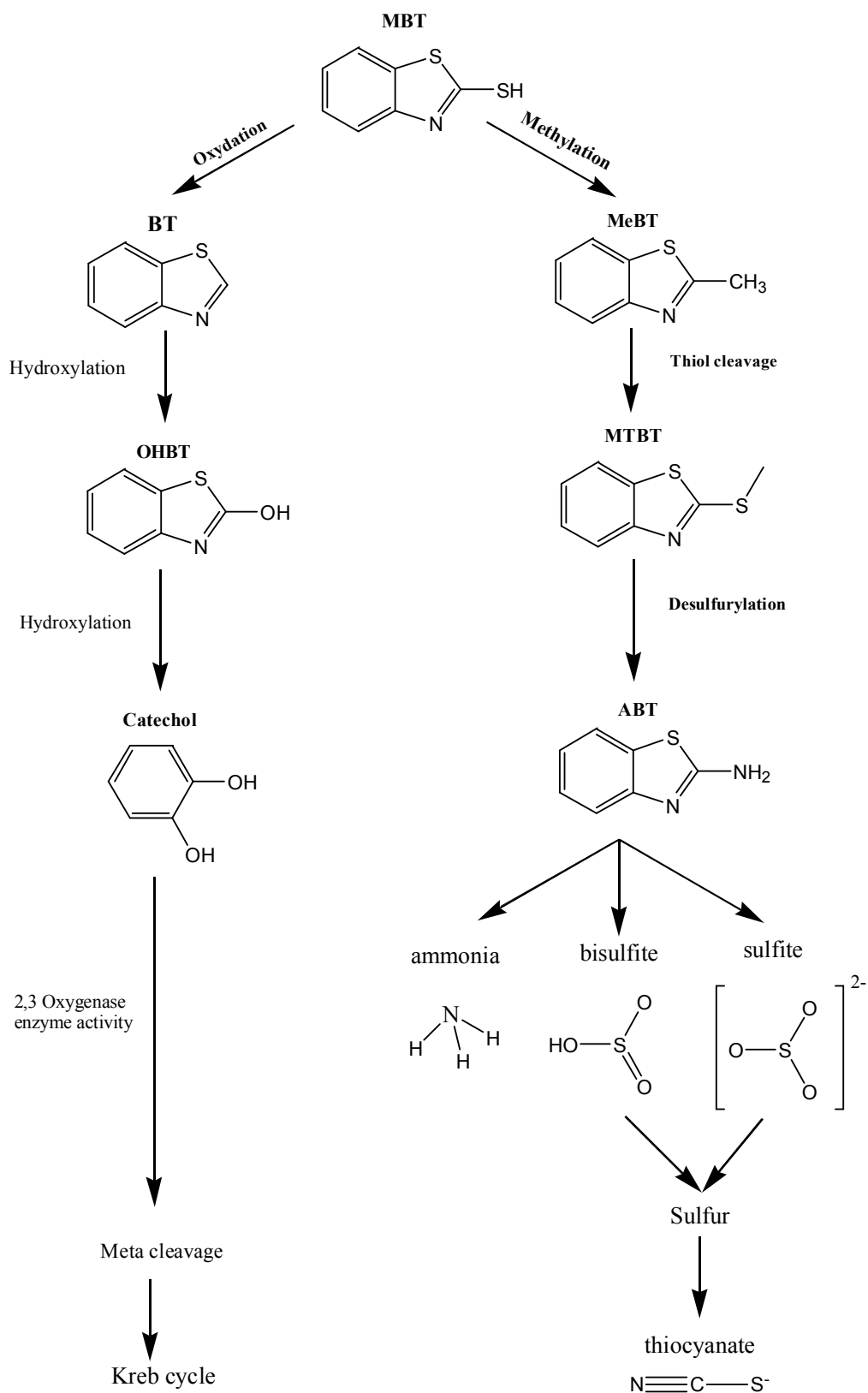
1.2.4 MBT Biodegradation

Data concerning the biodegradation of MBT are inconclusive. Some studies have suggested it is recalcitrant to biodegradation and have toxic effects on many bacteria, and its presence inhibits biodegradation of other compounds, including some of its own degradation products. [7].

Because of its antimicrobial effect, wastewater containing MBT is usually resistant to conventional biological treatment. For example, in the activated sludge system, MBT was found to be resistant and toxic towards activated sludges [71]. Moreover, MBT even inhibited the degradation of the other heterocycles in the degradation test of heterocycle mixtures. It was reported that microorganisms composing the activated sludge from municipal wastewater treatment plant could be killed after exposure to MBT solutions for 2–3 days [79]. De wever *et al.* [7] found that 100 mg/L of MBT was enough to completely inhibit bacterial growth. In addition to the conventional activated sludge process, two stage anaerobic and aerobic process [73].

M. A. Gaja *et al* [3] studied the removal of 2-mercaptobenzothiazole from solution by activated sludge, the authors noted that, the most rapid removal was with an industrial sludge, however, MBT was removed as rapidly by heat-killed as by “live” activated sludge.

Microaerobic degradation of 2-Mercaptobenzothiazole was investigated also by Umamaheswari. B *et al* [8] using an isolated bacterial strain CSMB1. It was identified as *Alcaligenes* sp. MH146 by genomic analysis. The isolate degraded 50 mg/L concentration of MBT which was measured in terms of Total Organic Carbon (TOC) (700 mg/L). A maximum degradation of 86% with a residual TOC concentration of 101 mg/L was obtained after 72 h, with the biomass growth of 290 mg/L. The presence of specific activity of catechol 2, 3 oxygenase was observed in all the tested derivatives of benzothiazoles and the benzene ring opening was observed through meta cleavage. By analyzing the 72 h incubated culture supernatant, MBT, and all its biotransformed products were degraded into polar compounds. It is concluded that microaerophilic isolate CSMB1 was able to degrade MBT and its intermediates by utilizing them as sole carbon and energy. With the analytical results obtained, a possible Microaerobic degradative pathway was proposed and illustrated for MBT (**Scheme I.1**).



Scheme I.1: Postulated microaerobic degradation pathway of MBT by isolated strain *Alcaligenas* sp. MH 146 strain CSMB1. [8].

De Wever *et al.* [74] have reported that the bacteria like *Corynebacterium pseudomonas* and *Escherichia coli* are capable of methylating the thiol group to produce 2-methylthiobenzothiazole (MTBT).

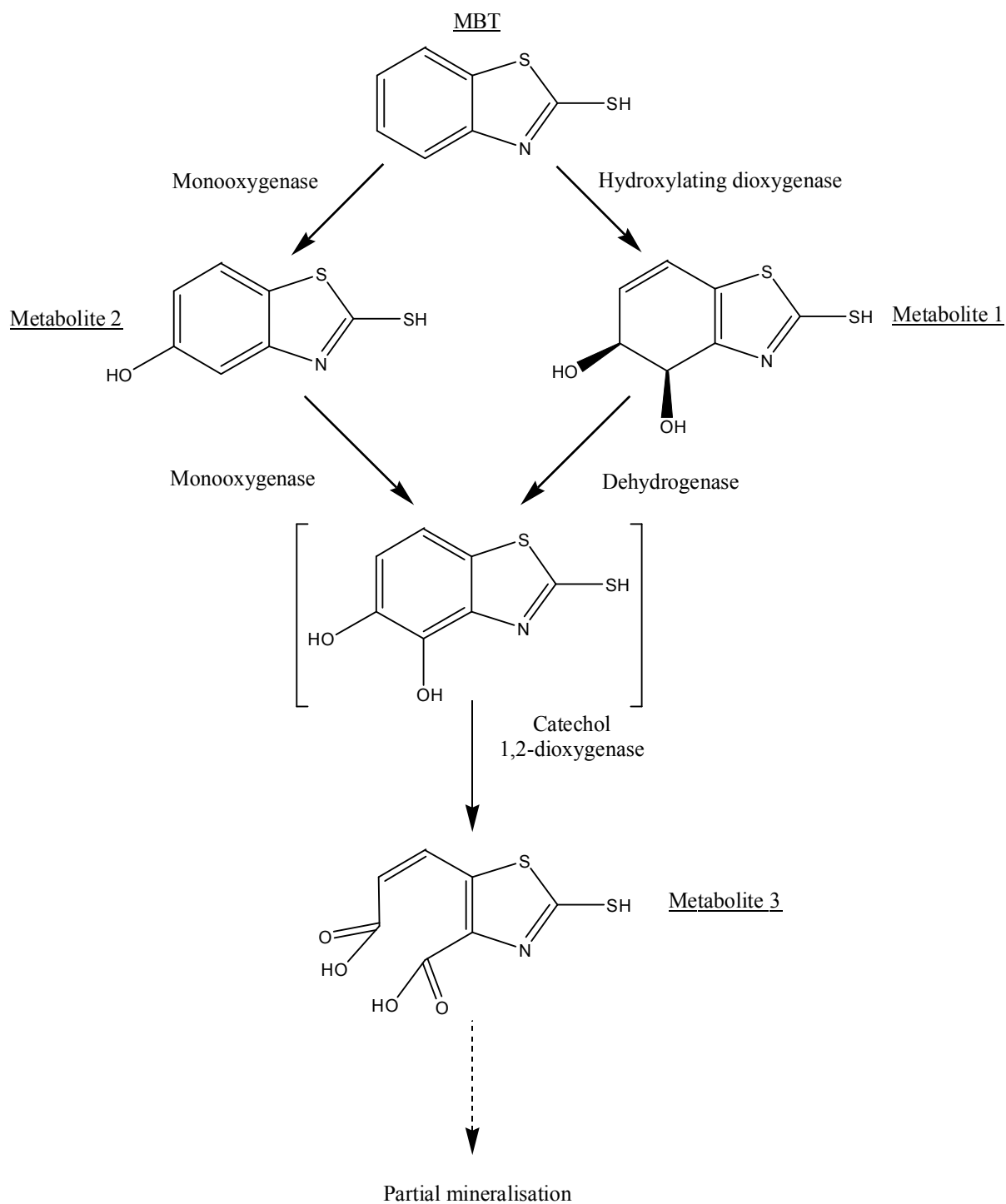
Rhodococcus erythropolis converts BT and BTSO₃ to 2-hydroxybenzothiazole (OHBT), which can be further hydroxylated to form 2,6-dihydroxybenzothiazole [75,76]. The conversions require the presence of the oxygen, the conversion of BTSO₃ to OHBT can take place under anaerobic conditions [75]. (**Scheme I.2**).

Nicolas Haroune *et al* [77] showed for the first time that MBT can be biotransformed and partially mineralized by a pure-culture bacterial strain of *Rhodococcus rhodochrous* OBT18, isolated from activated sludge from a wastewater treatment plant of an MBT-producing factory.

The authors found that, although MBT is known to be extremely recalcitrant, it can be biotransformed into four metabolites and that 30% of MBT was completely mineralized under experimental conditions. The transformation of MBT clearly results from enzymatic processes, as no degradation of MBT was observed in control experiments in which no cells, either live or heat-killed, were used. Although the experiments reported were not performed with growing cells, the results may give indications about processes that could occur in the environment.

Also, it was shown that 6-OH-MBT is less toxic than MBT, according to the standardized Microtox test performed. For an exposure time of 15 min, the 50% effective concentrations were 9.5 μM for 6-OH-MBT and 1.5 μM for MBT.

The structure of the metabolites formed and the metabolic pathway of MBT was identified by the authors as shown in the **Scheme I.2**.

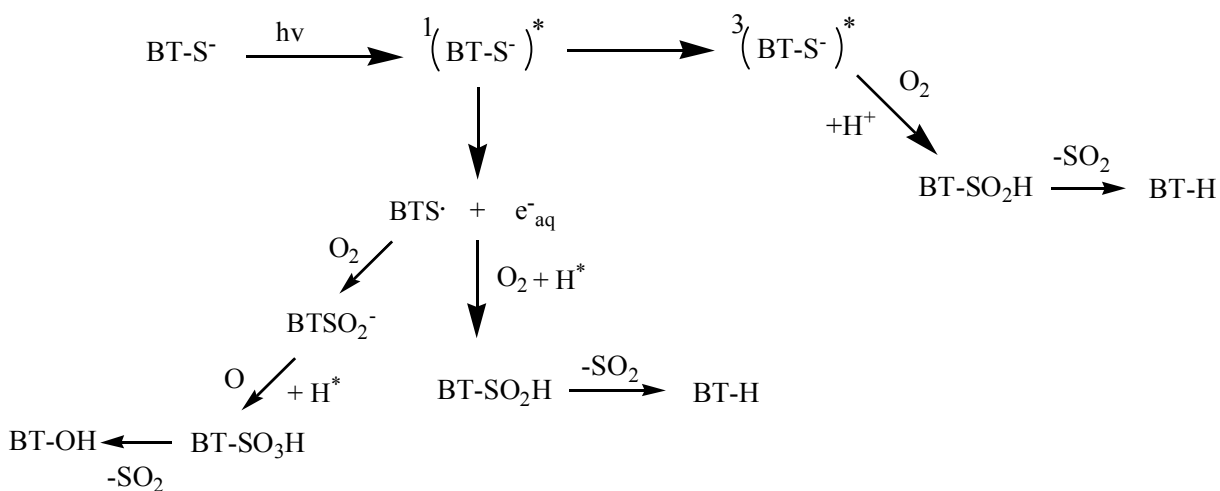


Scheme I.2: Proposed metabolic pathway of MBT in *R. rhodochrous* OBT18 [77].

I.2.5 MBT photodegradation

I.2.5.1 Direct photolysis

The investigation of the direct photolysis of MBT using 313nm irradiation was studied by Malouki et al [15] in milli-Q purified water and in natural water sampled in a lake; the authors observed that the anionic form was found to be photoconverted into benzothiazole (BT) and 2-hydroxybenzothiazole (2-HOBT) in aerated medium, (Scheme I.3). The yield of photoconversion was 0,02.



Scheme I.3: Proposed pathway of direct photolysis of MBT at 313 nm proposed by Malouki *et al* [15].

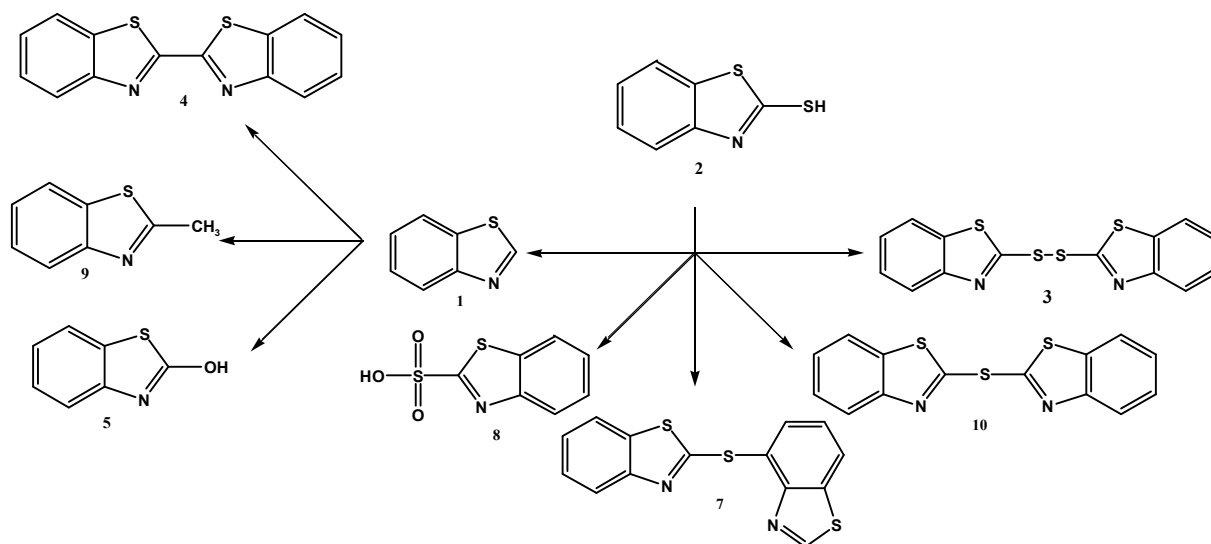
Moreover, the authors compared the disappearance of MBT in Milli-Q purified water (buffered at pH 8) and in natural lake water exposed to solar light. They observed that the disappearance of MBT was 4 times faster showing that chromophoric components of natural water of the lake powerfully contributed to the phototransformation of MBT in the aquatic environment [15,16].

Zuzana Zajíčková *et al* [78] also have investigated the direct photolysis of 2-mercaptobenzothiazole to identify the photodegradation products of this later with the benzothiazole and 2- mercaptobenzothiazole disulfide.

Their results showed that with both the quartz and Pyrex flasks; irradiation causes the formation of the same photoproducts. The major difference is in how fast the compounds are decomposing and in what ratios the individual products are being

formed. A quartz vessel allows for much faster occurring degradation since light of higher frequency passes through. Absorption of the light of higher frequency provides higher energy necessary to break a bond in a molecule.

The photolytic pathway proposed by the authors confirm that benzothiazole (1) is the principal photoproduct together with an oxygenated photoproduct 2-benzothiazolesulfonic acid (8), and its monomer 2,2'-thiobisbenzothiazole (10) which is formed in small amounts. Additional degradation products were detected as well, such as 2-methylbenzothiazole (9), 2-hydroxybenzothiazole (5) and 2,2'-bibenzothiazole (4) which are further degradation products of benzothiazole (1). The presence of the dimer 2-mercaptobenzothiazole disulfide (3) was detected at higher concentration of 2-mercaptobenzothiazole (1×10^{-2} M) in methanol upon irradiation in a Pyrex vessel or in acetonitrile as the irradiation medium. The formation of photoproducts is summarized in Scheme I.4.

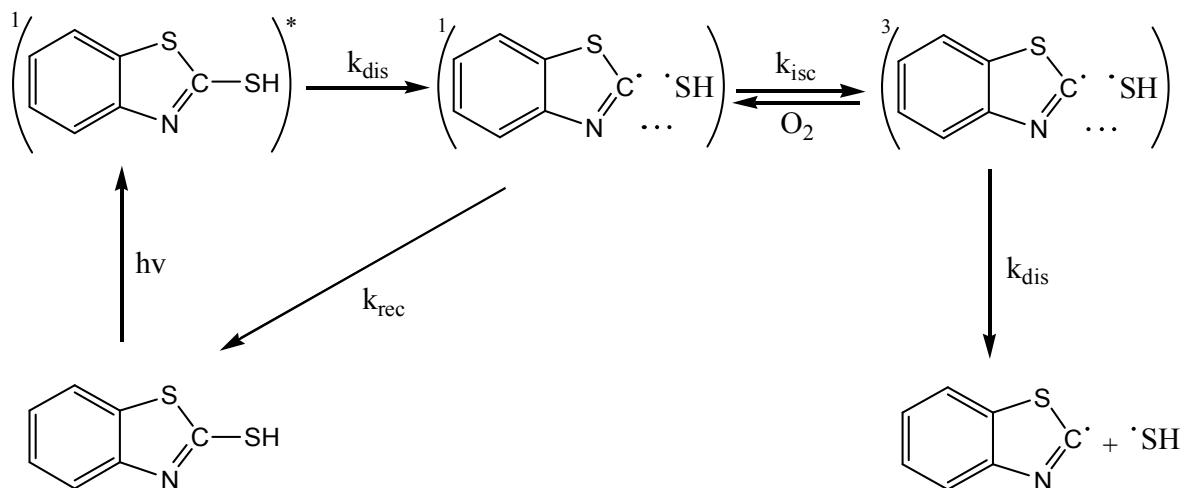


Scheme I.4: Photolytic pathway of direct photolysis of MBT proposed by Zajičková *et al* [78].

Maria Serdechnova *et al* [79] studied the photochemical degradation of MBT and 1,2,3-benzotriazole in aqueous solution and organic solvent, the authors found that upon UV irradiation the analysis of degradation products revealed the predominant formation of dimeric compounds from MBT and oligomeric structures from BTA.

The increase of the quantum yield of MBT and BTA photodegradation reactions under aerobic conditions both in aqueous and organic solvents was explained by an increase of

the spin-orbit conversion of the singlet radical pairs into the triplet radical pairs in the presence of oxygen. These triplet pairs further dissociate into free radicals, or convert to the parent compounds. At the early stage of UV irradiation, free radicals coupling lead essentially to the dimer formation in the case of MBT and to the formation of oligomers in the case of BTA irradiation.



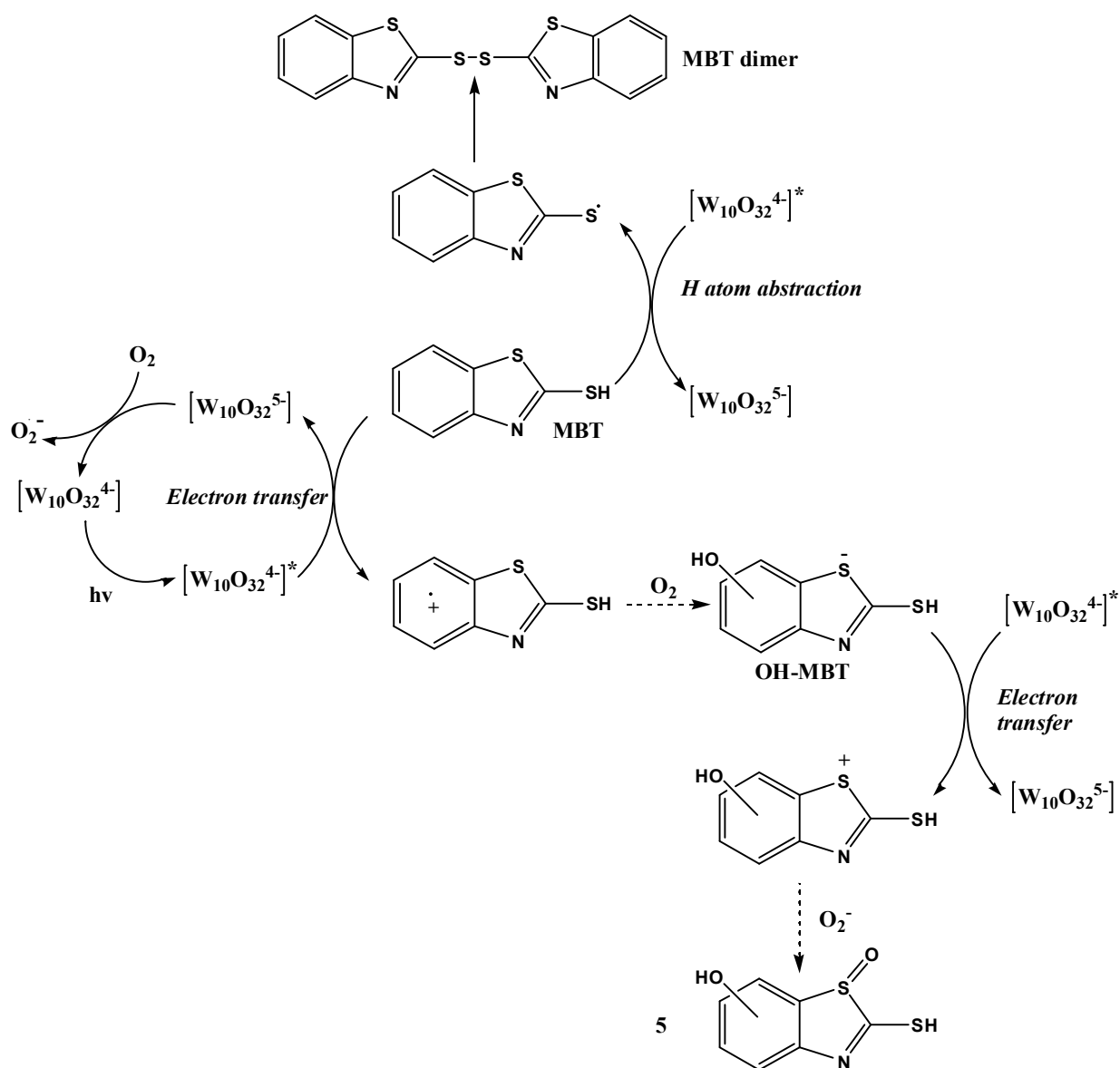
Scheme I.5: The proposed mechanism for MBT photodegradation, Maria Serdechnova et al [79].

I.2.5.2 Homogeneous photodegradation

a. Using DTA

Recently, Allaoui *et al* [6] studied the homogeneous photodegradation of MBT using decatungstate anions (DTA) under UVA light irradiation; they found that, the photodegradation was clearly increased by factor of six in the presence of DTA in aerated condition when compared with the direct photolysis.

The LC-MS study in negative electron spray ionization (-ESI) and LC-DAD techniques allowed them to propose the following mechanism pathway:

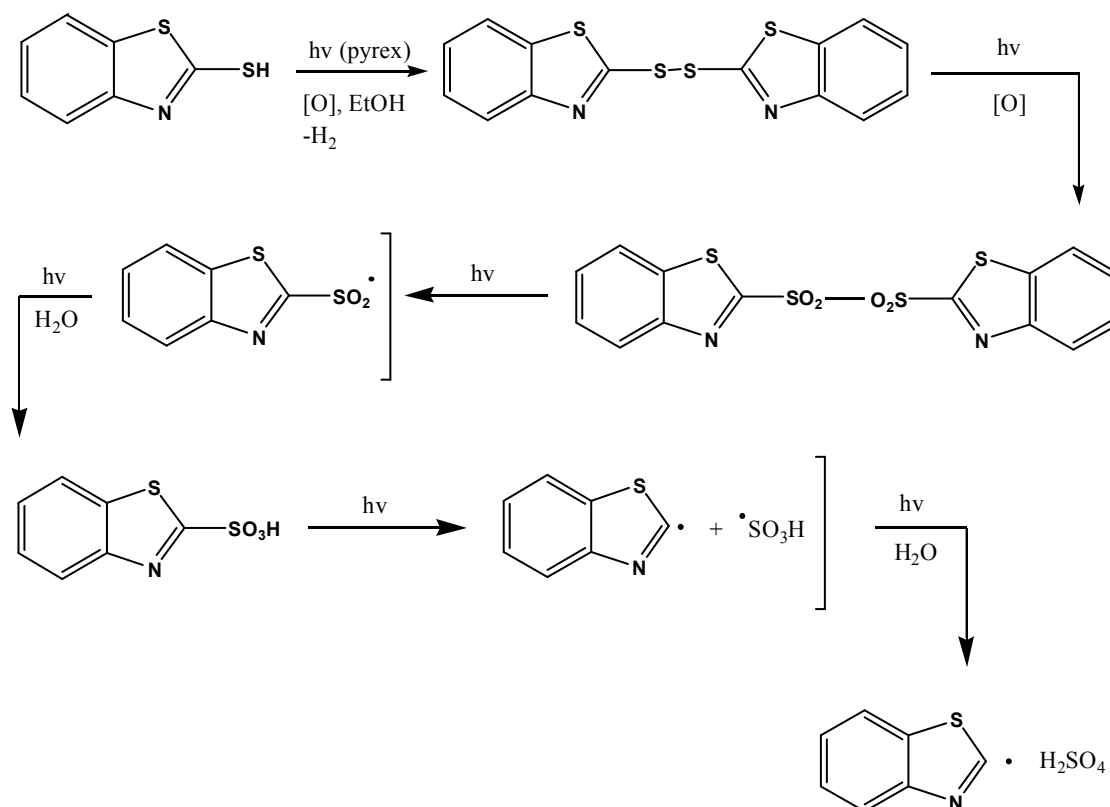


Scheme I.6: Degradation mechanism of MBT in the presence of DTA under irradiation at 365 nm [6].

The mechanism was explained by an Electron transfer and H atom abstraction processes involving $W_{10}O_{32}^{4-*}$ excited state species were involved in the degradation. In the primary step of the degradation, the hydroxylation of the aromatic ring leading to four OH-MBT isomers and the formation of disulfide form of MBT were observed. For longer irradiation time, a secondary electron transfer permitted the oxidation of OH-MBT isomers and the formation of sulfoxide derivatives.

Parkanyi and Abdelhamid [80] studied the photolysis of 2-mercaptobenzothiazole and identified the main stable photoproducts. MBT was irradiated in Pyrex reactor in the

presence of oxygen. When benzene or toluene was used as solvent, the authors observed the bis-(2-benzothiazolyl) disulfide as the major product of transformation. In solution of acetonitrile, methanol or ethanol, the bis-(2-benzothiazolyl)disulfone was obtained as the intermediate product while benzothiazole-2-sulphonate (BTSA) was the final product of the photodegradation (Scheme I.7).



Scheme I.7: Direct photolysis of MBT in organic solution [80].

This study carried out in pure water and in natural water showed clearly that the photoinduced degradation of benzothiazoles was more efficient than the photolysis. As a consequence, to eliminate efficiently benzothiazoles, different advanced oxidation processes have been tested: Fiehn *et al.* [9] studied MBT ozonolysis in pure water or in wastewaters of tanneries.

b. Ozonation

MBT was very reactive with ozone and different products were formed. The three major products observed were BT, benzothiazole-2-sulfite and traces of 2(3H)-benzothiazolone and OBT. These compounds were also degraded with ozone and could be mineralized with a longer treatment. The same results were obtained with the waters

from the tanneries but with longer ozonation time, showing that wastewaters containing high amount of MBT should easily be detoxified using ozone.

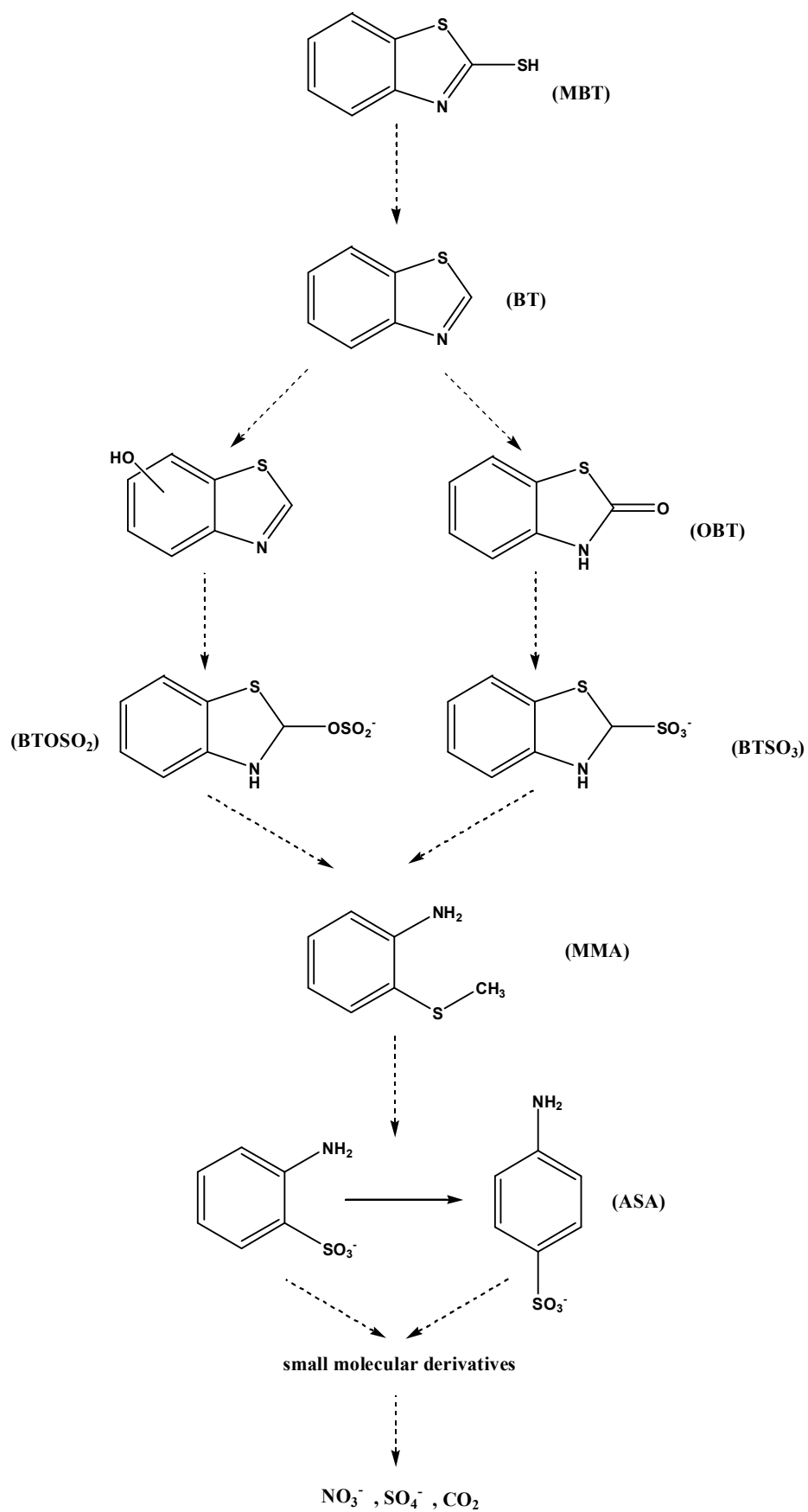
Recently, Valdés and Zaror [81] improved this process by combining the ozone oxidation with the presence of activated carbon. They obtained a great increase of BT degradation. They showed, with radical trap, that the activation of the reaction was due to oxidation reaction of BT at the surface of activated carbon.

More recently, Jan Derco *et al* [4] investigated the feasibility of ozonation process on the removal of 200 mg.L⁻¹ MBT from model wastewater of rubber industry; they remarked a total removal of MBT just after 20 min of ozonation. With a very good reproducibility of repeated ozonation trials including sampling and analysis was observed. However, the majority of dissolved organic carbon (DOC) and chemical oxygen demand (COD) remained in the reaction mixture. Benzothiazole (BT) and 2-hydroxybenzothiazole (OBT) intermediates were identified during degradation of MBT with ozone.

1.2.5.3 Heterogeneous photodegradation

The photocatalytic degradation of MBT in aqueous solution using: Nd³⁺-TiO₂, La³⁺-TiO₂ and Ce³⁺-TiO₂ was studied by F. B. Li *et al* [5,9-10].

F. B. Li *et al* [5] results, showed that the overall kinetic constant (k) of MBT degradation using Nd³⁺-TiO₂ was significantly higher than that using TiO₂ and an optimal content of neodymium ion doping was found to be 1.2% (molar ratio). The main intermediates during the MBT degradation were identified by LC/MS-MS, and the final products including sulfate ion, ammonium ion, and nitrate ion were also determined by ion chromatography. Only three main intermediates including benzothiazole, 2-hydroxybenzothiazole, and benzothiazole-2-sulfite were found during the MBT degradation using the TiO₂ catalyst, while five main intermediates including benzothiazole, 2-hydroxybenzothiazole, benzothiazole-2-sulfonate, benzothiazole-2-sulfite, and anilinesulfonic acid were found during the MBT degradation using 1.2% Nd³⁺-TiO₂.



Scheme I.8: Proposal pathway of the MBT photocatalytic degradation [5].

The oxidative degradation of 2-mercaptobenzothiazole at the interface of β -MnO₂ was investigated by Fangbai Li *et al* [13].

The effect of iron oxides and oxalate on the photodegradation of 2-mercaptobenzothiazole (MBT) was studied by Chengshuai Liu *et al* [12] and Xugang Wang *et al* [11] under UVA light irradiation.

Chengshuai Liu *et al* [12] results showed that, the degradation of MBT found to be depended strongly on the dosage of iron oxides and the initial concentration of oxalic acid (C_{0ox}). The authors found that, the optimal dosages of iron oxides were 0.40, 0.35, 0.30, 0.25 and 0.25 g/L for γ -FeOOH, IO-250, IO-320, IO-420 and IO-520, respectively, and the optimal C_{0ox} was 1.0 mM for all the five iron oxides. These results showed that MBT photodegradation could be enhanced greatly in the presence of oxalic acid.

Xugang Wang *et al* [11] investigated the effect of various factors on the photodegradation of MBT in natural environment with co-existence of iron oxides and oxalic, the authors investigated The effect of the dosage of iron oxide, initial concentration of oxalic acid (C_{0ox}), initial pH value, the light intensity and additional transition metal cations on MBT photodegradation in the γ -Fe₂O₃/oxalate suspension under UVA light irradiation. The optimal γ -Fe₂O₃ dosage was 0.4 g/L and the optimal C_{0ox} was 0.8 mM with the UVA light intensity of 1800 mW/cm². And the optimal dosage of γ -Fe₂O₃ and C_{0ox} for MBT degradation also depended strongly on the light intensity. The optimal initial pH value was at 3.0. The additional transition metal cations including Cu²⁺, Ni²⁺ or Mn²⁺ could significantly accelerate MBT degradation.

Habibi *et al.* [41] have reported the photocatalytic degradation of 2-MBT using titanium dioxide in the wastewater.

The photodegradation of 2-mercaptobenzothiazole disulfide, 2-mercaptobenzothiazole and benzothiazole has been investigated. Benzothiazole was found to undergo photodimerization into 2, 2'-bibenzothiazole, and in the presence of oxygen to give two additional photoproducts 2-hydroxybenzothiazole and 2-methylbenzothiazole. The major degradation products of 2-mercaptobenzothiazole are benzothiazole and 2-benzothiazolesulfonic acid, with 2,2'-thiobisbenzothiazole and 2-mercaptobenzothiazole disulfide as the minor degradation products.

Recently Ziyang Lu *et al.* [82] Studied the photodegradation of MBT by a novel imprinted $\text{CoFe}_2\text{O}_4/\text{MWCNTs}$ photocatalyst prepared through combination of hydrothermal method and suspension polymerization. The authors found that, the photocatalyst not only had high photocatalytic efficiency (57.09 %), but also possessed the strong ability to selective recognition and photodegradation of MBT. In addition, in the process of photodegradation reaction, h^+ and $\bullet\text{OH}$ were the main oxidative species, $\bullet\text{O}^{2-}$ played a very small role.

PART B: ADVANCED OXIDATION PROCESSES

In the last three decades, advanced oxidation processes (AOP) have been studied as promising alternative technologies for the treatment of contaminated ground, surface and wastewater containing hardly biodegradation substances, which would not be efficiently removed by conventional methods.

All of these processes are based on the *in situ* generation of highly reactive species, the hydroxyl radicals (HO^\bullet).

Under treatment by AOPs complex organic molecules can be either oxidized by HO^\bullet to smaller organics or completely mineralized to carbon dioxide (CO_2) and water (H_2O).

In the next paragraphs we will present an exploratory study on some of these AOP, with a special focus on: direct photolysis, $\text{H}_2\text{O}_2/\text{UV}$, homogeneous and heterogeneous Fenton and photo-Fenton processes.

I.1 CONCEPT AND FUNDAMENTALS

I.1.1 Hydroxyl radicals

The hydroxyl radicals (HO^\bullet) have a high oxidation potential ($E_0 = 2.8 \text{ eV}$), as shown in Table I.3 [83]. which are able to react with practically all classes of organic compounds, because they are reactive electrophilic (electron preferring) that react rapidly and no selectively with nearly all electron-rich organic compounds.

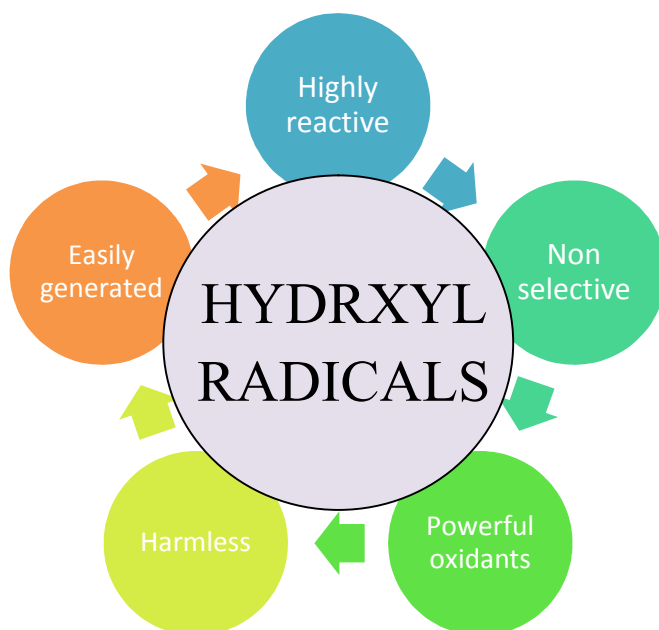


Figure I. 3: Some characteristics of hydroxyl radicals.

Most environmental contaminants react 1 million to 1 billion times faster with HO^\bullet than O_3 , a conventional oxidant [84] resulting in complete mineralization of these compounds, that is, the formation of carbon dioxide, water and inorganic salts, or their conversion into less aggressive products [85-87].

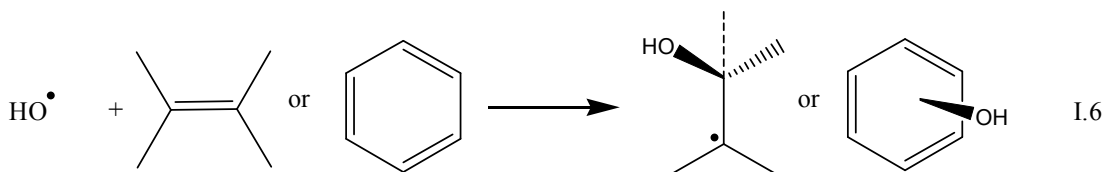
Table I.3: Oxidation potential of most commonly used oxidizers in water [88].

Oxidant	Oxidation potential (eV)
Fluorine (F_2)	3,03
Hydroxyl radical (OH^\bullet)	2,80
Ozone (O_3)	2,07
Hydrogen peroxide (H_2O_2)	1,77
Potassium permanganate (KMnO_4)	1,67
Chlorine dioxide (ClO_2)	1,50
Chlorine (Cl_2)	1,36
Bromine (Br_2)	1,09

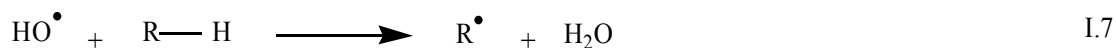
I.1.2 Mechanism

The possible oxidation reaction pathways involving the attack of hydroxyl radicals onto organic compounds are:

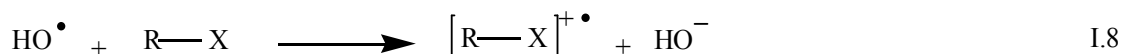
- Electrophilic addition of a hydroxyl radical to organic compounds (unsaturated or aromatic) that contain a π bond leading to the formation of organic radicals (Eq I.6)



- Hydrogen abstraction by reacting with a saturated aliphatic compound (Eq I.7).



And electron transfer with reduction of the hydroxyl radical into a hydroxyl anion by an organic substrate (Eq I.8) [89,90].



The hydroxyl radical attack on organic substrates may be influenced by the presence of a number of chemical species in water (or originating in the mineralization process), such as carbonate and bicarbonate ions [85]. These ions can react with the hydroxyl radicals (Eq I.9 and I.10), hence competing with the organic substrates through the hydroxyl radicals.



I.2 CLASSIFICATION OF AOPs

Hydroxyl radicals can be generated from several AOP, enabling the application of a better process for each specific treatment condition. According to Huang *et al.* [91], the AOP can be classified as homogeneous and heterogeneous. Domènech *et al.*

[92] presented this classification in terms of whether light is used in the process. Table I.4 shows a classification of AOPs according to these authors.

Table I.4: Type and classification of AOPs.

Non-photochemical	photochemical
Homogeneous	
Ozonation in alkaline media (O_3/OH^-)	Photolysis of water in vacuum ultraviolet (VUV)
Ozonation with hydrogen peroxide (O_3/H_2O_2)	H_2O_2/UV
Fenton (Fe^{2+} or Fe^{3+}/H_2O_2)	O_3/UV
Electro oxidation	$H_2O_2 /O_3/UV$
Wet air oxidation (WAO)	Photo-Fenton (Fe^{2+} or $Fe^{3+}/ H_2O_2/UV$)
Supercritical water oxidation (SCWO)	
Heterogeneous	
Catalytic wet air oxidation (CWAO), iron Oxide/ H_2O_2 ...	Heterogeneous photo catalysis: TiO_2/UV , ZnO/UV , SnO_2/UV , $TiO_2/H_2O_2/UV$...

AOPs could be classified also according to the method of which OH^\bullet radicals are generated (chemical, electrochemical, sonochemical, or photochemical). The main used AOPs are shown in Fig I.4

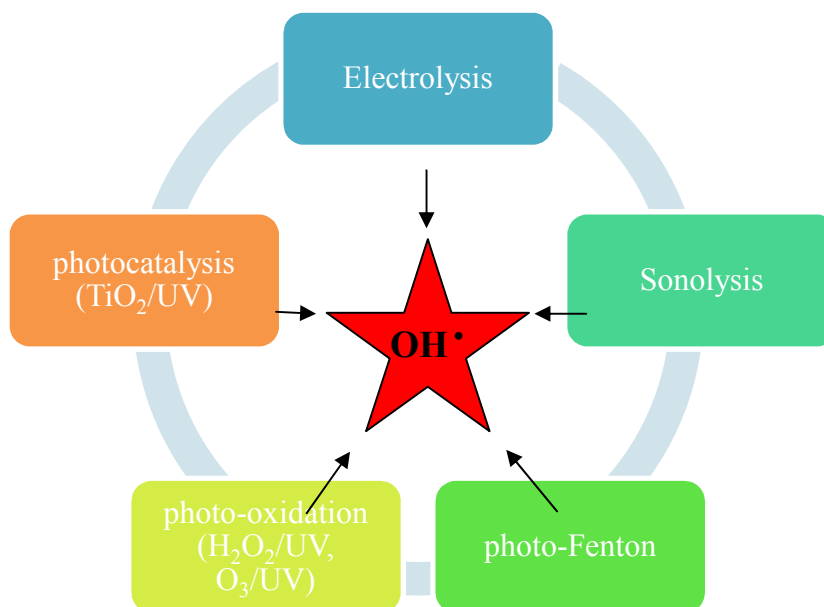


Figure I. 4: Main advanced oxidation process.

The AOPs are expensive processes owing to the high cost of reagents such as H_2O_2 and O_3 and electric energy when UV radiation is applied. For this reason they are considered in alternative treatment of wastewater that cannot be biologically treated.

Another significant aspect is the load of pollutants present in the wastewater, regularly expressed in terms of chemical oxygen demand (COD). The use of these processes is indicated only for wastewaters with COD usually below 10 g.L^{-1} , given that a higher COD index would require very high consumption of reagents, precluding the treatment [85].

For wastewaters with high organic load, can be more conveniently treated by means of wet oxidation or incineration (Fig I.5) [93], pretreatment operations, like dilution, coagulation and flocculation, are required in order to reduce the initial load [94]. In contrast, AOP can be applied in the treatment of contaminated waters with very low organic loads (in ppb) and which contain dissolved organic compounds which are difficult to remove.

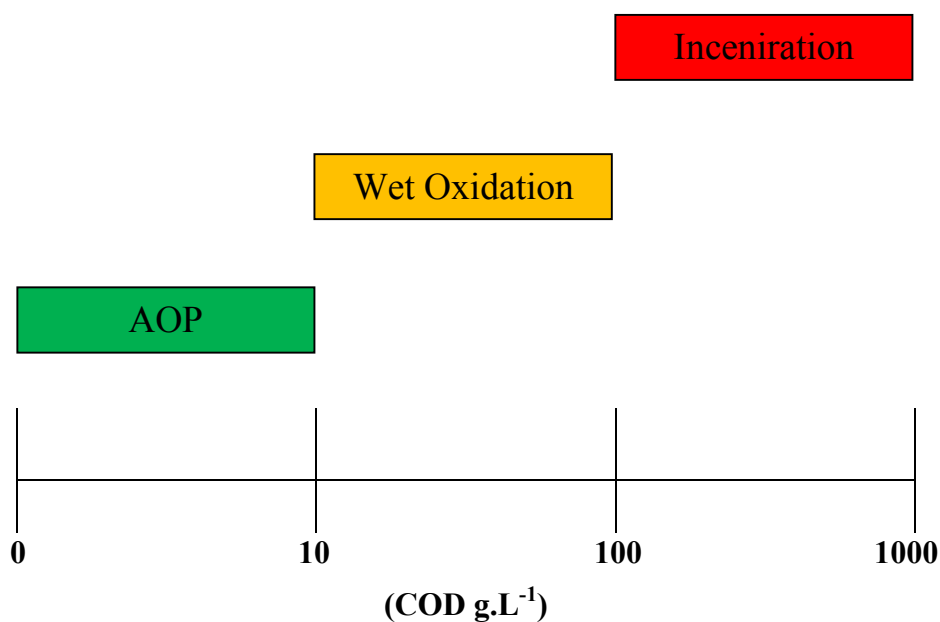


Figure I. 5: Suitability of water treatment technologies according to COD content [85].

One way of reducing the costs of AOPs is to use them as preliminary treatment operations to reduce toxicity, followed by biological treatment. This option has proven to be quite interesting from an economic point of view and has been studied by several authors [95-100].

In the next paragraphs we will focus more our study on describing four fundamental AOPs mainly used in this thesis namely: direct photolysis, UV/H₂O₂, Fenton and photo-Fenton processes.

I.2.1 UV PHOTOLYSIS and UV/H₂O₂ PROCESSES

UV-radiation is successfully used for disinfection, both drinking water and wastewater [101]. It has been shown that this type of oxidation can be useful for elimination of some organic compounds [102,103].

Low pressure UV lamps used for disinfection are monochromatic and emit light at a wavelength of 254 nm, which causes DNA damage of microorganisms present in water. Photodegradation of a compound is only possible when the compound is able to absorb light at the wavelength to which it is exposed [104].

Since not all compounds absorb light at 254 nm efficiently, the alternative would be to use medium or high pressure polychromatic lamps, which emit a radiation of a broad wavelength range, but use more energy.

In photochemical reactions, hydroxyl radicals may be generated by water photolysis [105]. (Eq I.11):



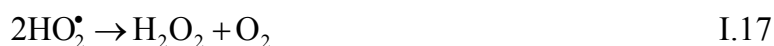
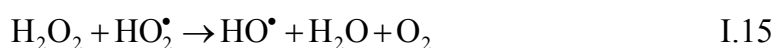
Photolysis involves the interaction of light with molecules to bring about their dissociation into fragments. This reaction is a poor source of radicals, and in the reaction medium large quantity of reaction intermediates that absorb part of the radiation are generated, which causes the photo-oxidation

In some cases the efficiency of the process can be enhanced by the addition of hydrogen peroxide (H₂O₂). In the UV/H₂O₂-process, UV-radiation causes photolytic decomposition of H₂O₂ leading to the formation of hydroxyl radicals (OH)[•] (Eq I.12).

The most commonly accepted mechanism for the photolysis of H₂O₂ is the cleavage of the molecule into hydroxyl radicals with a quantum yield of two OH[•] radicals formed per quantum of radiation absorbed (Eq I.12). This reaction is observed only at $\lambda < 300$ nm for concentration of H₂O₂ of 10⁻¹ mol.L⁻¹. On the other hand, H₂O₂ is known to dismute (Eq I.13).



Hydrogen peroxide can also react with hydroxyl radicals and the intermediary products formed thereby, according to the reaction mechanism described in a simplified way by Eq I.14 to I.18 [106].



The attack on organic compounds occurs due to the hydroxyl radicals (HO^\bullet) and hydroperoxyl (HO_2^\bullet) radicals formed. However, the hydroperoxyl radicals have a lower reduction potential (1.7 eV) than that of hydroxyl radicals (2.8 eV); therefore, their generation is not interesting to the process. Several studies have shown that the rise in the initial concentration of H_2O_2 increases the degradation rate of contaminants up to a maximum value, after which they begin to decline when they reach very high H_2O_2 levels [107-111]. López et al. [107], attribute this decrease in the $\text{H}_2\text{O}_2/\text{UV}$ process yield to hydroxyl radicals reacting with excess H_2O_2 (Eq I.14), instead of reacting with the organic substrates, leading to the formation of the hydroperoxyl radical HO_2^\bullet .

The photolysis of H_2O_2 is normally obtained with low or medium pressure mercury vapor lamps, both with high intensity, in order to reduce the amount of H_2O_2 needed. Nearly 50% of the energy consumed is lost in the form of heat or in emissions of wavelengths shorter than 185 nm, which are absorbed by the quartz jacket [112]. The germicide lamp is a widely used cheaper alternative; however, the efficiency is lower because it emits in the 210 to 240 nm range and H_2O_2 absorption reaches a maximum of 220 nm.

The UV/ H_2O_2 -process has been already investigated in numerous studies [113-115]. Three representative compounds of Benzothiazoles family, namely benzothiazole (BT), 2-mercaptobenzothiazole (MBT) and 2-hydroxybenzothiazole (OHBT) were found to

undergo efficient degradation under UV/H₂O₂, as a consequence of their high reactivity with the hydroxyl radical [14]. However, the great majority of these studies have been performed using contaminant concentrations that are much higher than the concentration ranges found in real waters.

The operational pH must be low (pH < 4) to prevent the effect of sequestering radical species, specifically ionic species such as carbonate and bicarbonate ions, leading to a better degradation rate.

I.2.1.1 Advantages

The advantages of using the H₂O₂/UV process can be attributed to the fact that:

- The reagent (H₂O₂) is totally soluble in water.
- There is no mass transfer limitation.
- It is an effective source of HO•.
- And there is no need for a separation process after treatment [112,116].

I.2.1.2 Disadvantages

- This technique requires a relatively high dose of H₂O₂ and/or a much longer UV-exposure time.
- The presence of residual hydrogen peroxide in the treated effluent will promote biological re-growth in the distribution system.
- The method is expensive due to the cost of necessary devices and the energy requirements.

I.2.2 HOMOGENEOUS FENTON AND PHOTO-FENTON PROCESS

Fenton and photo-Fenton processes have already been widely investigated and proved to be efficient somehow. Among all AOP processes, Fenton and photo-Fenton processes are the most promising and attracting methods, since this kind of process is proved to be efficient, easy to operate and low-cost.

I.2.2.1 Fenton process: $\text{Fe}^{2+}(\text{Fe}^{3+})/\text{H}_2\text{O}_2$

The year 1894 marked a new era in chemistry, with the postulation of the so-called Fenton reaction, named after H.J.H. Fenton himself. Although accidentally, it was found that iron ions, when combined with oxidizing agents, resulted in a solution with higher oxidative capacities than its separate components. The first “application” was the mix of hydrogen peroxide, tartaric acid, a base and iron (II) salt [117]. The identification of this finding marked the “Fenton reaction” or “Fenton reagent” and the first full publication which he authored indicated the principles of what we refer today as Fenton chemistry [118]:

1. The use of an oxidant,
2. A metal in its reduced form and,
3. The involvement of higher oxidation state of the used metal.

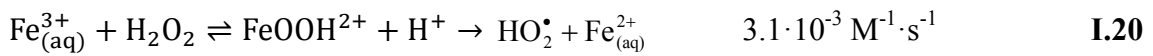
Although the initial formulation involved the application of iron (II) and H_2O_2 or hypochlorous acid, nowadays, we know that many metals can be used to facilitate the reaction, involving Cu, Cr, V, Ni, persulfate and/or organic peroxides can participate, and the H_2O_2 can be replaced by chlorine water or CaO [117,119–121].

However, Huang *et al.* [122], cited by Neyens *et al.* [123], mentioned that the application of Fenton’s reagent in oxidation processes to destroy toxic organic compounds was only attempted in the 1960s. There is considerable controversy about the reaction mechanism involving Fenton’s reaction. The classic Fenton reaction interpreted by Haber and Weiss [124], as cited by Bossmann *et al* [89], consists of an aqueous combination of hydrogen peroxide (H_2O_2) and ferrous ions (Fe^{2+}), in acid medium, leading to the decomposition of H_2O_2 into a hydroxyl ion and a hydroxyl radical, and the oxidation of Fe^{2+} to Fe^{3+} , as represented by Equation I.19.



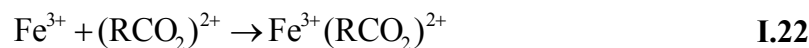
The Fe^{2+} and Fe^{3+} species, shown in a simplified form, correspond to the $[\text{Fe}(\text{OH})(\text{H}_2\text{O})_5]^+$ aqueous complexes, which, together with H_2O_2 , form the $[\text{Fe}(\text{OH})(\text{H}_2\text{O}_2)(\text{H}_2\text{O})_4]^+$ and $[\text{Fe}(\text{OH})(\text{H}_2\text{O})_5]^{2+}$ complexes, respectively, as reported by Bossmann *et al* [89].

As shown by Walling *et al* [125], the Fe^{3+} formed in Eq I.19 can react with the H_2O_2 present in the medium and be reduced to Fe^{2+} again, forming the hydroperoxyl radical, according to Eq I.20. This reaction, referred by Neyens *et al* [123] as Fenton-like, occurs more slowly than reaction I.19, as reported by Pignatello [87]. The Fe^{3+} ions also react with the HO_2^\bullet and are reduced to Fe^{+2} , as shown by Eq I.21.



The initial degradation rate using Fe^{+3} is much lower than that using Fe^{+2} , as pointed out also by Safarzadeh-Amiri *et al* [126]. And shown by Wang *et al* [127].

In most cases, the Fenton's reaction alone is not capable of degrading organic compounds and mineralizing them efficiently. The Fenton's reaction is effective up to the moment at which all the Fe^{2+} present in the medium is oxidized to Fe^{3+} , thus interrupting the generation of hydroxyl radicals and, consequently, the degradation of organic compounds. According to Balanosky *et al* [128], cited by Maciel *et al* [129], one of the factors that contribute to the interruption of the Fenton's reaction is that Fe^{3+} ions can form stable organic compounds (under normal conditions) with the degradation products (mainly the organic acids) present in the medium, as shown by Eq I.22, impairing the regeneration of Fe^{2+} .



I.2.2.2 Photo-Fenton process ($\text{Fe}^{2+}(\text{Fe}^{3+})/\text{H}_2\text{O}_2/\text{UV}$)

The Fenton's reaction was recognized as a powerful tool to degrade organic compounds when ultraviolet radiation is added to the system. This type of photoassisted reaction is referred to as "photo-Fenton-reaction" [130]. This was achieved when Pignatello [87] applied it in the treatment of wastewaters containing toxic organic pollutants in the early 1990s. It has served as a starting point for a number of studies related to the application of the photo-Fenton process.

According to Pignatello [87], UV irradiation strongly accelerates the degradation rate of organic pollutants from Fenton's reagent, which has the advantage of being sensitive to UV-Vis radiation for wavelengths above 300 nm. Under these conditions, the photolysis of Fe^{3+} complexes enables regeneration of Fe^{2+} and the occurrence of Fenton's reaction, if H_2O_2 is available. Faust and Hoigné [131] reported that the dominant species (between pH 2.5-5) in the photo-Fenton process is the ferric complex $\text{Fe}(\text{OH})^{2+}$, a simplified form of representing the aqueous complex $\text{Fe}(\text{OH})(\text{H}_2\text{O})_5^{2+}$, and the photolysis of this complex (wavelengths < 410 nm) is the largest source of hydroxyl radicals (Eq I.23). Other photoreactive species are also present in the reaction medium, such as $\text{Fe}_2(\text{OH})_2^{4+}$ and $\text{Fe}(\text{OH})^{2+}$, possibly leading to the formation of hydroxyl radicals [131].



Safarzadeh-Amiri *et al* [126] reported that Fe^{2+} regeneration can also occur with the photolysis of the complexes formed (Eq I.22) from Fe^{3+} and the organic products generated in the degradation process, as shown by Eq I.24.



Thus, the ferrous ions regenerated by Eq I.23 and I.24 can react again with the H_2O_2 in solution (Eq I.19) to generate more hydroxyl radicals, creating a photocatalytic cycle in the $\text{Fe}^{2+}/\text{Fe}^{3+}$ system.

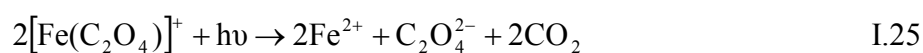
The use of radiation reduces significantly the concentration of ferrous ions required, compared with the dark Fenton reaction (in the absence of light). The concentration of ferrous ions must not be very high, as in the Fenton's reaction, in order to achieve good efficiency, since the addition of ferrous ions increases solution opacity, hindering radiation penetration and compromising Fe^{2+} regeneration when oxidized to Fe^{3+} . As a consequence, the degradation rate is diminished, as reported by Bhatkhande *et al* [132].

The disadvantages of the photo-Fenton process are associated with the low pH values required (normally below 4) and the need to remove iron after the reaction. However, as reported by Mota [133], iron removal may not be needed if is used at concentrations below the discard limit established by law. It is important to have prior

knowledge of the physical-chemical characteristics of the wastewater to be treated by this process because some substances or inorganic ions, such as Cl^- , SO_4^{2-} , H_2PO_4^- / HPO_4^{2-} present in the wastewater or added as reagents (FeSO_4 , FeCl_3 , HCl , H_2SO_4) may interfere in the reaction mechanism of the Fenton and photo-Fenton system, inhibiting the degradation process, as reported by De Laat *et al* [134] and Nadtochenko and Kiwi [135]. De Laat *et al* [134] suggest that the possible causes of these effects are the complexation reactions of the inorganic ion with Fe^{2+} or Fe^{3+} ions and the reactions with hydroxyl radicals that lead to the formation of less reactive inorganic radicals ($\text{Cl}^{\bullet-}$, $\text{Cl}_2^{\bullet-}$ and $\text{SO}_4^{\bullet-}$).

Machulek Jr *et al* [136] found that the formation of $\text{Cl}_2^{\bullet-}$ radical anions, due to the presence of chloride ions in the reaction medium, can be avoided by controlling pH at 3 during the reaction period, given that the degradation process of an organic substrate by the photo-Fenton process leads to the formation of acids and thus pH reduction. It occurs due to pH decrease lower than 2.5 in the presence of chlorides ions, leading to more intense formation of ferric chloride complexes (FeCl_2^+ and FeCl^{2+}). These complexes also undergo photolysis, thereby decreasing the amount of $\text{Fe}(\text{OH})^{+2}$, which is the main source of hydroxyl radicals in the photo-Fenton process, in addition to the formation of the $\text{Cl}_2^{\bullet-}$ radical anion, which can react with Fe^{2+} (oxidizing to Fe^{3+} without the formation of hydroxyl radicals) and the organic substrate.

One of the main advantages of using the photo-Fenton process compared with the other oxidation processes consists on using solar radiation in its reaction process. In this case, according to Machulek Jr *et al* [136], in the presence of oxalate ions ($\text{C}_2\text{O}_4^{2-}$), the Fe^{3+} present in the aqueous medium may form the $[\text{Fe}(\text{C}_2\text{O}_4)]^+$ complex (Eq I.25), which absorbs light at wavelengths below 570 nm (the larger part of the visible UV solar spectrum).



The possibility of using solar radiation represents an enormous saving from the energetic point of view, given that there will be no need to use lamps. The development of pilot wastewater treatment plants that use solar reactors applied to the advanced oxidation processes has been one of the main focus of research in the area [137-143].

I.3 PARAMETERS AFFECTING FENTON AND PHOTO-FENTON PROCESSES

Several parameters of the water as well as the conditions in which the process is carried out can influence the kinetics of Fenton and photo-Fenton process: pH, iron concentration, iron species, H₂O₂ concentration, initial contaminant concentration, irradiation sources, temperature and the presence of inorganic anions.

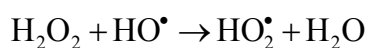
The influence of initial pH, H₂O₂ and iron concentration are briefly discussed in this section.

I.3.1 The effect of pH

The ideal pH in Fenton and photo-Fenton's reaction found in a number of studies is 3 [144-146,87] considered therefore to be the operating pH, because the pH value influences the generation of hydroxyl radicals (OH[•]) and thus the oxidation efficiency. At very low pH (< 2.5), the formation of complexes, such as [Fe(H₂O)₆]²⁺, occurs. These species react more slowly with H₂O₂ than [Fe(OH)(H₂O)₅]⁺, producing a lower amount of hydroxyl radicals, thus decreasing the system efficiency [145]. At pH value above 4, iron reacts with the hydroxide ions (HO⁻), precipitating the iron hydroxide (Fe(OH)₂ or Fe(OH)₃), which does not react with H₂O₂, consequently precluding strongly the degradation process. Therefore, an adjustment in pH is required in the wastewater to be treated before adding the Fenton reagents.

I.3.2 Effect of H₂O₂ concentration

The concentration of hydrogen peroxide has an important influence in the degradation of organic compounds. Degradation rate tends to increase with increasing hydrogen peroxide concentration which is explained by the effect of additionally produced OH[•] radicals [147]. However, above certain limit, the reaction rate levels off and sometimes is negatively affected, by the progressive increase of hydrogen peroxide concentration. This may be attributed to the auto-decomposition of H₂O₂ to oxygen and water, and the recombination of OH[•] radicals. Moreover higher concentration of hydrogen peroxide act as free-radical scavenger itself (Eq I.26), thereby decreasing the concentration of hydroxyl radicals and reducing compound elimination efficiency

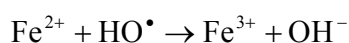


I.26

Thus, H_2O_2 should be added to treat wastewater an optimal concentration to achieve the best degradation, this optimum H_2O_2 concentration depends on the iron concentration and on the nature and the load of the pollutant.

I.3.3 Effect of the initial iron concentration

As in the case of H_2O_2 , degradation rate increase with the concentration of iron, but after an optimum the efficiency decrease even when the concentration is doubled. This is due to the fact that, at an Fe (II) concentration higher than the optimum, the rate of hydroxyl radicals originated from the decomposition of H_2O_2 is so high that much of hydroxyl radicals are consumed by the side reactions before they are utilized for the removal of the pollutant. Moreover, it would result in brown turbidity that hinder the absorption of the UV light required for photolysis and also would cause the recombination of OH^\bullet radicals. In this case, Fe^{2+} reacts with OH^\bullet radicals as scavengers (Eq I.27).



I.27

I.3.4 Effect of $[\text{Fe}^{2+}]/[\text{H}_2\text{O}_2]$ ratio

It is important to establish previously the optimal relationship between ferrous and hydrogen peroxide ions. When higher concentrations of ferrous ions than hydrogen peroxide ions are used, the hydroxyl radicals generated by Eq I.19 may react with excess ferrous ions, according to Eq I.27, decreasing the attack of hydroxyl radicals on organic substrates [123].

Guedes *et al* [148] observed that, although a $[\text{Fe}^{2+}]/[\text{H}_2\text{O}_2]$ ratio of 1:2 has a higher degradation rate, it is usually recommended to use the 1:5 ratio, which yields similar results and requires fewer reagents.

I.3.5 ADVANTAGES

- Fenton process requires very little energy compared to Photo-Fenton and other oxidation technologies that utilize O₃ or UV.
- Fenton & Photo-Fenton processes produce no vapor emissions and, therefore, require no off-gas treatment or air permits.
- The processes are carried out at room temperature and pressures.
- Since reactions take place in homogeneous phase, there are no mass transfer limitations.
- Iron is a highly abundant and non-toxic element. The photo-Fenton process can use photons within a broader wavelength range as compared to heterogeneous photocatalysis.

I.3.6 DISADVANTAGES

- An iron extraction system is needed to remove residual iron from the treated water, which may increase the costs for the system.
- A very low pH (<4) environment is necessary to keep the iron in solution. Therefore, pH adjustment before and after treatment will be required. The requisite acid and base injections will increase the operational & maintenance costs.
- The photo-Fenton process using artificial light involves an additional energy consumption to run the lamps.

I.4 HETEROGENEOUS FENTON AND PHOTO-FENTON PROCESS

Fenton's reagent is very attractive since its low cost, wide application range and mild operating conditions.

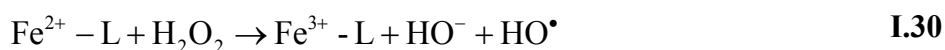
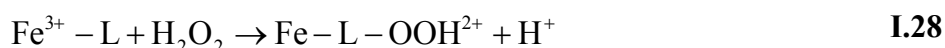
However, the application of homogeneous Fenton process is limited with significant disadvantages:

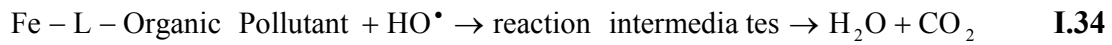
1. Homogeneous Fenton system needs up to 50–80 ppm of iron ions which is highly above the normal directives [149].
2. The tight range of pH (< 4) which requires strong conditioning before and after treatment.
3. The removal of the sludge containing iron ions complicates the overall process and makes the method uneconomical [150].

Thus, replacement of the homogeneous catalysts with heterogeneous catalysts becomes an imperative alternative.

Various heterogeneous Fenton-like catalysts have recently been developed and can be used. The ideal heterogeneous catalysts are supposed to be inexpensive, available for wide pH range, as well as have high catalytic activity and stability. At present, the catalyst supports include organic [151,152] and inorganic materials (such as zeolite, carbons and clays) [153,154]. can be useful from a practical point of view to avoid the above-mentioned limitations [155]. Among these supports, clays have been reported to be good candidates as catalyst supports because they are natural, abundant, cost-effective, environmentally benign as well as their unique properties and structures. [156].

Alireza Khataee *et al* [157] reported the mechanism of heterogeneous Fenton-like process in the presence of iron based compounds such as iron rich laterite soil (laterite) by the following equations:

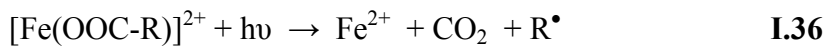




Where L stands for laterite. Moreover, heterogeneous Fenton-like process can be coupled with a light source [158,159]. In heterogeneous photo-Fenton-like process, which is utilized as a strong method for wastewater remediation [160,161], the effect of UV-vis irradiation can be explained with the photo-reduction of Fe^{+3} to Fe^{+2} to keep the catalytic cycle (Eqs. I.28-I.34) and produce extra radicals by the following equation:



Depending on the ligand type, hydroxyl radicals or other radicals (R) from specific organic ligands such as carboxylic ligand, (Eq. I.36), can be generated during the degradation process as intermediates which can return Fe^{2+} ions to the catalytic cycle (Eqs. I.36 and I.37) [162-164].



I.5 Developments of the Fenton Reaction

Following the fundamental research of Fenton reaction, remarkable developments have been made to advance its application in water treatment [165,166]. A variety of Fenton reactions are outlined in Table I.5.

Table I.5 shows that the efforts exerted to develop the Fenton reaction focused on pH extension, in situ supply of H_2O_2 via the cathodic reduction of oxygen, in situ supply of Fe^{2+} via the electrochemical anodic oxidation of elemental iron, avoidance of iron loss, and Fe(II) regeneration by illuminating the sludge iron sources [167]. Although all these modifications of the classic Fenton reaction cannot be coupled in one system, the heterogeneous photo-Fenton reaction unifies most of them and poses a promising Fenton based technology. Obviously, it overcomes the pH limitation, prevents the iron loss after use like that in the reaction using free iron ions as the iron sources, and

utilizes light to favor Fe(II) generation from Fe(III). The in situ supply of electrogenerated H₂O₂ can also be coupled into this system to form a photoelectro-Fenton system [168,169]. Iron-oxalate can also be utilized in a heterogeneous photo-Fenton system by fixing the iron ions on silica fabric [167]. Therefore, the heterogeneous photo-Fenton reaction covers almost all developments of the Fenton reaction and has certainly attracted much attention in recent years.

Table I.5: Varieties of Fenton reactions.

	Reagents	pH	Iron loss	light
Classic Fenton	H ₂ O ₂ , Fe ²⁺	2-4	Yes	No
Fenton-Like	H ₂ O ₂ , Fe ³⁺	2-4	Yes	No
Photo-Fenton	H ₂ O ₂ , iron complex, free iron ions	Acidic to neutral	Yes	Yes
Heterogeneous Fenton	H ₂ O ₂ , solid iron oxide	Wide range	No	No
Electro-Fenton	Electrogenerated H ₂ O ₂ , Free iron ions; H ₂ O ₂ , Electrogenerated Fe ²⁺	2-4	Yes	
Heterogeneous photo-Fenton	H ₂ O ₂ , solid iron oxide	Wide range	No	Yes
Heterogeneous photoelectro-Fenton	Electrogenerated H ₂ O ₂ , solid iron oxide	Wide range	No	Yes

II

EXPERIMENTAL

II. Experimental

II.1 Chemicals

All chemicals used in this study were of the highest quality commercially available and used without any further purification.

Table II.1: Chemicals products used in the study and their origins.

Product	Origin
<ul style="list-style-type: none">• 2-mercaptobenzothiazole (MBT) (99% P).• Tert-butanol (99.5% purity).• Hydrogen peroxide 33% (w/v).• Potassium hydroxide (KOH) (85%).• Perchloric Acid (HClO₄)(65%).• Iron(III) Chloride anhydrous(FeCl₃).• Iron(III) Chloride Hexahydrates (FeCl₃.6H₂O) (98 %).• Ammonium iron (II) sulphate Hexahydrate (NH₄)₂FeS₂O₈.• Ammonium Nitrates (NH₄NO₃)(99%).• Oxalic acid 2-hydrate (COOH)₂.2H₂O.• Citric acid monohydrate (C₆H₈O₇.H₂O).• Sulfuric Acid (H₂SO₄) (96%).• Nitric Acid (HNO₃) (69%).• Methanol (CH₃OH) (Grade HPLC).• EDTA (Na₂H₂C₁₀H₁₂N₂O₈.2H₂O).• Sodium bicarbonate (NaHCO₃).	<ul style="list-style-type: none">• Fluka.• Janssen Chimica.• Panreac.• Panreac Quimica.• Carlo Erba.• Fluka Chemika.• Aldrich/Merck.• Prolabo Chemicals• Sigma-Aldrich.• Fluka/Sigma Aldrich• Sigma-Aldrich• Sigma-Aldrich• Panreac Quimica.• Panreac Quimica.• Panreac Quimica.• Sigma Aldrich.

Natural clay was obtained from El-Hoggar region, city of Tamanghasset in the extreme south of Algeria, and used without any previous chemical treatment except for appropriate grinding and sieving (80 meshes of diameter sieve).

Milli-Q water was obtained from a Millipore device with a resistivity of 18.2 MΩ·cm at 298K used for HPLC analyses.

Solutions were prepared with distilled water. pH was adjusted by adding KOH or HClO₄ solution and controlled using a *Hanna* pH-meter. De-oxygenation of solutions was performed by bubbling Argon during all irradiation time, at room temperature.

II.2 Experimental procedure

II.2.1 Adsorption study

Adsorption experiments were carried out at room temperature. 0.025 g (25mg) of NCP was added into 50 mL MBT solution with an initial concentration of 5.10⁻⁵M (8,36 mg/L). The obtained suspensions were maintained under constant magnetic stirring during the necessary time to reach adsorption equilibrium.

The adsorption tests are performed at natural pH, room temperature and stirring at different time intervals. After equilibrium, the aqueous phase was separated by centrifugation by Nahita Centrifuge or filtered with Millipore membrane of 0.22µm. (**Fig II.1**). Absorbance measurements were performed using uviline 9400 UV/Visible spectrophotometer at wavelength corresponding to the maximum absorbance of the MBT solution ($\lambda = 320$ nm).

The adsorbed amount is calculated using the following formula:

$$Q_{\text{ads}} = \frac{(C_0 - C_{\text{eq}}) \cdot V}{m} \quad (\text{II.1})$$

Where:

Q_{ads}: adsorption capacity of the NCP (mg/g).

C₀: initial concentration of MBT at t = 0 (mg/L).

C_{eq}: concentration of MBT at the equilibrium (mg/L).

V: volume of the solution (L).

m: mass of the NCP (g).

II.2.2 Heterogeneous degradation and photodegradation study

In the degradation experiments, $0.5\text{g}\cdot\text{L}^{-1}$ of the natural clay powder (NCP) were added to a $5.0\cdot 10^{-5}$ M MBT solution and stirred magnetically for 15 min to establish the adsorption–desorption equilibrium, while the lamp was warmed up before inserting it in the reaction medium and starting the photodegradation experiments. The first sample was taken at the end of the dark adsorption period, just before the lamp was inserted, in order to determine the starting concentration of the compound in solution, which was taken as C_0 for each experiment. Then, the suspensions were irradiated at constant stirring speed.

During the irradiation, discrete samples of the suspension were collected at regular times for analysis. To remove the suspended clay, the samples were centrifuged at 16000 rpm for 5 min using a Nahita centrifuge. Sometimes we used also Millipore filter 0,22 μm as shown in figure II.1.

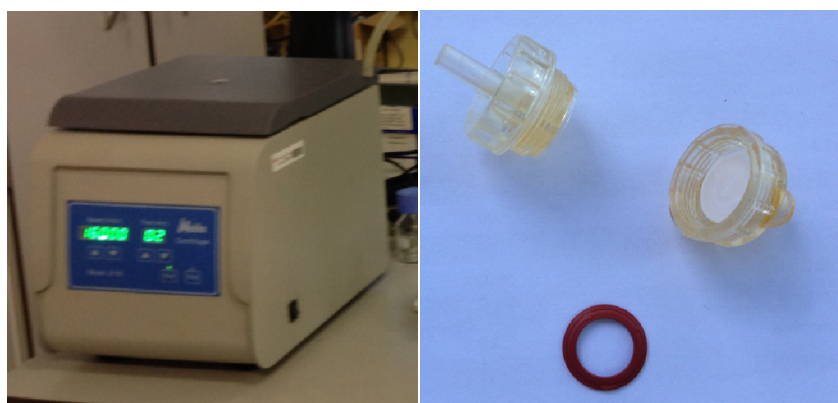


Figure II.1: Nahita Centrifuge and Filter holder used to separate NCP from MBT solutions.

II.3 Irradiation systems

II.3.1 irradiation at 254 nm

The irradiation experiments at 254 nm were carried out with 750 mL UV photoreactor system, equipped with a Heraeus TNN 15/32 low-pressure Hg immersion-vapor lamp, TQ 150, which $\lambda_{exc} = 254$ nm, cooled by water flow, The photon flux at 254 nm was 3.33×10^{-8} Einstein s^{-1} . The temperature of the system was kept to within 298.0 ± 0.1 K by circulation water.

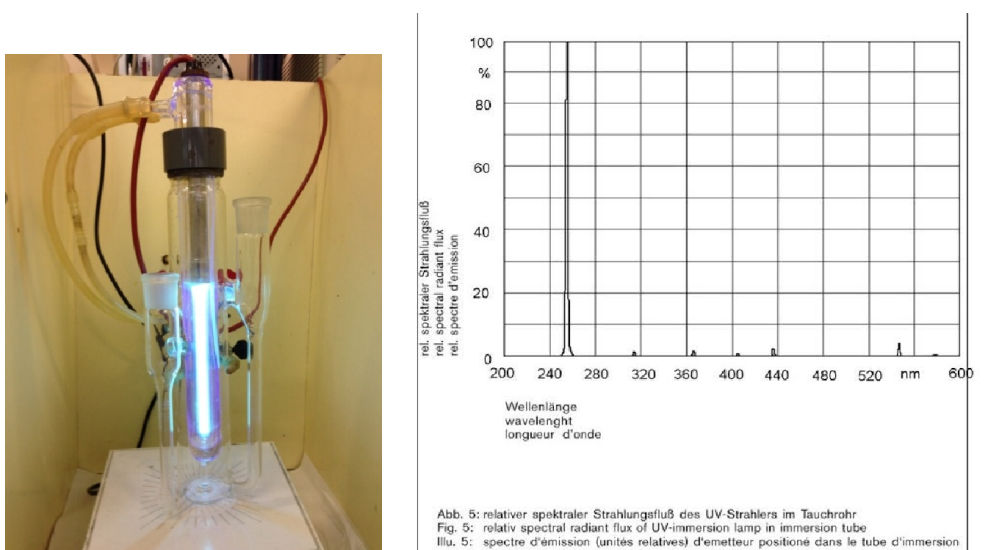


Figure II.2: quartz photoreactor used in the lab equipped with UV lamp 254 nm and its emission spectrum.

II.3.2 Irradiation at 366 nm

The irradiation experiments at NUVA visible light were carried out in a Pyrex glass photoreactor (200 mL), as shown in Figure II.3, open to the air. The light source was a Heraeus medium-pressure Hg lamp TQ 150, for which the more intense emission lines occur at $\lambda_{exc} = 254, 313, 366, 405, 436, 546$ and 578 nm (Fig II.4). The lamp is cooled by water circulation to 298.0 ± 0.1 K. The irradiation spectrum (Fig II.5) was cut off below 366 nm using a Duran 50 glass jacket.

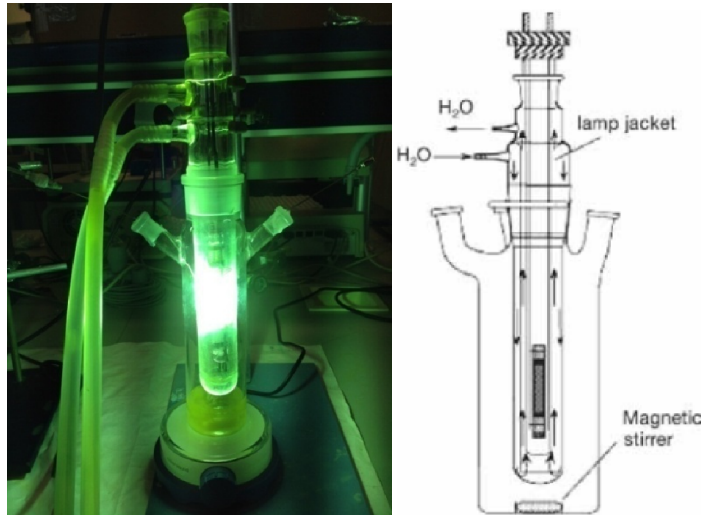


Figure II.3: Pyrex glass photoreactor used in the lab equipped with Vis lamp at 366 nm.

Abb. 5: relativ spektraler Strahlungsfluß des UV-Strahlers im Tauchrohr
 Fig. 5: relativ spectral radiant flux of UV-immersion lamp in immersion tube
 Illu. 5: spectre d'émission (unités relatives) d'émetteur positionné dans le tube d'immersion

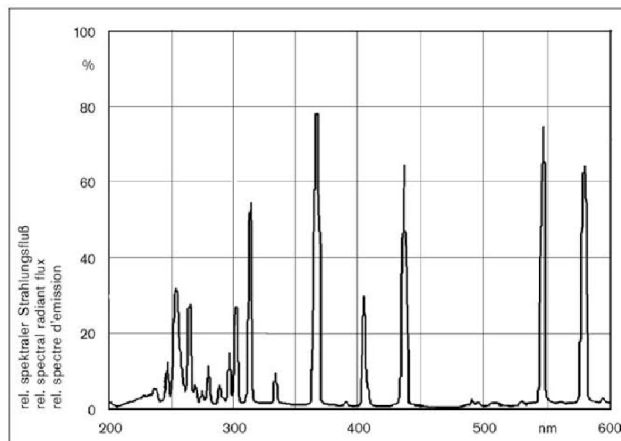


Figure II.4: Emission spectrum of the Vis lamp at 366nm.

Abb. 6: Transmission von Quarzglas und Duran 50
Fig. 6: transmission from quartz glass and Duran 50
Illu. 6: transmission de verre en quartz et Duran 50

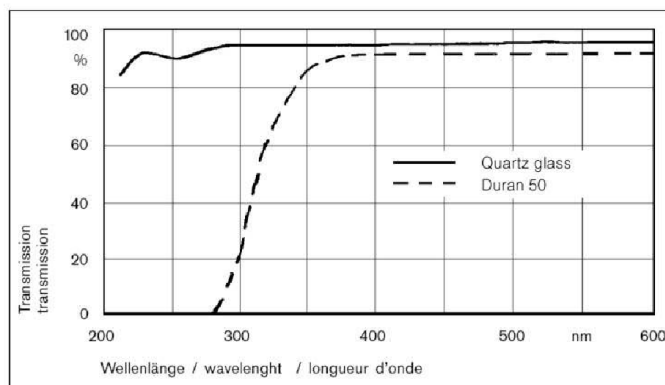


Figure II.5: Transmission spectrum of the Quartz and Glass tubes.

As we can see, the Glass tube of Duran 50 cuts off all the UV radiations from the Vis lamp.

II.4 Analytical techniques

After the centrifugation of the sample, the clean transparent solutions were analysed. The photodegradation process was monitored by the change in concentration of MBT, following the UV/Vis change in the characteristic bands of MBT as a function of irradiation time.

II.4.1 UV-Visible absorption analysis

Absorption spectra were registered using a double beam UV-Vis spectrophotometer (Libra Biochrom) and UV-1800 SHEMADZU spectrophotometer, covering 190-1100 nm. Measurements were made at $\lambda_{\max}=320$ nm of MBT solution at natural pH, using quartz cells of 1 cm optical path length.



Figure II.6: UV-Vis Spectrophotometers used in this study.

II.4.2 HPLC analysis

MBT was also monitored using HPLC instrument with P4000 pump, AS3000 Auto Sampler and spectra system UV6000LP detector. The mobile phase was MeOH/Milli-Q water 60:40 ratio, the detection wavelengths were at $\lambda = 280$ and 320 nm. Separation was carried out using KROMAPHASE C18 column (150 x 4.6 mm x 5 μ m) at a flow rate of 1 mL/min.



Figure II.7: HPLC instrument used in this study.

II.4.3 HPLC-MS analysis

The photoproducts identification were carried out by HPLC-MS, using a Thermo Scientific, LTQ Orbitrap Discovery apparatus, equipped with an electrospray interface operating in positive ion mode (ESI+). A Phenomenex Kinetex XB-C18 (100 mm \times 2.10 mm, 2.6 μ m) column was used. The analyses were carried out using full-scan data dependent MS scanning from m/z 50 to 400.

The structures of photoproducts were tentatively proposed by interpretation of MS spectra using Xcalibur software.

II.5 Kinetic treatment

Kinetics were monitored at the maximum wavelength of MBT (see below), at 298 K and at the natural pH of the solution (pH *ca.* 6.3), produced by the mixture of dissolved reagents and suspension of NCP particles).

Direct photolysis and adsorption kinetics were routinely treated according to either a first order or a pseudo-first order kinetic model, eq. (II.2):

$$r = k_{obs} \cdot C \quad \text{(II.2)}$$

UV-Vis photocatalytic degradation processes are usually adequately described by a Langmuir-Hinshelwood kinetic model [198] as in Eq. (II.3):

$$r = k_{LH} \cdot \Theta = k_{LH} \cdot \frac{K_{LH} \cdot C}{1 + K_{LH} \cdot C} \quad (\text{II.3})$$

Where:

C is the MBT concentration once the adsorption-desorption equilibrium has been established,

k_{LH} ($\text{mol} \cdot \text{s}^{-1} \cdot \text{cm}^{-2}$) is an apparent kinetic rate constant per unit of surface area,

and Θ (cm^2) accounts for the coverage of catalyst surface by MBT.

K_{LH} is the Langmuir-Hinshelwood adsorption constant. Assuming $K_{LH} \cdot C \lll 1$, eq. (II.3) reduces to eq. (II.2), with $k_{obs} \approx k_{LH} \cdot K_{LH}$, k_{obs} being the limiting apparent pseudo-first order kinetic rate constant.

II.6 Characterisation analyses

II.6.1 SEM-EDS analysis

Natural clay mineral of yellowish-brown color (Fig II.8), was crushed into small particles (powder) of less than 80 mesh, and then micrographed by scanning electron microscopy (SEM) to verify its morphology, Some random areas were analysed by energy dispersive X-ray spectroscopy (EDS) for quantitative chemical composition analysis of the surface.



Figure II.8: NCP used in this study.

II.6.2 BET analysis

The BET specific surface area and pore distribution of the sample were determined by N₂ adsorption-desorption isotherms using a Micromeritics TriStar II Plus instrument. The measured temperature was that of liquid nitrogen (77.4 K). The control, acquisition and data processing software was Microactive for Tristar II Plus, v. 2.03 (Micromeritics).

II.6.3 UV-Vis DRS analysis

The optical properties of the natural clay mineral were registered by UV-Visible diffuse reflectance spectroscopy using Evolution 260 Bio Thermo Scientific spectrophotometer (Fig II.9). The sample was dispersed in distilled water at neutral pH to give a colloidal suspension, and the spectra were obtained using a 1cm path length quartz cell.



Figure II.9: UV-Visible diffuse reflectance spectrophotometer used in the study.

II.6.4 x-ray fluorescence spectroscopy (XRF)

The chemical composition of the clay was determined by X-ray fluorescence (XRF) analysis. Data were obtained using a 4 kW wavelength dispersion X-ray fluorescence spectrometer, model S4 Pioneer (Bruker-AXS). The evaluation of results was done using SpectraPlus software v. 1.70 (Socabim).

II.6.5 x-ray diffraction spectroscopy (XRD)

X-ray diffraction spectra measurements were performed using a Siemens-Bruker D5000 diffractometer, with Bragg-Brentano geometry and Theta/2-Theta configuration,

equipped with graphite monochromator, and scintillation counter detector. The data collection was carried out from 5–80° with a step size of 0.05° and an acquisition time of 2.5 s. The data processing software was: DiffracPlus v. 8.0.0.2 (Socabim).

III

RESULTS AND DISCUSSION

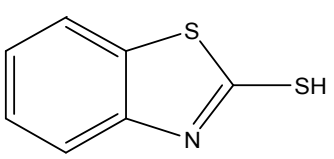
III. RESULTS AND DISCUSSION

III.1. Contaminant properties

III.1.1. Physico-chemical properties

The main physico-chemical properties of MBT are gathered in the following table.

Table III.1: Physico-chemical properties of MBT.

Structure of MBT	
Molecular formula	C ₇ H ₅ NS ₂
Molecular weight	167.24g/mol
Physical state	Powder
Color	yellow
Odor	malodorous
pH	7 (0.12g /L (25°C))
pKa	6,93 (dissociation constant at 20°C)
Melting point	177-179°C
Soluble in	Dilute caustic soda, alcohol, alkalis acetone, benzene, chloroform.
Solubility in water at 25C°	51 mg/L (pH 5), 118 mg/L (pH 7), 900 mg/L (pH 9)
Stability	Stable under all normal conditions.
Density	1.42g /cm ³

III.1.2 Spectroscopic properties

The UV-Vis spectrum of the molecular form of 5.0·10⁻⁵M aqueous MBT (Fig III.1) showed three characteristic maxima: 320 nm ($\epsilon=23287 \text{ L}\cdot\text{mol}^{-1}\cdot\text{cm}^{-1}$), 230 nm ($\epsilon = 13657 \text{ L}\cdot\text{mol}^{-1}\cdot\text{cm}^{-1}$) and 203 nm ($\epsilon= 18677 \text{ L}\cdot\text{mol}^{-1}\cdot\text{cm}^{-1}$). Moreover, the spectrum

shows a shoulder at 252 nm ($\epsilon = 5364 \text{ L}\cdot\text{mol}^{-1}\cdot\text{cm}^{-1}$). These spectral features, $n\rightarrow\pi^*$ and $\pi\rightarrow\pi^*$ electronic transitions, represent a significant overlap with the sunlight emission in the region above 300 nm. Thus, MBT is likely to undergo photo-oxidation under natural or simulated sunlight irradiation.

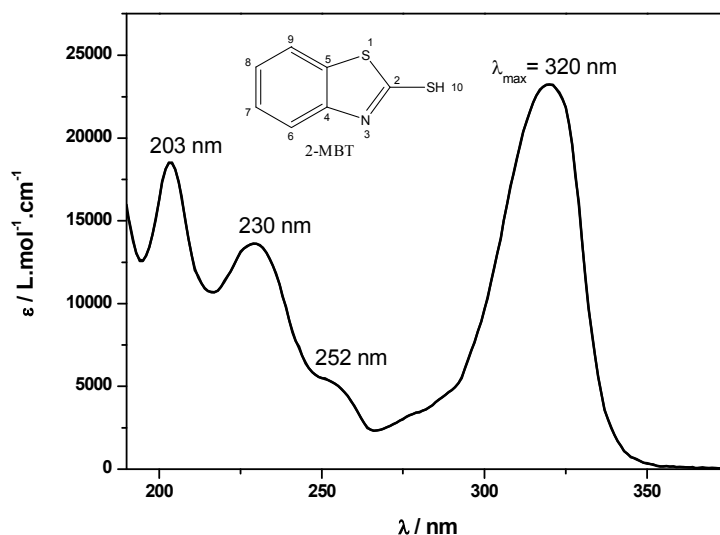


Figure III.1: UV-Vis spectrum of aqueous $5.0 \cdot 10^{-5} \text{ M}$ MBT, natural pH.

On the other hand, at basic pH values, a significant hypsochromic and hypochromic effects were observed (Fig III.2). For instance, $\lambda_{\text{max}}=320 \text{ nm}$ decreases to 308 nm (blue shift), while $\epsilon_{320}=11664 \text{ M}^{-1}\cdot\text{cm}^{-1}$ decreases to $\epsilon_{308}=8810 \text{ M}^{-1}\cdot\text{cm}^{-1}$.

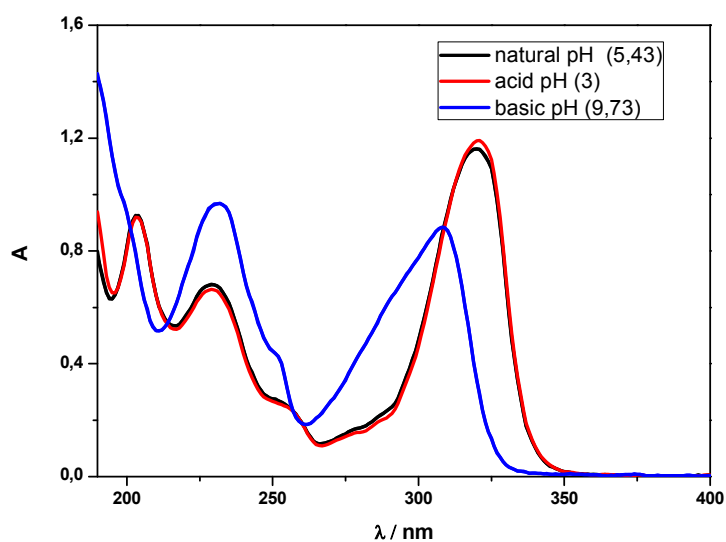


Figure III.2: Evolution of UV-Vis spectrum of MBT in acidic and basic medium.

Several authors have determined the substrate pKa [15,170]. The found value was 6.95 ± 0.05 . This value of pKa indicates clearly that both forms can play an important role in the photo-transformation of the substrate under environmental conditions.

The molecular form has a thiol-thione tautomerism. The thione form would be largely predominant [171].

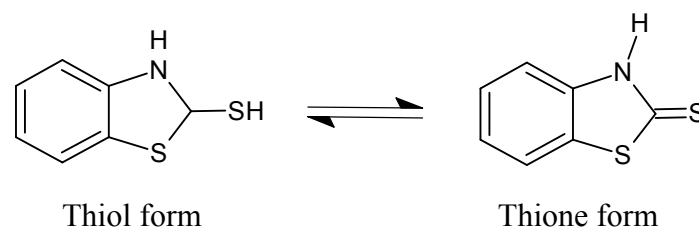


Figure III.3: Tautomerism thiol-thione of MBT.

The principal spectroscopic characteristics of molecular and anionic forms are presented in the following table.

Table III.2: Spectroscopic properties of MBT in aqueous solution ($5.10^{-5}M$).

Molecular form		Anionic form	
λ max (nm)	ϵ ($M^{-1}.cm^{-1}$)	λ max (nm)	ϵ ($M^{-1}.cm^{-1}$)
320	11664	308	8810
352	2823	352	4217
230	6745	232	9636
203	9273	/	/

III.2 CHARACTERISATION STUDY OF THE NATURAL CLAY

III.2.1 SEM-EDS analysis

The morphology of the clay sample as revealed by SEM shows irregular shapes, with agglomerates of *ca.* 1 μm , composed of fine long crystal nanometric needles, observed with typical size 200 nm length x 20 nm width, as shown in Figure III.4 and Figure III.5. The observed edges are compatible with orthorhombic crystals.

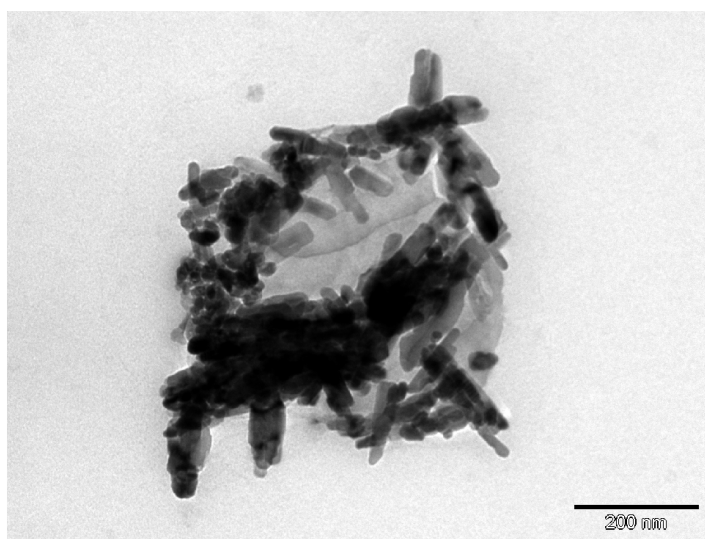


Figure III.4: SEM image of a randomly taken sample of the NCP.

Randomly taken EDS analyses of the raw sample (Table III.3), indicate the presence of aluminum, silicon, calcium, titanium and phosphorus in small amounts, with oxygen and iron as main elements with 34.3% and 48.1% respectively. The amount of Fe and O would suggest the clay may be composed of either iron oxide Fe_2O_3 or iron hydroxide - FeOOH . The Si/Al ratio *ca.* 1.2 points to a rather weathered clay, reflecting a high Si-loss, which is in agreement with goethite ($\alpha\text{-FeOOH}$) or hematite ($\alpha\text{-Fe}_2\text{O}_3$).

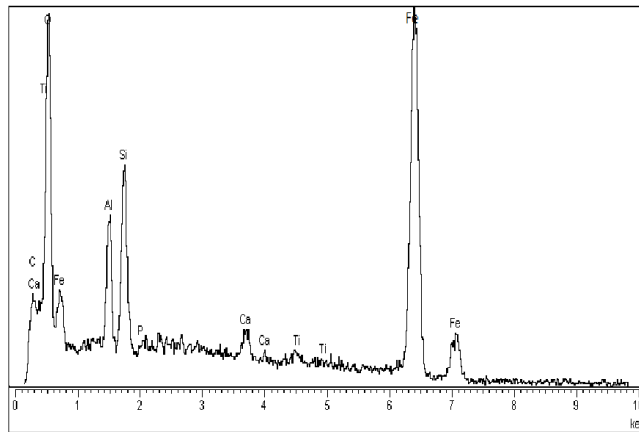


Figure III.5: EDS for a randomly taken portion of the NCP.

Table III.3: EDS analysis of NCP.

Elemental composition (weight %)						
O	Al	Si	P	Ca	Ti	Fe
34.29	6.83	8.38	0.36	1.38	0.63	48.13

III.2.2 BET analysis

BET isotherms showed a specific surface area of *ca.* $30.2 \text{ m}^2 \cdot \text{g}^{-1}$, and an average particle size of $0.1985 \text{ }\mu\text{m}$, in good agreement with the size of the agglomerates observed by SEM, the BJH pore volume and pore diameter were: $0,051 \text{ cm}^3 \cdot \text{g}^{-1}$ and $70,3 \text{ \AA}$ respectively, the obtained results are summarized in the following table:

Table III.4: BET analysis of the NCP.

Surface area	
BET surface area	30.22 m ² /g
Langmuir Surface Area	145.48 m ² /g
t-Plot Micropore Area	0.90 m ² /g
t-Plot External Surface Area	29.31 m ² /g
BJH Adsorption cumulative surface area of pores between 17.000 Å and 3 000.000 Å diameter	29.16 m ² /g
BJH Desorption cumulative surface area of pores between 17.000 Å and 3 000.000 Å diameter	30.61 m ² /g
D-H Adsorption cumulative surface area of pores between 17.000 Å and 3 000.000 Å diameter	29.03 m ² /g
D-H Desorption cumulative surface area of pores between 17.000 Å and 3 000.000 Å diameter	30.48 m ² /g
Pore Volume	
t-Plot Micropore volume:	0.00023 cm ³ /g
BJH Adsorption cumulative volume of pores between 17.000 Å and 3 000.000 Å diameter	0.05125 cm ³ /g
BJH Desorption cumulative volume of pores between 17.000 Å and 3 000.000 Å diameter	0.05180 cm ³ /g
Pore size	
BJH Adsorption average pore diameter (4V/A)	70.29 Å
BJH Desorption average pore diameter (4V/A)	67.67 Å
D-H Adsorption average pore diameter (4V/A)	70.27 Å
D-H Desorption average pore diameter (4V/A)	67.62 Å
Average Particle Size	1985.19 Å

III.2.3 XRF Analysis

XRF results, expressed as % in oxides, confirmed (Table III.5) that the clay is rich mainly in Fe₂O₃, which represents 77.7 % of the total composition, followed by SiO₂ (11.5 %), Al₂O₃ (6.5 %) and CaO (1.3%), respectively. Other components are also present although in very low percentages, not exceeding 1%.

Table III.5: Chemical composition % of NCP obtained by XRF.

SiO₂	11.5	CuO	0.040
Al₂O₃	6.5	ZrO₂	< 0.005
K₂O	0.058	NiO	0.035
Fe₂O₃	77.7	Rb₂O	< 0.003
MgO	0.35	SrO	0.025
TiO₂	0.46	Na₂O	< 0.008
CaO	1.3	SO₃	0.35
P₂O₅	0.75	Cl	0.11
ZnO	0.056	Y₂O₃	< 0.003
MnO	0.14	BaO	< 0.003

III.2.4 UV-Vis DRS Analysis

A broad and intense band in the region 250-600 nm of the UV/Vis diffuse reflectance spectroscopy was observed for suspensions of the NCP (Figure III.6), with a maximum at around 380 nm. The reflectance was also significant in all the range between 600 and 800 nm, primarily associated to iron and the presence of iron oxide. The intense reflectance in the range between 250-600 nm results mainly from ligand to metal charge transfer transition (LMTC) from O²⁻p → Fe³⁺ 3d. However, the Vis absorption edge, which gives the iron oxides their red to yellow colours, does not result from LMTC transitions, but is the consequence of very intense Fe³⁺ ligand field Fe³⁺-L pair transitions (respectively LF and MMP transitions). The UV/Vis spectrum of the sample suggests the presence of goethite [197].

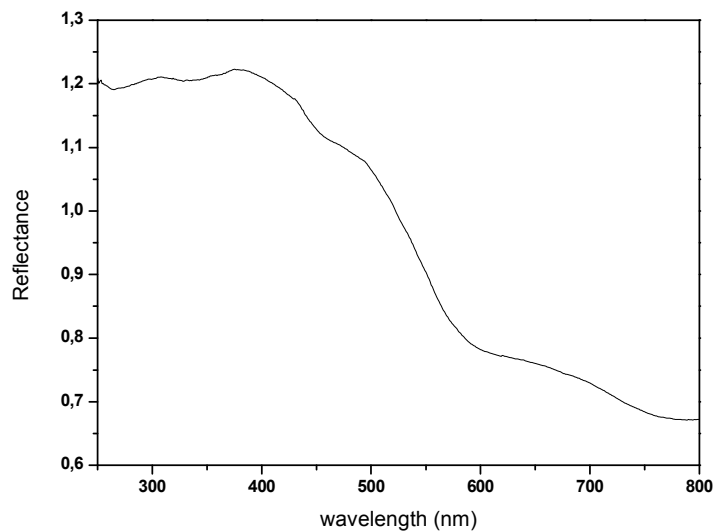


Figure III.6: UV-Vis diffuse reflectance spectrum of NCP.

III.2.5 XRD Analysis

XRD of the clay (Figure III.7) showed a diffraction pattern that is undoubtedly attributed to the presence of goethite, quartz and kaolinite (JCPDS files 29-0713, 46-1045 and 14-0164, respectively), with goethite (FeO(OH)) as the most dominant component of the clay. This is in agreement with SEM-EDS observations and confirms, out of doubt, that the natural clay is rich in Fe³⁺ and therefore useful for the heterogeneous photo-Fenton process.

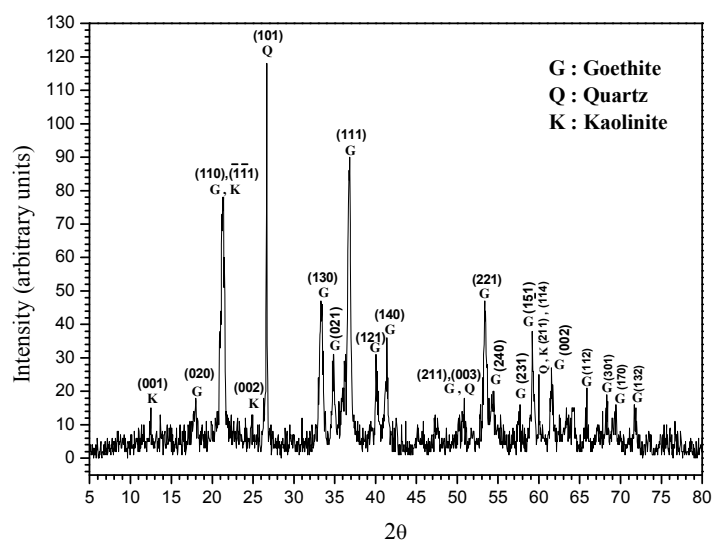


Figure III.7: X-ray diffractogram of the natural clay powder.

III.3 ADSORPTION STUDY

III.3.1 MBT adsorption onto NCP (effect of contact time)

Before starting the heterogeneous degradation experiments, we decided to study first the adsorption behavior of MBT on the NCP. Hence, an estimation of MBT adsorption capacity on the surface of natural clay powder was investigated during 150 min in the dark, with $[MBT]=5.0 \cdot 10^{-5}$ M and $0.5 \text{ g} \cdot \text{L}^{-1}$ NCP. The results showed a very fast adsorption in the first 15 min, estimated at about 11 %, *i.e.*, $5.5 \cdot 10^{-6}$ M of the initial MBT concentration. When the amount of NCP was doubled to $1.0 \text{ g} \cdot \text{L}^{-1}$, much higher adsorption, *ca.* 28 % of MBT, was observed within the 10 first min of contact at the same temperature.

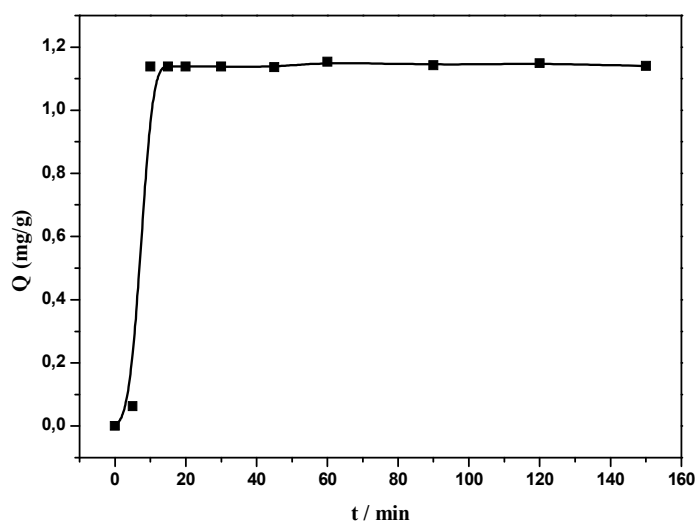


Figure III. 8 : Effect of contact time on MBT adsorption onto NCP
 $[MBT]=5.0 \cdot 10^{-5}$ M, $0.5 \text{ g} \cdot \text{L}^{-1}$ NCP, $T = 298$ K.

III.3.2 Effect of operational parameters

The effect of various parameters affecting the adsorption of MBT onto NCP namely: initial MBT concentration, NCP dose, agitation speed and initial pH of the solution; have been investigated, and they are presented in the following paragraphs, followed by the results of kinetics and adsorption isotherms studies.

III.3.2.1 Effect of initial MBT concentration

The effect of initial MBT concentration on the adsorption process onto the surface of natural clay powder was investigated; the isotherm adsorption which was represented by the variation of the adsorbed quantity Q_e (mg/g) as a function of C_e (mg/l) at equilibrium ($Q_e = f(C_e)$) is shown in Fig III.9. It is clear that the adsorbed amounts of MBT increases proportionally with initial concentration increase.

This result indicates that the higher concentration of MBT is in the solution, the more molecules will diffuse towards the surface of the clay, and consequently the retention becomes more important.

On the other hand, high initial MBT concentration increases the fraction of area covered with NCP and provides necessary driving force to overcome the resistance to the mass transfer of MBT onto the interface which increases the adsorption capacity.

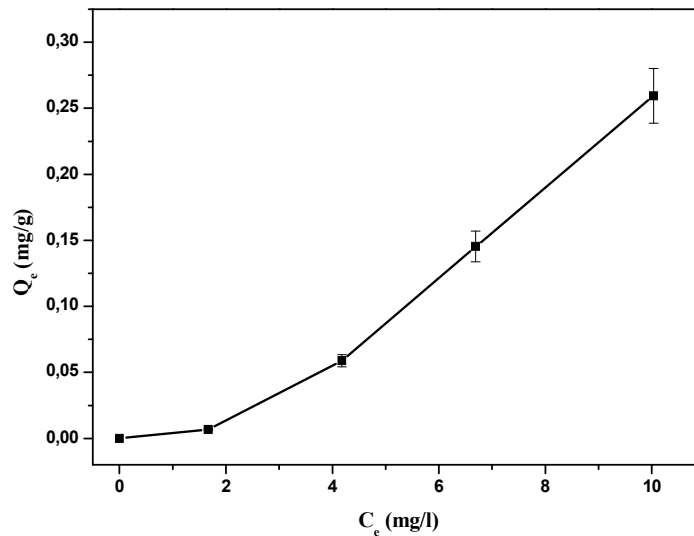


Figure III.9: Effect of initial MBT concentration on its adsorption capacity.

III.3.2.2 Effect of agitation speed

The results of the influence of the agitation speed variation on the adsorption of MBT (5.10^{-5} M) are shown in figure III.10. The NCP dose, initial MBT concentration and temperature are kept constant. The study was performed by varying the agitation speed from 250 to 1400 rpm using a magnetic stirrer.

From the results, it can be seen that the adsorption capacity of MBT decreases slowly from 250 to 800 rpm and then decrease significantly at a higher agitation speed.

As suggested by the authors [187] cited by Krzysztof Kusmierk *et al* [188], this observation is due to the fact that at very high agitation speed, the kinetic energy of both MBT molecules and the natural clay particles increased enough, resulting in the detachment of the loosely bound adsorbate molecules.

Based on these results, we can conclude therefore that for a better adsorption of MBT on the NCP, the agitation rate of the reaction mixture should be between 250 and 800 rpm.

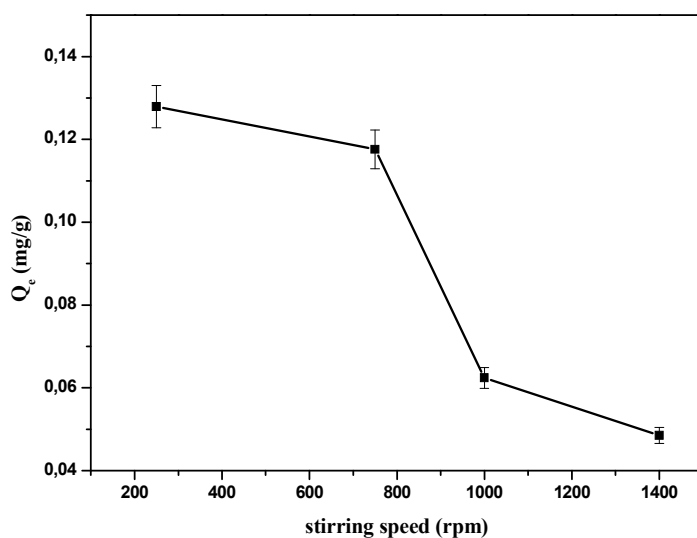


Figure III.10: Effect of agitation speed (rpm) on the adsorption capacity of MBT.

III.3.2.3 Effect of natural clay dose

The study of the influence of natural clay dose on the adsorption capacity of MBT led us to vary the initial amount of the NCP while the initial concentration of the substrate in solution remains constant ($5 \cdot 10^{-5} \text{M}$ i.e.: 8,36 mg/L).

The obtained results (Fig III.11), showed that the increase in NCP dose until certain limit has a proportional effect on the retention capacity and consequently on the adsorbed amount of MBT due to the availability of more binding sites for adsorption.

Hence, the optimum amount of the adsorbent was 1.5 g/L, Above this value, further increase in NCP amount did not improve the adsorption capacity and a decrease in the adsorbed amount of MBT was observed, which mean that the number of adsorption sites of NCP remaining stable and saturated by MBT molecules, In addition, a large quantity of adsorbent creates agglomeration of particles, leading to a reduction of the total adsorption surface and, consequently, a decrease in the amount of adsorbate per unit of adsorbent mass.

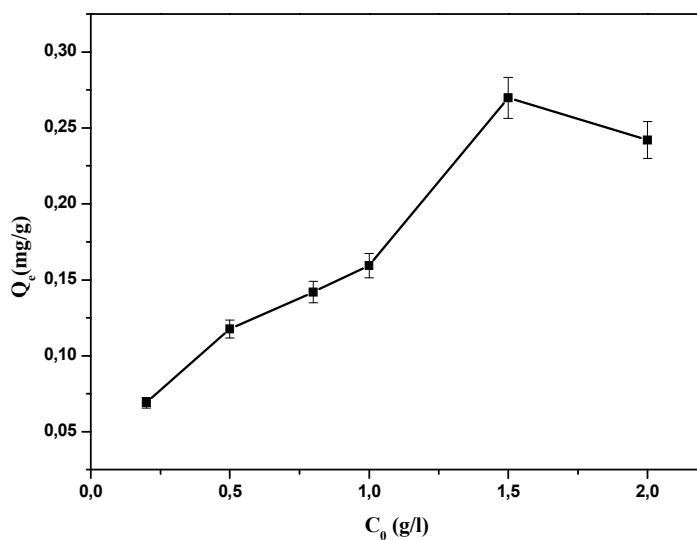


Figure III.11: Effect of natural clay dose on MBT retention.

III.3.2.4 Effect of initial pH

The initial pH of the solution is an important factor which must be taken into consideration during the adsorption study.

The adsorption experiments were carried out at pH range 2-12, the results showed that the adsorption capacity increase with increasing pH to reach a maximum at pH 12.

Generally, there are two possible mechanisms influencing the adsorption of organic compounds onto clay: (1) electrostatic attraction between the negatively charged adsorbate and positively charged adsorbent; (2) chemical adsorption between the adsorbate and the adsorbent. As for MBT, it exists as thione and thiol tautomeric forms in equilibrium (as shown in figure III.3) with pKa value of 6.95.

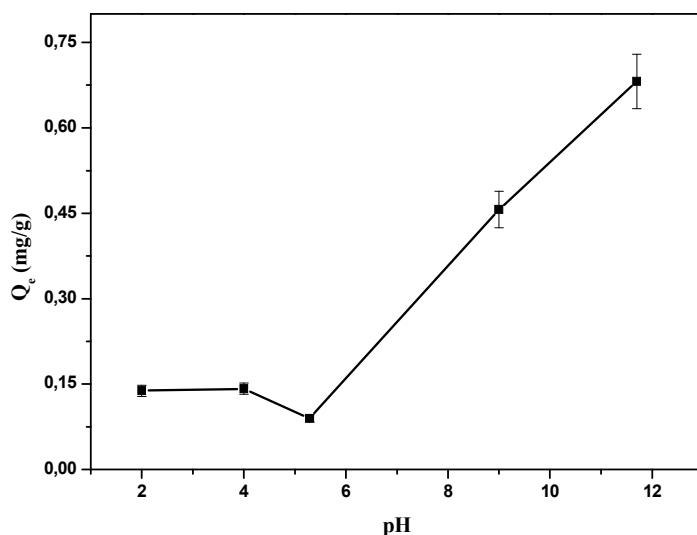


Figure III.12: Effect of initial pH on the adsorption of MBT by NCP.

With the increasing in pH beyond the pH value at the point of zero charge (pHpzc), the number of positive charge sites decreased and the number of negative charge sites increased. This phenomenon favors the positive sorption of MBT due to the electrostatic attraction.

For the interval between pH 2 and 4 below the pHpzc value, a stability of the adsorbed quantity is noted. This can be explained by the fact that at low pH values, the surface of the adsorbent would be surrounded by H^+ which decreases the interaction of ions of

MBT with the sites of the adsorbent, on the other hand at high pH, the H⁺ concentration decreases which generates a good interaction between the pollutant ions and the sites of the surface. These results showed that alkaline conditions favor the adsorption of MBT, and indicated that high pH existed electrostatic interaction between MBT and NCP. Thereafter, the experiments should be carried out at basic initial pH.

III.4 ADSORPTION ISOTHERMS

To study the adsorption isotherms of MBT onto NCP, volumes of 50 mL of different concentrations of MBT are brought into contact with a mass of 25mg of the NCP. The experimental conditions are similar to those of adsorption study.

The adsorption isotherms are the representation of the amount of solute adsorbed per unit weight of adsorbent as a function of the equilibrium concentration in the bulk solution at constant temperature. Langmuir and Freundlich adsorption isotherms are studied because they are commonly used for their simplicity of artwork to describe the adsorption phenomenon of MBT onto the surface of studied NCP.

III.4.1 Langmuir isotherm

The Langmuir isotherm is valid for monolayer adsorption onto a surface of adsorbent with a finite number of identical sites. The surface is uniform with no interaction between the adsorbed molecules. The homogeneous Langmuir adsorption isotherm is represented by the following equation.

$$q_e = q_m \cdot bC_e / (1 + bC_e) \quad \text{(III.1)}$$

Where:

q_e is the amount adsorbed at equilibrium (mg/g), C_e the equilibrium concentration (mg/l), q_m : the maximum adsorption capacity (mg/g) (characteristic of the formation of the monolayer of adsorbed molecules), and b a constant related to the adsorption energy (l/mg).

The linear form of Langmuir equation may be written as:

$$\frac{1}{q_e} = \frac{1}{q_m} + \frac{1}{q_m \cdot b \cdot C_e} \quad \text{(III.2)}$$

By plotting $(1/q_e)$ as a function $(1/C_e)$ we obtained the curves of (Fig III.13), corresponding to the linearity expression of the Langmuir model, this curve allowed us to determine the value of q_m and b .

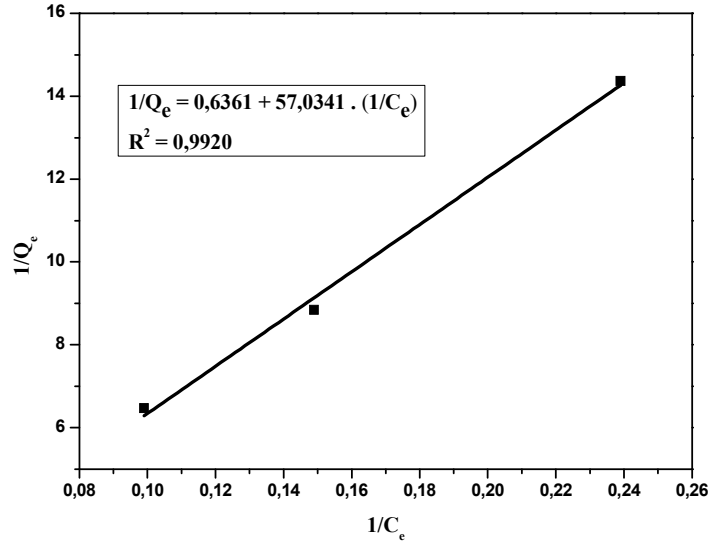


Figure III.13: The Langmuir isotherm of MBT adsorption on the NCP.

III.4.2 Freundlich isotherm

The Freundlich isotherm is an empirical equation assuming that the adsorption process takes place on heterogeneous surfaces, and adsorption capacity is related to the concentration of MBT at equilibrium. The heterogeneous Freundlich adsorption isotherm is represented by the following equation:

$$q_e = K_F \cdot C_e^{1/n} \quad \text{(III.3)}$$

Where K_F is Freundlich constant related to the adsorption capacity (mg/g) and $1/n$ is the heterogeneity factor.

The linear form of Freundlich equation may be written as:

$$\log(q_e) = \log K_f + \frac{1}{n} \cdot \log C_e \quad \text{(III.4)}$$

The values of K_F and n are determined by plotting $\log(q_e)$ as a function of $\log(C_e)$, we obtained the curve of figure III.14 Corresponding to the expression linearity of the Freundlich model.

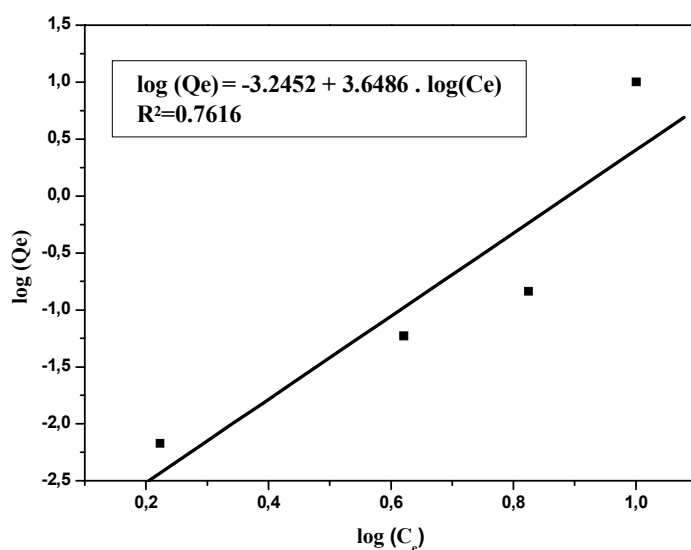


Figure III.14: Freundlich isotherm of MBT adsorption on clay.

The isotherm parameters for the adsorption of MBT onto NCP for both Langmuir and Freundlich isotherms are summarized in Table III.6. It can be seen from the results that the adsorption of MBT onto NCP fits the Langmuir isotherms model ($R^2 = 0,99$) much better than Freundlich isotherm model ($R^2 = 0,76$). This can be ascribed to the effective chemisorption of MBT onto NCP.

The quantity of the MBT increases more rapidly for low concentrations in solution and then equilibrates to reach a plateau, corresponding to saturation of the adsorption sites and that reflecting an adsorption in monolayer.

Table III.6: Summary of the Freundlich and Langmuir constants.

Freundlich			Langmuir		
n	K_F	R^2	b	q_m	R^2
3,6486	$5.68 \cdot 10^{-4}$	0.7616	0.257	$3.26 \cdot 10^{-3}$	0.9920

In the present study the heterogeneity factor in the Freundlich isotherm model equal to 3,6486, this factor can reflect also the heterogeneity in site energy and the adsorption intensity. In the case of our study value of $1/n = 0.27$ smaller than 0.5 which indicates that the adsorbate is easily adsorbed, when the value of $1/n$ greater than 2, indicates that the adsorbate is hardily adsorbed [189,190].

III.5 ADSORPTION KINETICS OF MBT

A series of adsorption experiments were carried out to investigate the adsorption kinetics of MBT on NCP surface at natural pH and room temperature. The pseudo first-order kinetic model (Eq.III.5) and the pseudo second-order kinetic model (Eq.III.6) were used

$$\ln(q_e - q_t) = \ln q_e - K_1 \cdot t \quad \text{(III.5)}$$

$$\frac{t}{q_e} = \frac{1}{K_2 \cdot q_e^2} + \frac{1}{q_e} \cdot t \quad \text{(III.6)}$$

Where: $k_1(\text{min}^{-1})$ and $k_2(\text{g}/(\text{mg} \cdot \text{min}))$ are the rate constants of the pseudo first-order and pseudo second-order kinetic models, respectively.

The pseudo-first order model assumes that the adsorption process is controlled by only one adsorbing site, and the pseudo-second order model is based on the conception that the adsorption process is a chemical one, involving valence forces by the exchange or sharing of electrons between adsorbate and adsorbent [191,192].

III.5.1 Pseudo-First-order kinetic

A linear plot of $\ln(q_e - q_t)$ versus t was used to determine the values of k_1 and the equilibrium adsorption capacity (q_e). The model parameters used to evaluate the experimental data and the corresponding correlation coefficient are presented in Table III.7.

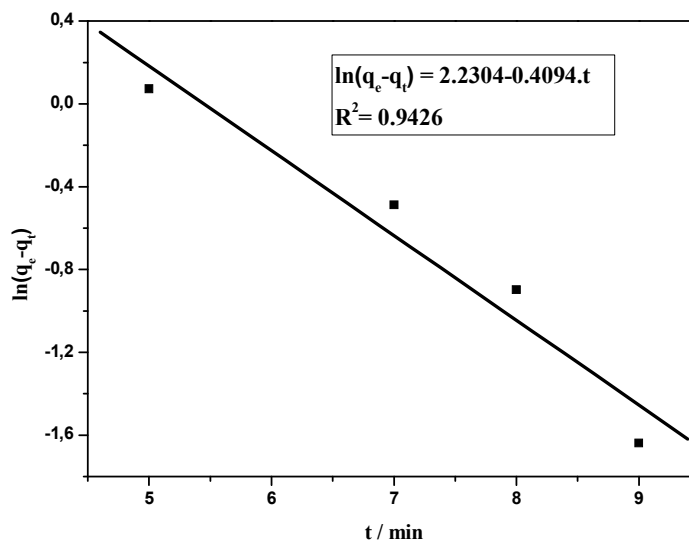


Figure III.15: First order adsorption kinetics for the adsorption of MBT on NCP.

III.5.2 Pseudo-Second-order kinetic

The straight line plots of t/q_t versus t permits the calculation of k_2 and q_e (Fig III.16). The results are shown in Table III.7. According to the Figure III.16, the pseudo-second-order model was found to be less appropriate with the experimental results.

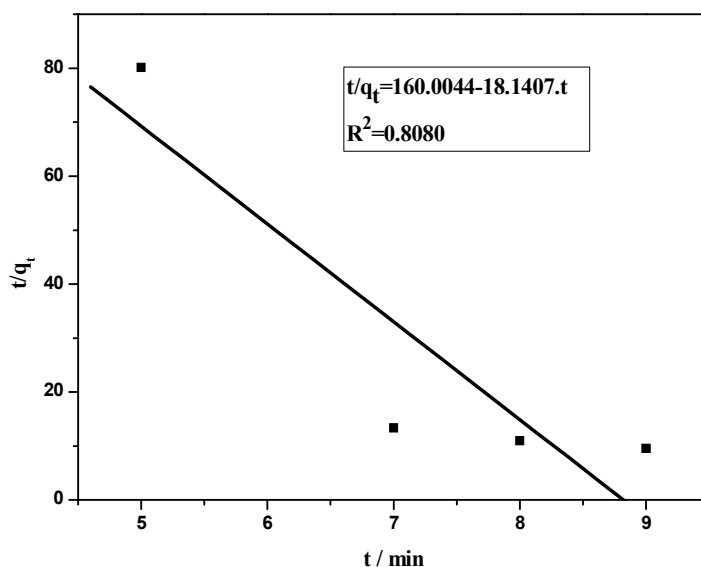


Figure III.16: Second order adsorption kinetics for the adsorption of MBT on NCP.

Comparisons between the resulted correlation coefficients (Table III.7) clearly indicated that the value of the correlation coefficient R^2 for the pseudo-first order model was 0.94 better than the pseudo-second order model ($R^2=0.80$), which mean that the adsorption kinetics of MBT onto NCP follow pseudo-first order adsorption kinetics model much better than pseudo-second order kinetics model and provide a suitable description for the adsorption of MBT on NCP adsorbent.

Table III.7: Pseudo first-order and pseudo second-order adsorption kinetic parameters for MBT adsorption onto NCP.

Pseudo-First-order kinetic			Pseudo-Second-order kinetic		
q_e (mg/g)	k_1 (min^{-1})	R^2	q_e (mg/g)	k_2 ($\text{mg.g}^{-1}.\text{min}^{-1}$)	R^2
9,303	0.409	0.9426	-0,055	2,056	0.8080

III.6 DEGRADATION STUDY

In this part of our study and for the sake of simplicity, we decided to use $0.5 \text{ g}\cdot\text{L}^{-1}$ as experimental load of NCP in the degradation experiments and assumes the Langmuir model, i.e., a true adsorption-desorption equilibrium forming a single layer of MBT onto a homogeneous surface of NCP, with equivalent and homogeneously distributed adsorption sites. Alterations of the adsorption properties of the NCP or of the adsorption-desorption equilibrium are considered negligible once the solution started to be irradiated.

III.6.1 Heterogeneous Fenton System :(MBT/H₂O₂/NCP)

III.6.1.1 Thermal effect of Natural Clay and H₂O₂

Before starting the study of MBT degradation by the system: MBT/H₂O₂/Clay, it is necessary first to check the effect of the thermal oxidation of MBT by the NCP and H₂O₂ alone in the dark. For that, two solutions were prepared: $5.0\cdot 10^{-5} \text{ M}$ MBT and 0.5 g/L clay, $5.0\cdot 10^{-5} \text{ M}$ MBT and 10^{-3} M H₂O₂. From the obtained results, it can be concluded that no thermal effect was observed for both solutions, and the decrease in concentration for the first solution concerning the adsorption of MBT on the surface of NCP, this adsorption was achieved after 15 min of contact, which corresponds to the equilibrium time of MBT with the clay as discussed earlier in the adsorption study (Section III.3.1).

III.6.1.2 Influence of operational parameters

a. Effect of initial MBT concentration

The influence of initial MBT concentration was studied for various concentrations ($10^{-5} - 7,5\cdot 10^{-5} \text{ M}$), at natural pH = 5.43 and at room temperature for fixed amount of NCP (0.5 g/L) and hydrogen peroxide (10^{-3} M).

From the results showed in the figure III.17, it can be seen that the degradation of MBT is more rapid for lower concentrations. This phenomenon can be explained by the fact that the increasing in the initial MBT concentration increases the probability of reactions between MBT molecules and hydroxyl radicals generated in the medium.

But under constant conditions of the heterogeneous Fenton process, the amount of MBT and its intermediates increased, while the amount of HO• radicals produced stayed constant, Thus, the concentration of HO• radicals was not enough to degrade high concentrations of MBT. Consequently, the removal rate of the pollutant decreased as the concentration increased [193].

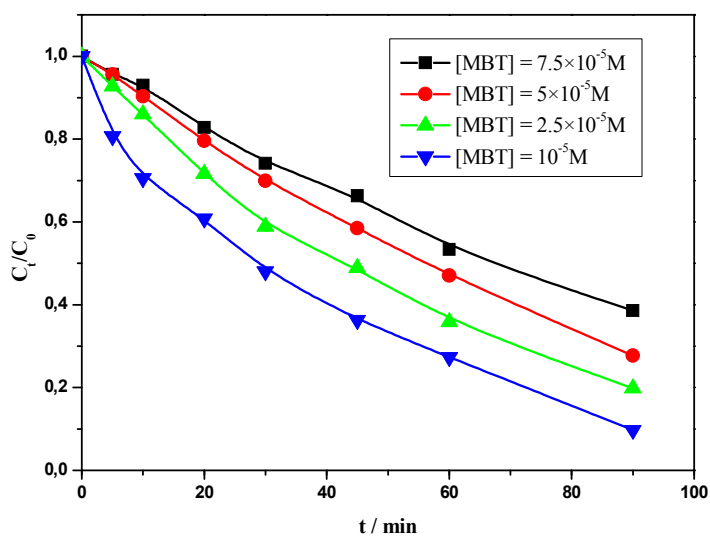


Figure III.17: Effect of initial MBT concentration on its degradation by heterogeneous Fenton process.

In order to obtain the kinetic information, the experimental results were fitted with a pseudo-first-order equation (III.7). The curve of $\ln(C_0/C_t)$ versus time was plotted and is presented in Fig. III.18. As can be seen from the results, the reaction rate of the pseudo-first-order kinetic model (K_{app}) is decreased from $0,02439 \text{ min}^{-1}$ to $0,01028 \text{ min}^{-1}$ with increasing initial MBT concentration from 10^{-5} to $7,5 \cdot 10^{-5} \text{ M}$.

$$\ln(C_0/C_t) = k_{app}t \quad \text{(III.7)}$$

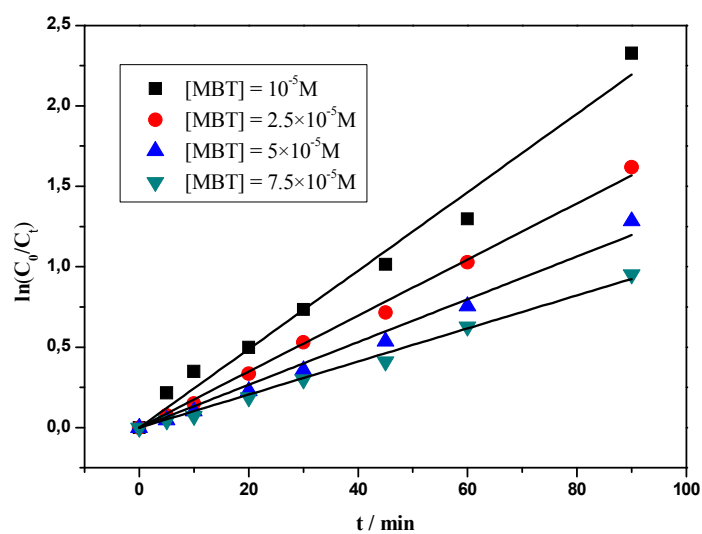


Figure III.18: Kinetic study of the degradation of MBT by heterogeneous Fenton process.

Table III. 8 : Effect of initial MBT concentration on the rate constant, half-life time of the reaction and the correlation coefficient.

[MBT] (M)	k_{obs} (min^{-1})	$t_{1/2}$ (min)	R^2
10^{-5}	0,02439	28,42	0,99095
$2,5 \cdot 10^{-5}$	0,01742	39,8	0,9979
$5 \cdot 10^{-5}$	0,0133	52,11	0,9925
$7,5 \cdot 10^{-5}$	0,01028	67,42	0,9965

These results show that the degradation of MBT by heterogeneous Fenton process is indeed following first-order kinetics model.

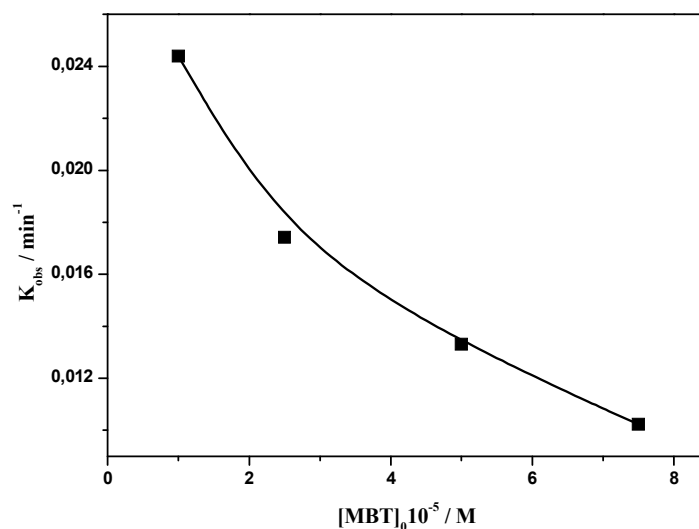


Figure III.19: Effect of the initial concentration on the apparent degradation rate constant of MBT.

b. Effect of initial concentration of hydrogen peroxide

The initial concentration of hydrogen peroxide is a key factor influencing MBT degradation by heterogeneous Fenton process MBT/H₂O₂/Clay. To study this factor, a series of experiments with an initial MBT concentration of 5.0·10⁻⁵ M and 0.5g/L of NCP were carried out in the presence of different initial concentrations of hydrogen peroxide.

It has been confirmed in the literature that the simultaneous presence of iron oxide and H₂O₂ greatly accelerates the degradation of MBT. Figure III.20 confirmed that the degradation of MBT is highly dependent on the initial concentration of H₂O₂; MBT degradation was significantly increased when the initial H₂O₂ concentration increased from 10⁻³ to 10⁻²M. However, several studies [107-111] have shown that, the excessive increase in the initial concentration of H₂O₂ above certain limit has negatively affected the degradation efficiency, because higher H₂O₂ level act as free-radical scavenger itself causing an auto-inhibition effect of the hydroxyl radicals, this later reacting with excess H₂O₂ (Eq III.8), instead of reacting with the organic pollutant, leading to the formation of HO₂• radicals which is less reactive than HO• radicals.



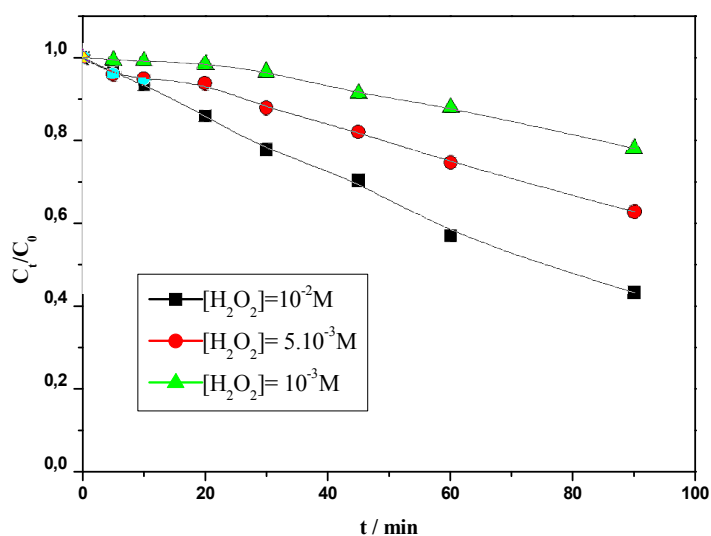


Figure III.20: Influence of $[H_2O_2]$ on the degradation efficiency of $5.0 \cdot 10^{-5} M$ MBT.

c. Effect of pH

Initial pH is a very important parameter too, influencing the performance of both homogeneous and heterogeneous Fenton processes, the effect of this factor on the degradation of $5.0 \cdot 10^{-5} M$ MBT was studied at pH values 2, 4, 9 and 12 by addition of, hydrochloric acid (HCl) for the acid medium, or sodium hydroxide (NaOH) for the basic medium. The concentration of H_2O_2 was $10^{-3} M$. The results are shown in figure III.21.

The obtained results showed that the degradation of MBT strongly depends on the pH values, a significant inhibition was observed at pH acids (2 and 4), MBT did not eliminated almost when the initial pH was less than 4. However the degradation efficiency was better at basic pHs, It can be seen that the maximum amount of MBT degradation occurred at pH 9 and reach a total degradation at around 100 min, then it slightly decreased with a further increase in the pH of the solution (pH 12).

These results indicated that heterogeneous Fenton process can be operated in a wide pH range, the best degradation efficiency can be achieved at basic pH. Thus it becomes more advantageous than the traditional homogeneous Fenton process.

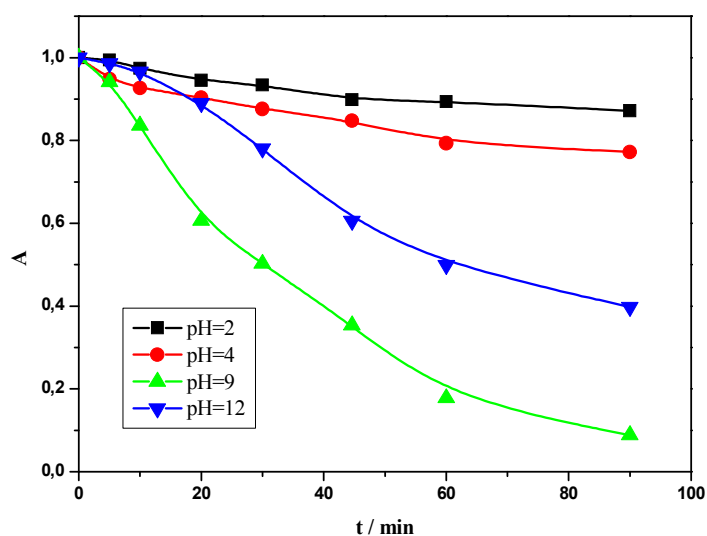


Figure III.21: Effect of initial pH on the degradation of $5 \cdot 10^{-5}$ M MBT

d. Effect of clay dose

Before studying the effect of this parameter, we determined first the equilibrium time for each dose, the results are shown in Fig III.22.

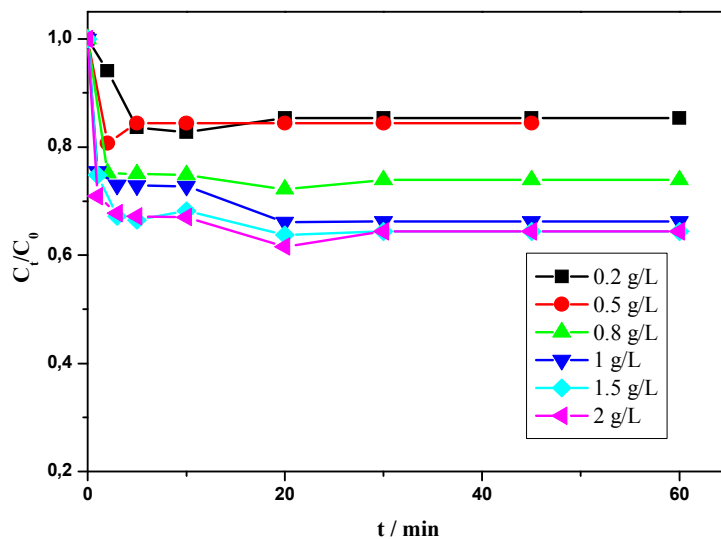


Figure III.22: Determination of equilibrium times for each NCP dose.

The effect of the initial NCP dose on the degradation efficiency of $5 \cdot 10^{-5} \text{M}$ MBT was investigated by varying the NCP dose from 0.2 g/L to 2 g/L (Fig III.23). The obtained results showed that the effectiveness of MBT degradation increased with increasing NCP concentration, as a result of the correspondingly higher NCP surface area available for the reaction, thus promoting the generation of hydroxyl radicals [194,195]. In addition to the increase of dissolved iron concentration in the solution [196]. On the other hand, above 0.8 g/L, the solution becomes saturated by the clay particles (screen effect) which cause a reduction in the efficiency of degradation processes.

In conclusion, the dose of 0.8 g/L represents the optimum value of clay. This value makes it possible to achieve a degradation rate of 92.6% after 2 hours reaction time.

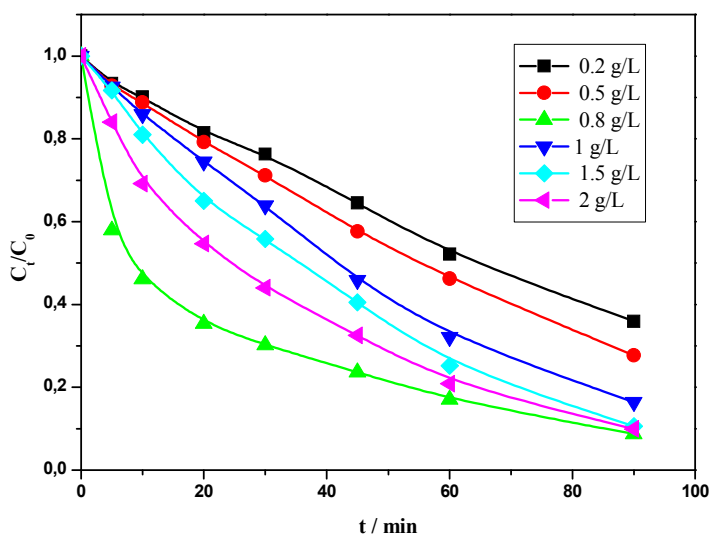


Figure III.23: Effect of NCP dose on the degradation efficiency of $5 \cdot 10^{-5} \text{M}$ MBT by heterogeneous Fenton process.

III.6.2 PHOTO-FENTON SYSTEM (MBT/H₂O₂/Clay/UV)

III.6.2.1 Degradation of MBT under different conditions

Preliminary studies were carried out to investigate the degradation efficiency of $5.0 \cdot 10^{-5}$ M MBT under different conditions. Figure III.24 shows a very low effect of UVA-Vis irradiation on the degradation when just MBT was only irradiated. Introduction of NCP while the sample is irradiated with UVA leads to a degradation *ca.* 51.5% within 180 min. Addition of H₂O₂ significantly improves the degradation process, reaching a degradation extent of 67% in 120 min. However, H₂O₂ alone didn't show any effect. Replacement of the UVA-Vis source by a germicidal one emitting at 254 nm (UVC) enhanced the oxidizing power of the system and increased the extent of degradation from 78% to 88% in less than 90 min.

The observed degradation enhancement can be explained on the basis of the generation of highly reactive oxygen species (ROS) [85]. As described in the introduction, in addition to the photocatalysis effect caused also by different semiconductors present in the clay mineral as shown in XRF analysis, which explain the degradation efficiency of the process NCP/UVA.

These ROSs and specially HO[•] are highly oxidative, show low selectivity, and may react with essentially any persistent organic pollutant, due to their high oxidation potential (see above).

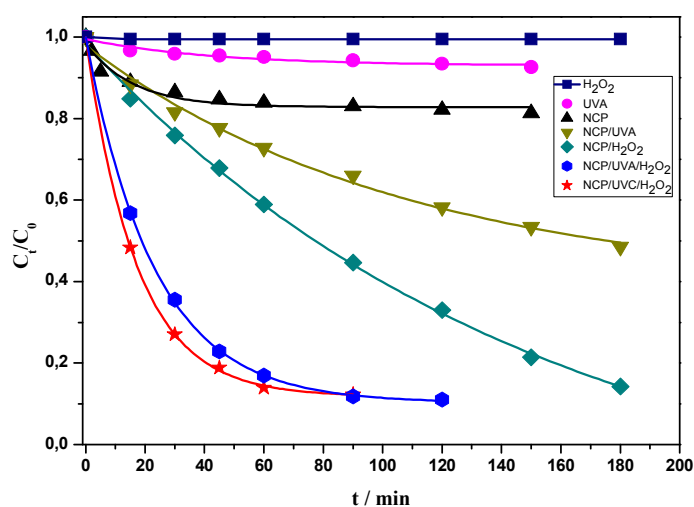


Figure III.24: Degradation of MBT under different conditions. [MBT]= $5.0 \cdot 10^{-5}$ M, [H₂O₂]₀= $1.0 \cdot 10^{-3}$ M, $0.5 \text{ g} \cdot \text{L}^{-1}$ NCP, natural pH, T=298 K.

Table III.9 compiles the observed first-order or pseudo-first order rate constants obtained under different experimental conditions. The obtained results show that H₂O₂ does not react with MBT, and UVA photolysis, with *ca.* 7% transformation of MBT in 2.5 h, is highly ineffective, presumably due to the predominance of photophysical deactivation pathways for the generated excited states.

The Fenton process (NCP/H₂O₂) is relatively effective, with *ca.* 86% transformation in 3 h and a lifetime $t_{1/2}=103$ min. The combination NCP/UVA, that initiates the photo-Fenton process, improves slightly the reaction rate, with a lifetime $t_{1/2}=77$ min, but is less effective from the point of view of transformation efficiency, reaching only *ca.* 49%. The synergistic combination of Fenton and photo-Fenton processes, NCP/UVA/H₂O₂ yields best results, improving both the reaction rate, with lifetime $t_{1/2}=16$ min and *ca.* 90% conversion in 2 h. Finally, the use of higher energy radiation, with NCP/UVC/H₂O₂ contributes to reduce slightly the transformation lifetime to $t_{1/2}=12$ min, almost without change in the conversion, *ca.* 88%.

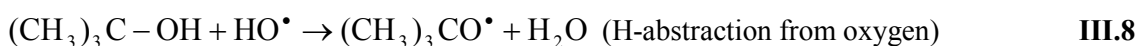
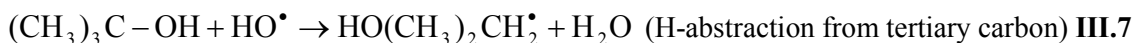
Table III.9: Rate constants obtained for the degradation of MBT under different conditions. [MBT] = $5.0 \cdot 10^{-5}$ M, natural pH, T=298.0 K.

Experimental conditions	$k_{\text{obs}} / \text{min}^{-1}$
0.5 g·L ⁻¹ NCP	0.006±0.001
1 mM H ₂ O ₂	No reaction
UVA	0.0024±0.0007
0.5 g·L ⁻¹ NCP/ 1 mM H ₂ O ₂	0.0067±0.0007
0.5 g·L ⁻¹ NCP/UVA	0.009±0.001
0.5 g·L ⁻¹ NCP/UVA/1 mM H ₂ O ₂	0.0431±0.0006
0.5 g·L ⁻¹ NCP/UVC/1 mM H ₂ O ₂	0.058±0.001

III.6.2.2 Role of the hydroxyl radical

To confirm the role of HO• radicals and to what extent they might be involved in the degradation of MBT in aqueous solution by heterogeneous photo-Fenton process, an excess of $1.0 \cdot 10^{-2}$ M *tert*-BuOH was added to the solution by using the same experimental conditions.

It is well-known that *tert*-BuOH can selectively scavenge HO• radicals, According to the reactions advanced by Kanhaiya *et al.* [173] it form less reactive tert-butoxide radicals when reacted with in-situ generated HO• radicals, as in eqs III.7 and III.8: [174].



The results, shown in Figure III.25, revealed an inhibition of *ca.* 21% (86% reduction in the reaction rate) in the efficiency of MBT degradation after 120 min of irradiation ($k=0.008\pm 0.001 \text{ s}^{-1}$, $t_{1/2}=86 \text{ min}$, 71% transformation) as compared to the process in the absence of *tert*-BuOH ($k=0.0431\pm 0.0006 \text{ s}^{-1}$, $t_{1/2}=16 \text{ min}$, 90 % transformation). Though this result clearly shows the involvement of HO• radicals, it also implies these are not the only reactive species involved in the process; otherwise, the 200-fold excess of *tert*-BuOH would completely hinder the reaction. Hence, besides the photolysis process described above, and since at the reaction pH HO_2^\bullet would be fully protonated, HO_2^\bullet may participate as described in eq I.21.

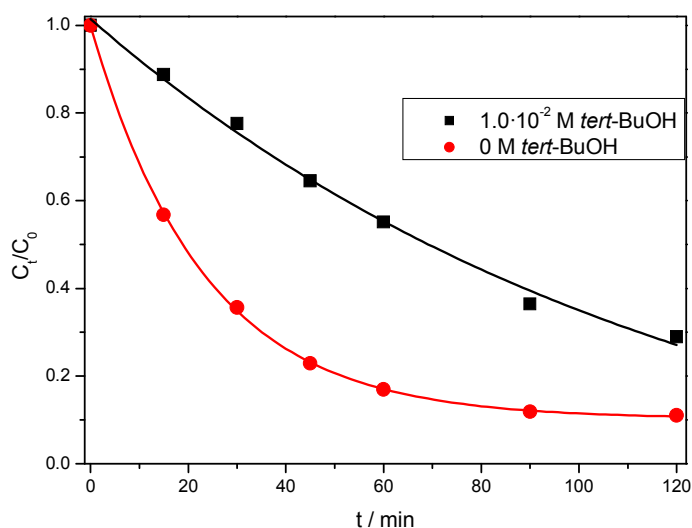


Figure III.25: Effect of *tert*-BuOH on the rate of degradation of aqueous MBT. $[\text{MBT}] = 5.0 \cdot 10^{-5} \text{ M}$, $[\text{H}_2\text{O}_2]_0 = 1.0 \cdot 10^{-3} \text{ M}$, $0.5 \text{ g} \cdot \text{L}^{-1} \text{ NCP}$ upon UVA/Vis irradiation, natural pH, $T=298.0 \text{ K}$.

III.6.2.3 Effect of operational parameters

We have studied the influence of different operational parameters: pH, H₂O₂ concentration, catalyst dosage and substrate concentration, all of which play a significant role on the efficiency and rate of degradation both for homogeneous and heterogeneous photo-Fenton processes.

a. Effect of pH

pH is the main influencing factor for the precipitation of iron oxides, and also determines the adsorption onto the surface of the catalyst. There have been different reports on the optimal pH for wastewater treatment efficiency [175] ranging from pH=3 to natural or even alkaline medium. Figure III.26 shows the effect of the pH on the efficiency of degradation of aqueous MBT in acidic, neutral and alkaline media. The highest reactivity was observed at pH=10 ($k_{\text{pH}=10}=0.105\pm 0.001 \text{ s}^{-1}$, $t_{1/2}=7 \text{ min}$), followed by natural pH ($k_{\text{nat pH}}=0.0431\pm 0.0006 \text{ s}^{-1}$, $t_{1/2}=16 \text{ min}$), and pH 2.6 ($k_{\text{pH}=2,6}=0.012\pm 0.002 \text{ s}^{-1}$, $t_{1/2}=56 \text{ min}$). The observed efficiency of the process, in terms of MBT transformation, was approximately the same, *ca.* 90% in 2 h for the three pH values. Agglomeration of ferric species was observed at pH=2.6, an indication of the instability of the participating iron species in acidic pH. These results are in good agreement with previous reports: since iron can form complexes with several Lewis bases, it has been suggested that in the presence of complexing agents the need for acidification could be circumvented [176-179]. The fact that the rate of degradation of MBT is higher in alkaline medium is probably due to the important solubility of iron species at this pH and the increase in the availability of active sites on the catalyst surface. Also, in acid medium a strong scavenging effect of HO• radicals by H⁺ is expected [180].

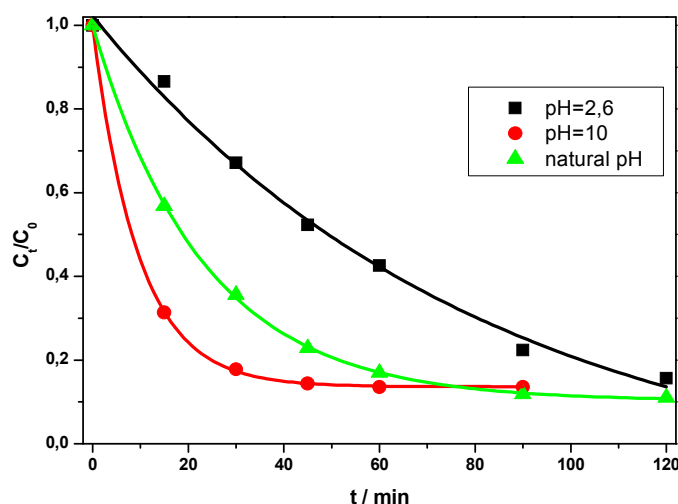


Figure III.26: Effect of pH on the heterogeneous photodegradation of aqueous MBT. $[MBT] = 5.0 \cdot 10^{-5} \text{ M}$, $[H_2O_2]_0 = 1.0 \cdot 10^{-3} \text{ M}$, $0.5 \text{ g} \cdot \text{L}^{-1}$ NCP upon UVA/Vis irradiation. $T = 298.0 \text{ K}$.

b. Effect of MBT concentration

Figure III.27 shows the effect of $[MBT]$ on its photo-Fenton heterogeneous degradation upon UVA-Vis irradiation ($\lambda \geq 366 \text{ nm}$). Within experimental error, the observed rate constants were approximately the same: $k_{\text{obs}} = 0.041 \pm 0.001$, 0.0431 ± 0.0006 and $0.038 \pm 0.002 \text{ M}^{-1} \cdot \text{s}^{-1}$, for concentrations $2.5 \cdot 10^{-5}$, $5.0 \cdot 10^{-5}$ and $7.5 \cdot 10^{-5} \text{ M}$, respectively. The same lack of effect was observed for the transformation efficiency (*ca.* 90 %). This indicates that, at the studied MBT concentrations, there are still active sites available for adsorption onto the surface of the NCPs.

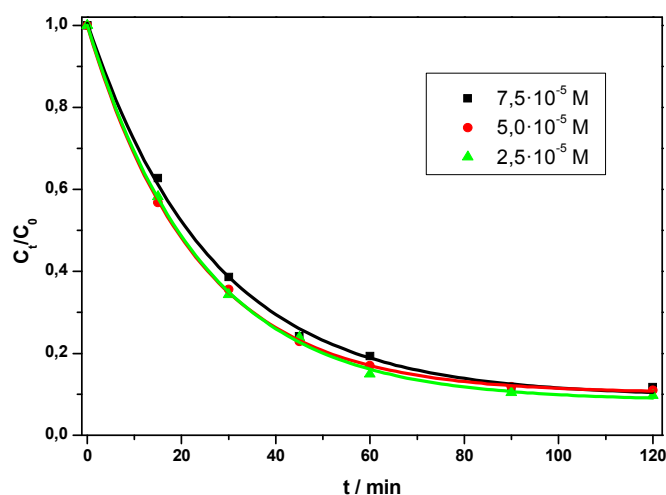


Figure III.27: Effect of MBT concentration on its photo-Fenton heterogeneous degradation. $[MBT] = (2.5-7.5) \cdot 10^{-5} \text{ M}$, $[H_2O_2] = 1.0 \cdot 10^{-3} \text{ M}$, $0.5 \text{ g} \cdot \text{L}^{-1}$ upon UVA/Vis irradiation, natural pH, $T = 298.0 \text{ K}$.

c. Effect of H₂O₂ concentration

The effect of [H₂O₂] on the removal of MBT from aqueous solution is shown in Figure III.28, and the corresponding pseudo-first order rate constants collected in Table III.10.

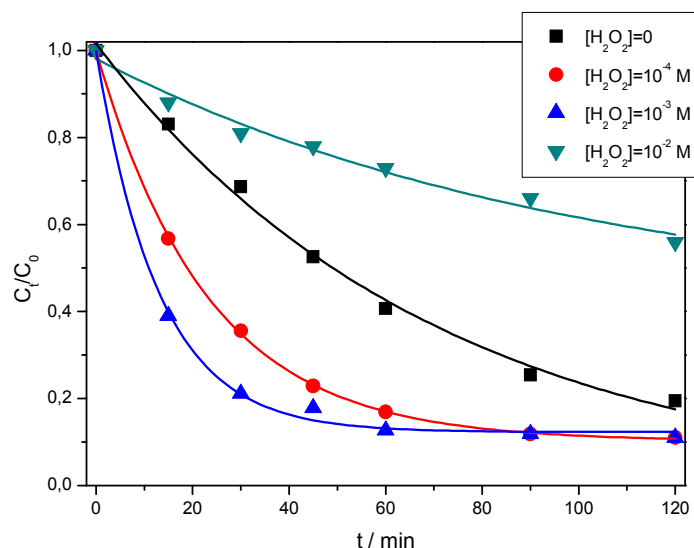


Figure III.28: Effect of H₂O₂ on the heterogeneous photo-Fenton degradation of aqueous MBT. [MBT] = 5.0 · 10⁻⁵ M, 0.5 g · L⁻¹ NCP upon UVA/Vis irradiation, natural pH, T=298 K.

Table III.10: Effect of H₂O₂ on the rate constant for heterogeneous photo-Fenton degradation of aqueous MBT. [MBT] = 5 · 10⁻⁵ M, [NCP] = 0.5 g · L⁻¹ upon UVA/Vis irradiation, natural pH, T=298.0 K.

[H ₂ O ₂] / M	k _{obs} / min ⁻¹
0	0.010 ± 0.003
1.03 · 10 ⁻⁴	0.009 ± 0.001
1.0 · 10 ⁻³	0.0431 ± 0.0006
1.0 · 10 ⁻²	0.077 ± 0.004

k_{obs} increases with [H₂O₂], but less as the concentration increases. A reduction in the extent of transformation is observed as the concentration of H₂O₂ increases, reducing the transformation efficiency. Both the tendency observed for the reaction rate and for the extent of reaction point to an inhibition of the process at higher H₂O₂ concentrations, which is explained in terms of a HO[•] radical scavenging effect caused by H₂O₂.

d. Effect of the load of NCP

Figure III.29 shows the effect of the load of NCP on the heterogeneous photo-Fenton degradation of MBT and Table III.11 summarizes the corresponding rate constants.

The rate of degradation increases linearly with growing concentrations of NCP, as shown in the inset of Fig. III.29. The direct proportionality observed shows the experimental conditions correspond to a true photocatalytic regime and, as pointed out previously for the dependence with [MBT], there are enough active sites available for adsorption on the surface of the NCPs. Under these conditions, the efficiency in the use of light by the photocatalyst is optimal, with no scattered photons.

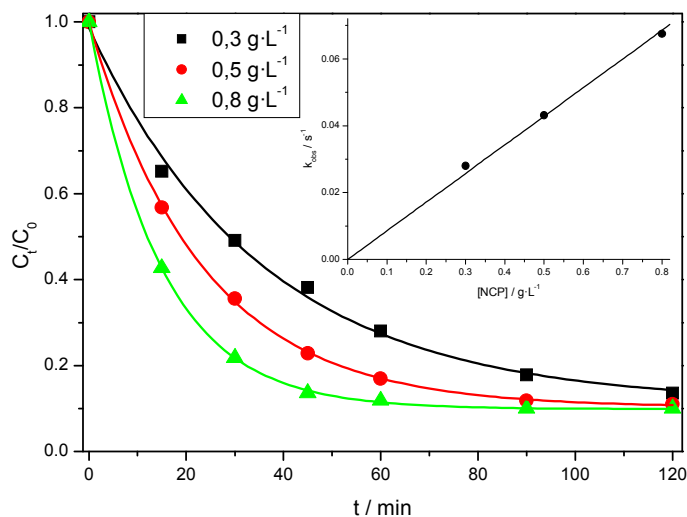


Figure III.29: Effect of the load of NCP on the rate of heterogeneous photo-Fenton degradation of MBT. [MBT]= $5.0 \cdot 10^{-5}$ M, [H₂O₂]= $1.0 \cdot 10^{-3}$ M, UVA/Vis irradiation, natural pH, T=298 K. Inset: dependence k_{obs} vs. [NCP].

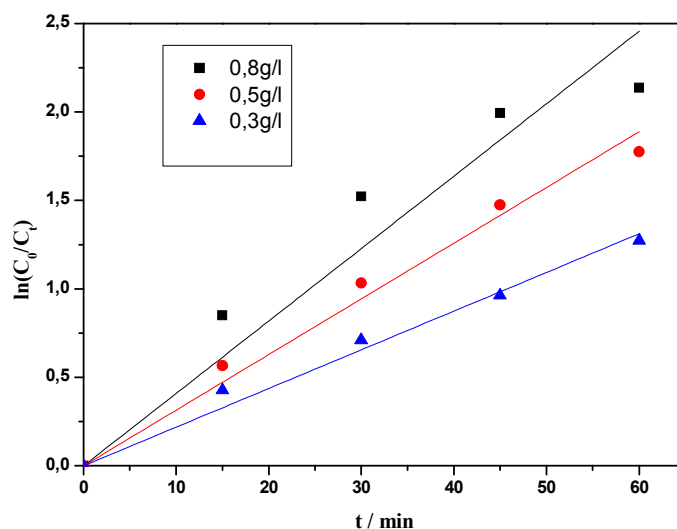


Figure III.30: Kinetic study for the degradation of MBT by heterogeneous photo-Fenton process.

Table III.11: Effect of the load of NCP on the rate constant for the heterogeneous photo-Fenton degradation of aqueous MBT. [MBT]= $5.0 \cdot 10^{-5}$ M, [H₂O₂]= $1.0 \cdot 10^{-3}$ M, UVA/Vis irradiation, natural pH, T=298 K.

[NCP] / g·L ⁻¹	k _{obs} / M ⁻¹ ·min ⁻¹
0.3	0.028±0.002
0.5	0.0431±0.0006
0.8	0.0675±0.0007

e. Effect of oxygen

The effect of the partial pressure of oxygen was studied and the results are shown in Fig. III.31. P(O₂) (v/v) was controlled by diluting it in Argon gas before saturation. The extent of reaction is approximately the same after 2 h, while the reaction rate increases with the concentration of oxygen in solution (Table III.12), a clear indication of the relevance of ROS in the heterogeneous photo-Fenton process. The observed increase in k_{obs} is, however, not linear, which points to the participation of different ROS in the process, that are generated at different rates and with different yields. Torres *et al.* [181]

investigated the reactivity of Bisphenol A (BPA) with HO^\bullet in UV- Fe^{3+} treatment, hypothesizing that monohydroxylated BPA products could be formed via HO^\bullet attack followed by reaction with O_2 to form peroxy radicals (ROO^\bullet). Finally, important reactivity is still observed in the absence of O_2 , which reveals the relevance of the Fenton and photo-Fenton processes described above on the MBT degradation.

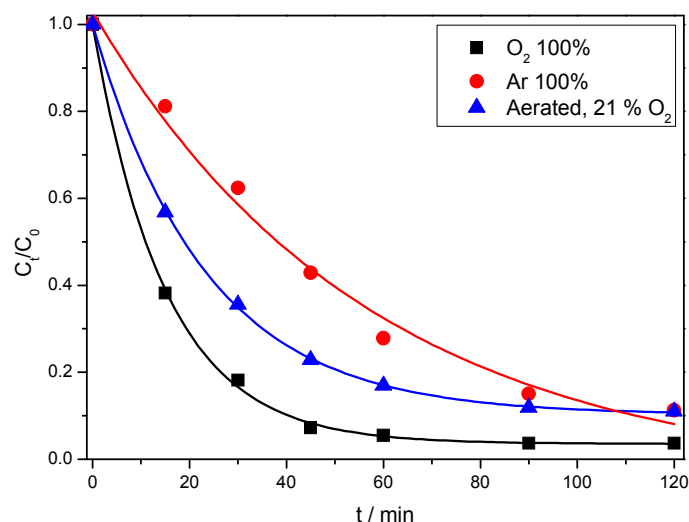


Figure III.31: Effect of the concentration of dissolved O_2 on the rate of degradation of MBT by heterogeneous photo-Fenton process. $[\text{MBT}] = 5.0 \cdot 10^{-5} \text{ M}$, $[\text{NCP}] = 0.5 \text{ g} \cdot \text{L}^{-1}$ upon UVA/Vis irradiation, $[\text{H}_2\text{O}_2] = 1.0 \cdot 10^{-3} \text{ M}$, natural pH, $T = 298 \text{ K}$

Table III.12: Effect of the partial pressure of O_2 on the rate constant for the heterogeneous photo-Fenton degradation of aqueous $5.0 \cdot 10^{-5} \text{ M}$ MBT, $[\text{NCP}] = 0.5 \text{ g} \cdot \text{L}^{-1}$ upon UVA/Vis irradiation, $[\text{H}_2\text{O}_2] = 1.0 \cdot 10^{-3} \text{ M}$, natural pH, $T = 298.0 \text{ K}$.

$P(\text{O}_2)$ (v/v)	$k_{\text{obs}} / \text{M}^{-1} \cdot \text{min}^{-1}$
0	0.018 ± 0.003
21	0.0431 ± 0.0006
100	0.067 ± 0.002

f. Effect of oxalic and citric acids

The effect of oxalic and citric acids on the UVA-Vis heterogeneous photo-Fenton degradation efficiency of MBT from aqueous solution has been studied in the absence of H_2O_2 . As shown in Figure III.32, within 150 min oxalic and citric acids show no thermal effect in the absence of UVA-Vis irradiation. When the solutions were irradiated, the same efficiency of degradation obtained for the process in the NCP/UVA (absence of carboxylic acids) was observed after 60 min in the case of oxalic acid and 150 min for citric acid. The shape of the (C_t/C_0) vs. t dependence was quite similar in both cases: the observed dependence shows what could be regarded as an induction period (longer for citric acid) followed by a decay that is not fit by a first order kinetic model in any of both cases.

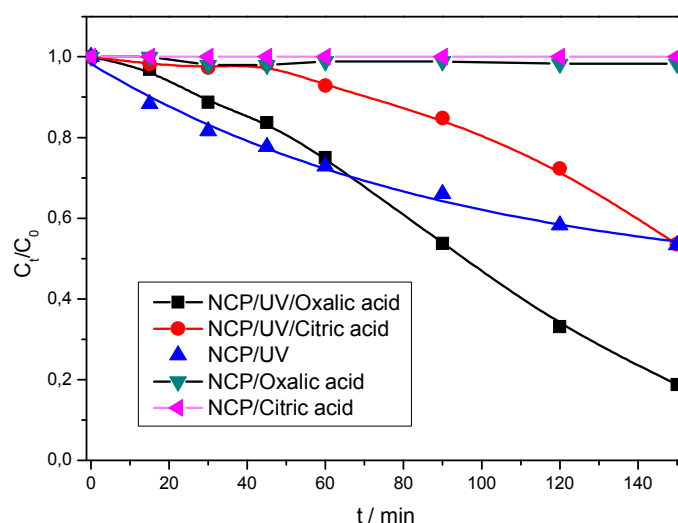


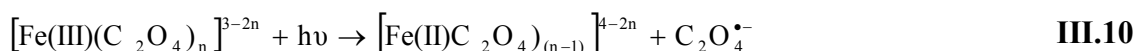
Figure III.32: Effect of oxalic acid and citric acid on the heterogeneous photo-Fenton degradation of aqueous MBT. $[\text{MBT}] = 5.0 \cdot 10^{-5} \text{ M}$, $\text{NCP} = 0.5 \text{ g} \cdot \text{L}^{-1}$ upon UVA/Vis irradiation, $[\text{OA}]$, $[\text{CA}] = 1.0 \cdot 10^{-3} \text{ M}$, $\text{pH}_0 = 6.8$, $T = 298 \text{ K}$

The higher efficiency observed of oxalic acid is probably due to the formation of iron complexes with carboxylate ions (Fe^{3+} -carboxylate), which increases the solubility of iron oxides present in the mineral matrix. This hypothesis may explain also the observed induction period: the complexation equilibrium must be reached before Fe^{3+} can be made available.

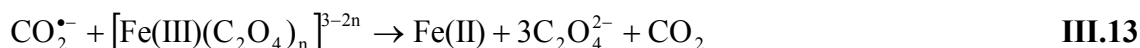
Fe³⁺-carboxylate complexes differ in stability and photoreactivity toward the studied compound. Therefore, the lower reactivity of citric acid can be related to the lower quantum yield of Fe³⁺-citric toward formation of Fe²⁺ ($\Phi=0.59$) as compared to the quantum yield of Fe³⁺-oxalic acid ($\Phi = 1.0-1.2$).[182]

The profiles with carboxylic acids resemble the typical profiles of autocatalyzed processes. The overall degradation at the end of the experiment with oxalic acid was around 82 % after 2.5 h, and 47% for citric acid (the same extent of reaction reached with NCP/UV treatment). The observed behavior can be explained by the fact that the formation of Fe³⁺-oxalate complexes, according to eq. III.9, initially limits the photoreduction of Fe³⁺, but then improves the dissolution of iron, which leads to the observed increase of degradation.

Under UV-Vis light irradiation, these complexes could be excited and transformed to Fe²⁺-oxalate complexes and C₂O₄^{•-}, as in eq. III.10:



The so-formed oxalate radical anion C₂O₄^{•-} decomposes to a carbon dioxide radical anion (CO₂^{•-}) and CO₂, eq. III.11. The CO₂^{•-} radical anion may react with dissolved oxygen, eq. III.12 and ferrioxalate complexes, eq. III.13, regenerating Fe²⁺.



Oxalic acid reacts simultaneously as a donor of proton and ligand, and the dissolution of iron is assumed to take place via an electrochemical photoreduction process.[183, 184] Charge transfer processes between the predominant oxalate species, namely ferric oxalate [Fe(III)(C₂O₄)_n]³⁻²ⁿ, and ferrous oxalate [Fe(II)(C₂O₄)_(n-1)]⁴⁻²ⁿ, and oxalate take place on the surface of NCP, introducing additional complexity on the observed heterogeneous photo-Fenton process.

III.6.2.4 MINERALIZATION EFFICIENCY

To determine the degree of mineralization reached upon treatment, duplicated samples were collected at the beginning of the experiment and after 2 h of photo irradiation under different conditions, and then TOC was evaluated. Table III.13 compiles the TOC removal results under different conditions. TOC percent removal was calculated once [MBT] did not show any further change, typically after 2 h of reaction.

Table III.13: effect of different operational parameters on TOC removal from MBT solutions. $[\text{MBT}]_0 = 7.75 \text{ mg}\cdot\text{L}^{-1}$, $[\text{H}_2\text{O}_2]_0 = 1.0 \cdot 10^{-3} \text{ M}$, $[\text{NCP}] = 0.5 \text{ g}\cdot\text{L}^{-1}$, $T = 298.0 \text{ K}$.

Experimental conditions	TOC / $\text{mg}\cdot\text{L}^{-1}$	% TOC removal
pH=2.6, UVA	2.48	68
Natural pH, UVA	3.79	51
Natural pH, UVC	4.63	40
pH=10, UVA	5.12	34
Ar-saturation, UVA	2.73	65
O ₂ -saturation, UVA	4.63	40

The obtained results show that the mineralization is not reached within typical MBT transformation time, *i.e.*, it leads to a number of reaction intermediates that are relatively persistent. Lower pH values lead to increased TOC removals, in agreement with the possibility of Fe^{3+} regeneration under appropriate acidity conditions (pH *ca.* 2.7-2.8), as described by eqs.I.20 and III.14.



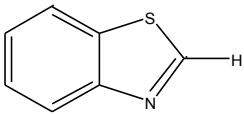
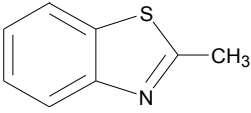
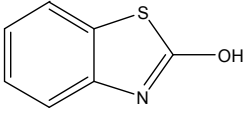
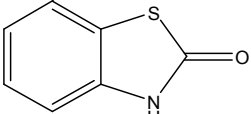
The presence of O₂ seems to worsen the mineralization, which could be associated to the generation of less reactive intermediates, possibly through peroxidation and / or hydroperoxidation processes. Finally, while UVC leads to a faster transformation of MBT than UVA, the process is more efficient for UVA in terms of TOC removal, which must be attributed to the generation of more persistent, less reactive intermediates. In sum, the best operational conditions to attain a high TOC removal are the use of UVA in combination with low pH values and absence or low concentrations of O₂.

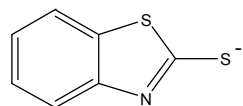
III.6.2.5 Identification of intermediates and reaction mechanism

MBT solutions were irradiated and analysed by LC-ESI-MS in positive mode ionization in order to identify the main photoproducts after 60 min of irradiation, taking into account the available literature [5-6,15,77-79,185-186]. The obtained results are compiled in Table III.14 and compared to published data.

Very similar chromatograms were obtained from solutions of aqueous $5.0 \cdot 10^{-5}$ M MBT and NCP for the different operational conditions described above. Only the main peaks were identified, and appropriate structures proposed, considering the observed (m/z) ratios. The main photoproducts found were benzothiazole (BT) and 2-benzothiazolesulfonate. The oxidation of MBT is mainly accomplished by reaction with HO^\bullet photogenerated at the surface of NCP in the presence of H_2O_2 . Detection of polyhydroxylated photoproducts is indicative of ongoing further degradation.

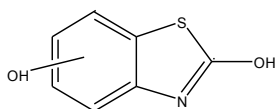
Table III.14: Identified photoproducts and comparison with others reported in the literature.

Compound	Method and reference
 BT (m/z = 135)	This study (NCP/ H_2O_2 /UVA-Vis) Direct photolysis [15], [78] Nd^{3+} - TiO_2 /UV _{365\text{nm}} [5]}
 MeBT (m/z = 149)	Direct photolysis [78]
 BT-OH (m/z = 151)	Present study (NCP/ H_2O_2 /UVA-Vis) Direct photolysis [15], [78]
 OBT (m/z = 151)	Nd^{3+} - TiO_2 /UV _{365\text{nm}} [5]}



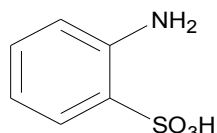
BT-S⁻ (m/z = 166)

Direct photolysis [15]



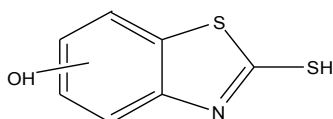
diOH-BT (m/z = 167)

This study (NCP/H₂O₂/UVA-Vis)



ASA (m/z = 173)

Nd³⁺-TiO₂/UV_{365nm} [5]

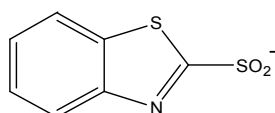


OH-MBT (m/z = 183)

This study (NCP/H₂O₂/UVA-Vis)

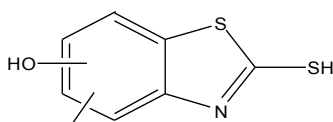
Direct photolysis [77]

DTA/UV_{365nm} [6]



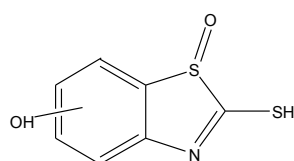
BT-SO₂⁻ (m/z = 198)

Direct photolysis [15]



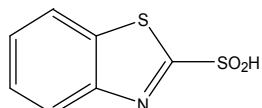
diOH-MBT (m/z = 199)

This study (NCP/H₂O₂/UVA-Vis)



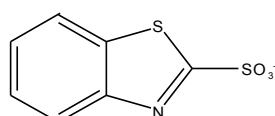
(m/z = 199)

DTA/UV_{365nm} [6]



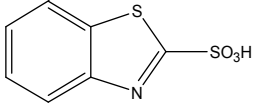
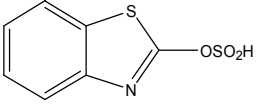
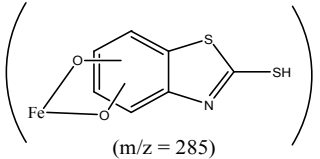
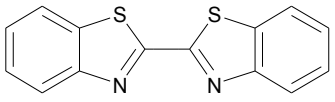
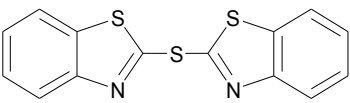
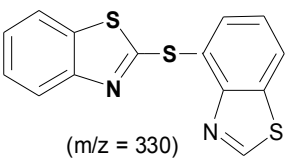
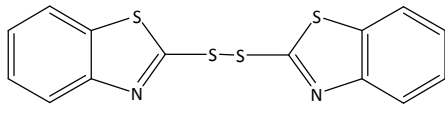
BT-SO₂H (m/z = 199)

Direct photolysis [15]



BTSo₃⁻ (m/z = 214)

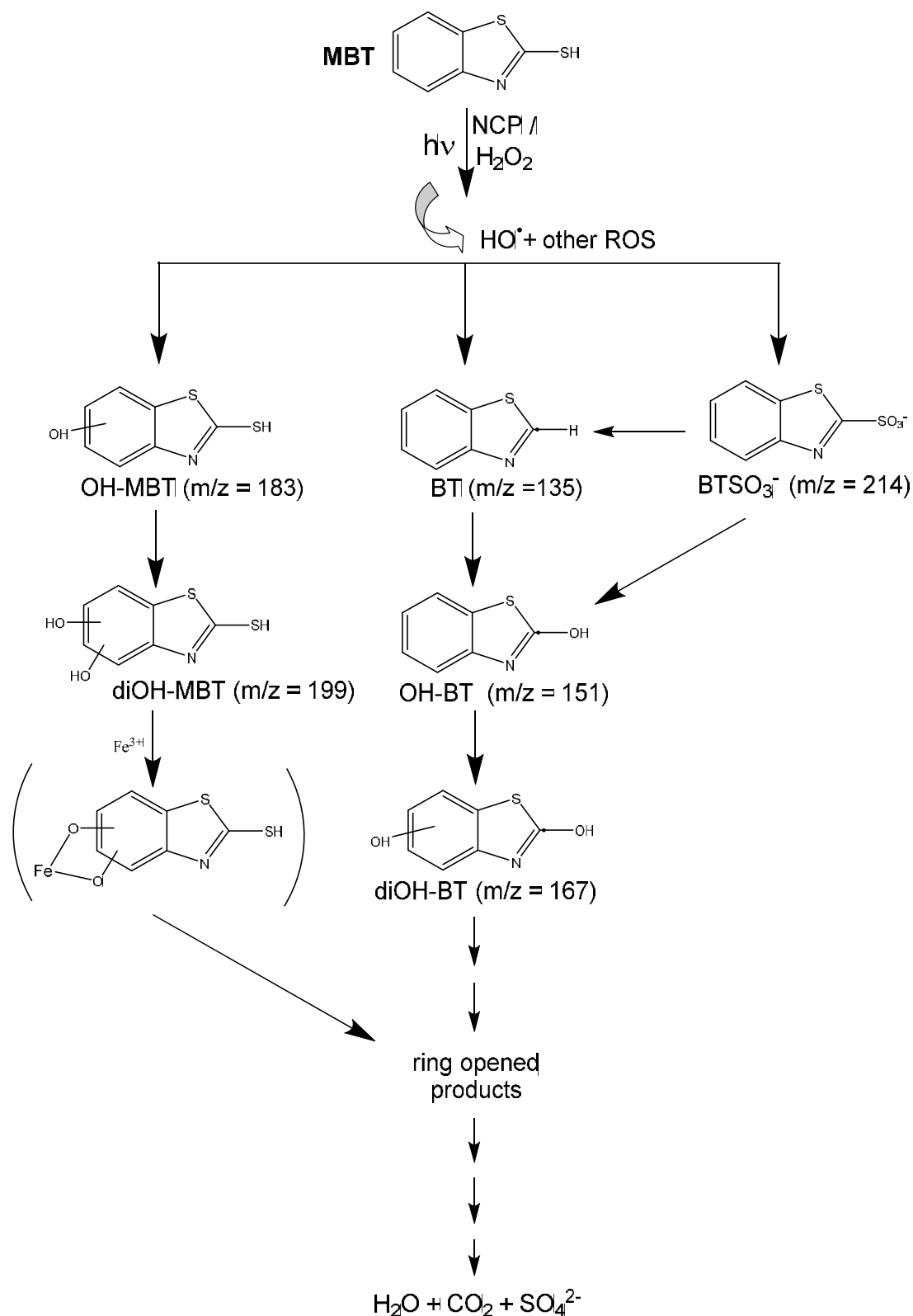
This study (NCP/H₂O₂/UVA-Vis)

 <p>BT-SO₃H (m/z = 215)</p>	<p>Direct photolysis [15], [77]</p> <p>Nd³⁺-TiO₂/UV_{365nm} [5]</p>
 <p>BTOSO₂ (m/z = 215)</p>	<p>Nd³⁺-TiO₂/UV_{365nm} [5]</p>
 <p>(m/z = 285)</p>	<p>This study (NCP/H₂O₂/UVA-Vis)</p>
 <p>(m/z = 296)</p>	<p>Direct photolysis [77]</p>
 <p>(m/z = 314)</p>	<p>Direct photolysis [77]</p>
 <p>(m/z = 330)</p>	<p>Direct photolysis [77]</p>
 <p>Dimer (disulfide form) (m/z = 332)</p>	<p>Direct photolysis [77]</p> <p>DTA/UV_{365nm} [6]</p>

Considering the different photoproducts identified, we have proposed a mechanism (Scheme III.1) for MBT heterogeneous photo-Fenton degradation in the presence of NCP.

Some of the main reaction pathways observed are: **i)** hydroxylation of the benzene ring, **ii)** hydroxylation of the carbon in thiazole ring, **iii)** S-oxidation. These transformations are expected to lead to the opening of the benzene ring and complete mineralization of the product.

➤ Degradation mechanism



Scheme III.1: Proposed mechanism of photodegradation of MBT in the presence of NCP under simulated sunlight irradiation at 366 nm. (Between brackets: hypothesized, undetected structure).

IV. GENERAL CONCLUSION

In the present thesis, our goal was to investigate the efficiency of using untreated natural clay rich in iron oxides as clean and green catalyst in the removal of MBT from water by heterogeneous Fenton and photo-Fenton processes.

First of all, we investigated the adsorption capacity of MBT onto NCP also its degradation at dark in the presence of H_2O_2 (heterogeneous Fenton process), and then under simulated sunlight (UVA-Vis) irradiation, we have investigated and focused our study on the efficiency of heterogeneous photo-Fenton process on the photodegradation of MBT in aqueous solutions. After appropriate crushing and sieving, the characterisation study by SEM and EDS analyses gave us some insights on the morphology and chemical structure of the NCP, the specific surface area was $30.2 \text{ m}^2 \cdot \text{g}^{-1}$, XRF and XRD results indicated the presence of an important amount of Fe^{3+} as an iron oxide goethite.

The results of the adsorption study indicated that the adsorption process was very fast and reached the equilibrium within 15 min. The kinetics data were fitted to pseudo-first order and pseudo-second order models, and it was found that the best fitting corresponded to the pseudo-first order kinetic model. The effect of experimental parameters including adsorbent dosage, contact time and initial pH were investigated. The adsorption isotherms were also studied. The results showed that the equilibrium data were well represented by the Langmuir isotherm equation ($R^2 > 0,99$).

Better adsorption efficiency was observed at alkaline pH and at low agitation speed. As MBT concentration and NCP dose increased, the adsorption amount also increased and the adsorption was favorable.

For the degradation study of MBT by heterogeneous Fenton process, the operational factors influencing the degradation indicated that NCP dose should not be overdosed, the optimum concentration was $0,8 \text{ g/L}$, the degradation efficiency was highly depended in the initial pH and H_2O_2 concentration, however, in contrast to what it was found in the literature, the best degradation efficiency was obtained at alkaline pH in the presence of NCP.

The photodegradation study of MBT by heterogeneous photo-Fenton process follows pseudo-first order kinetics, the species responsible for the photo-degradation was found to be mainly HO^\bullet , as the presence of *tert*-BuOH notably slowed down MBT photodegradation rate and reduced the percentage of MBT conversion. The kinetic study revealed that the photodegradation rate was strongly affected by dissolved O_2 , pH, H_2O_2 and NCP dose. The degradation in the presence of oxalic acid was found to be much more relevant for the process than that of citric acid. The formation of carboxylic acids-iron complexes slow down the process during the first 60 min, and then speeds it up by dissolving solid iron species. The photoproducts identified by LC-MS point to the formation of BT followed by 2-benzothiazolesulfonate and polyhydroxylated products. The highest TOC removals were obtained using UVA at low pHs, in the absence of O_2 . The obtained results support the use of NCPs rich in iron oxides as inexpensive, clean and efficient photocatalysts for the abatement of persistent organic micropollutants in water.

All in all, heterogeneous Fenton and photo-Fenton oxidation processes for water treatment containing MBT and using NCP rich in iron oxides is vital from the economic and environmental point of view, and appears as an alternative to the homo/heterogeneous conventional oxidation processes.

V. ANNEXES

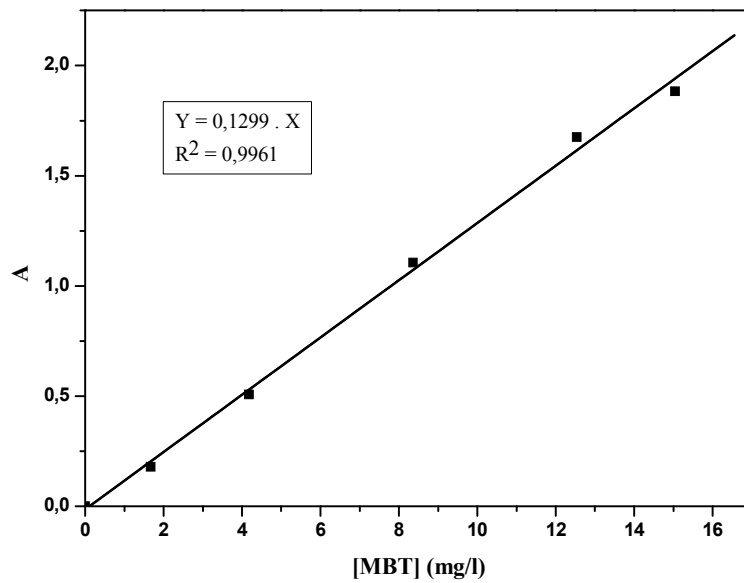


Figure A.1: Calibration curve of [MBT] at maximum wavelength 320 nm.

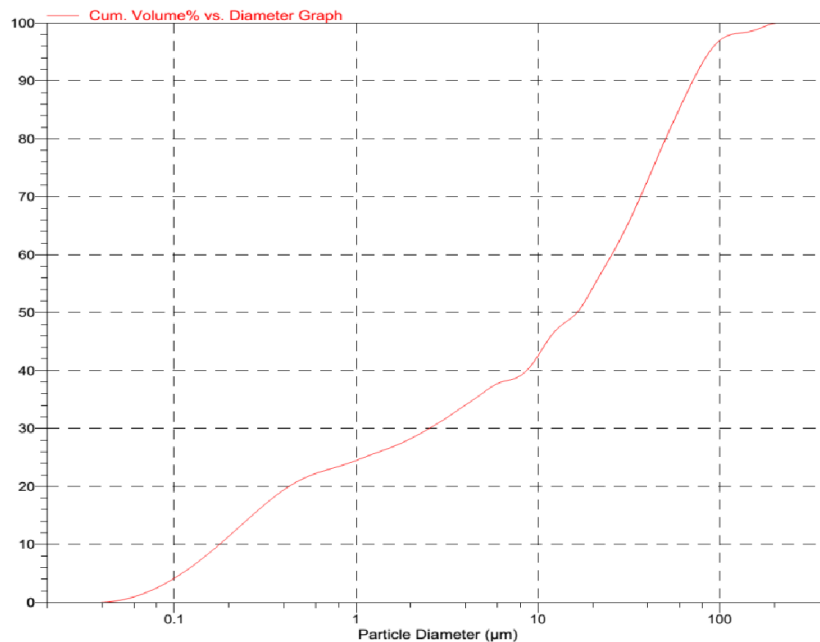


Figure A.2: Cumulative Volume Finer vs. Particle Diameter Graph for the used NCP

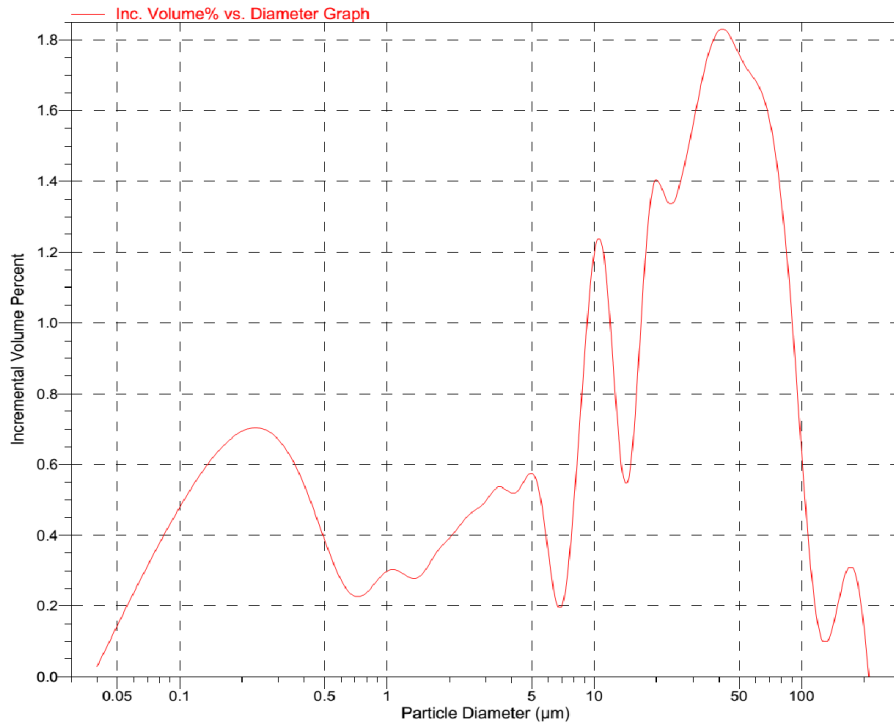


Figure A.3 : Incremental volume percent vs. Particle diameter graph

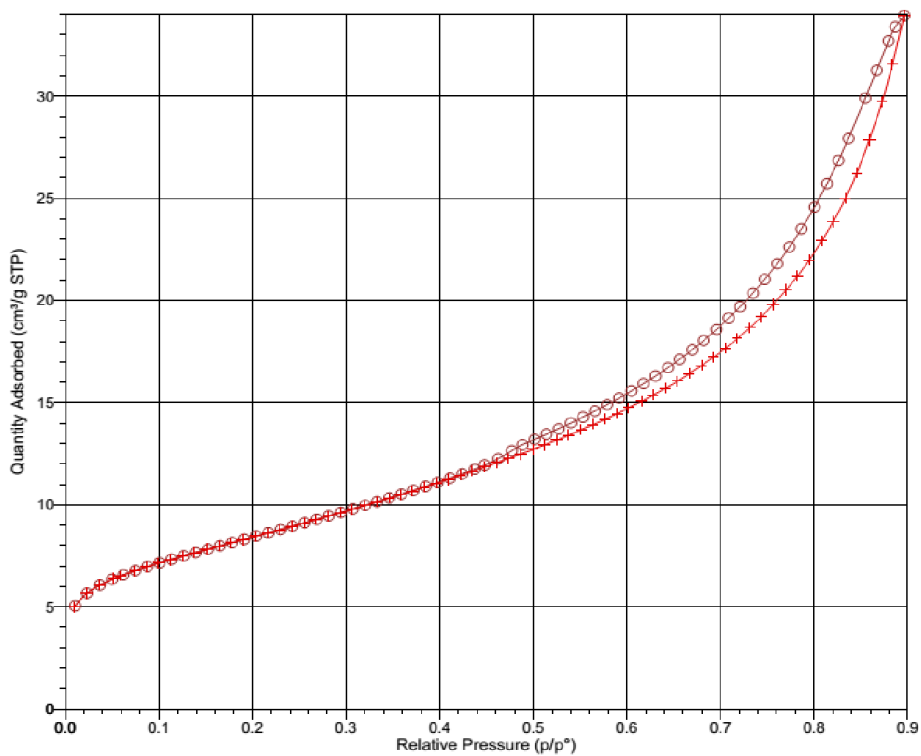


Figure A.4: Adsorption isotherm of the NCP

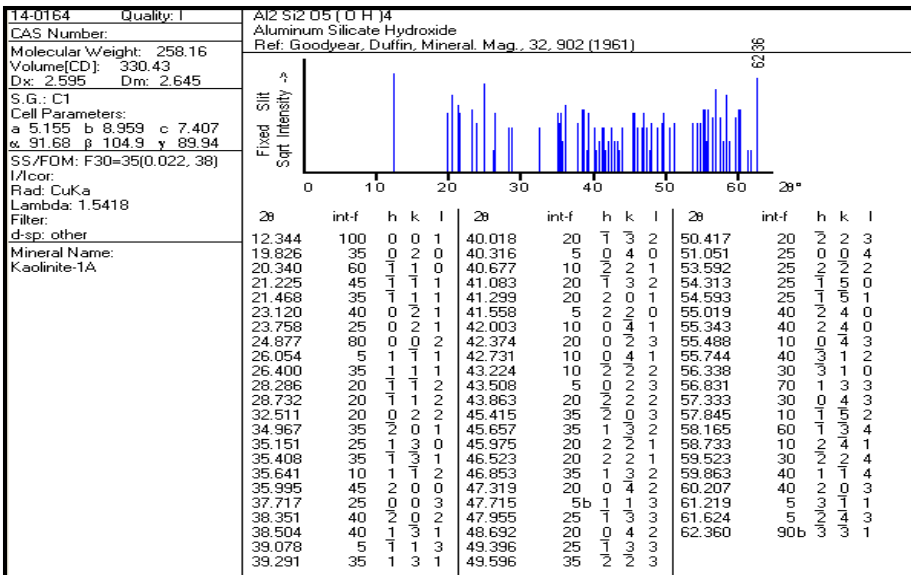
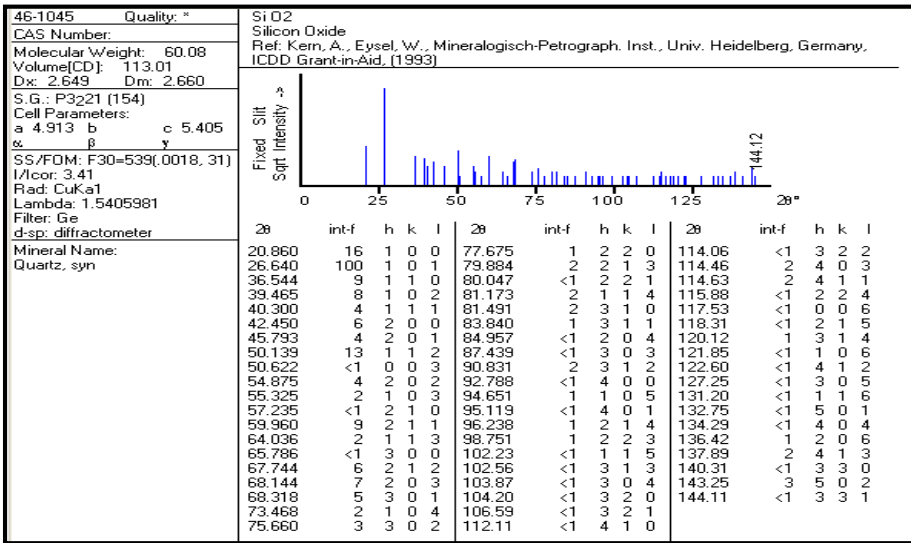
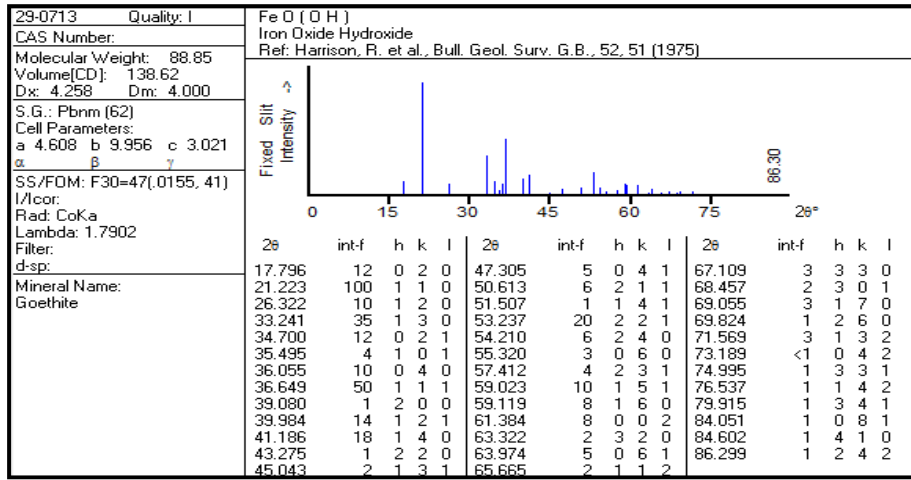


Figure A.5: JCPDS files: 29-0713, 46-1045 and 14-0164 respectively of the characterized natural clay by XRD.

VI. REFERENCES

- [1] http://www.notre-planete.info/environnement/eau/eau_contamination.php
- [2] H. Valdés, F. A. Murillo, J. A. Manoli, and C. A. Zaror, Heterogeneous catalytic ozonation of benzothiazole aqueous solution promoted by volcanic sand, *Journal of Hazardous Materials*. 153(3) (2008)1036–1042.
- [3] M. A. Gaja and J. S. Knapp, Removal of 2-Mercaptobenzothiazole by Activated Sludge: A Cautionary Note, *Journal of Water Research*. 32 (1998) 3786–3789.
- [4] J. Derco, A. Kassai, M. Melicher, J. Dudas, Removal of the 2-Mercaptobenotiazole from Model Wastewater by Ozonation, *Journal of Hindawi Publishing Corporation*, Volume 2014, Article ID 173010,7 pages. <http://dx.doi.org/10.1155/2014/173010>.
- [5] F. B. Li, X. Z. Li, K. H. Ng, Photocatalytic Degradation of an Odorous Pollutant: 2-Mercaptobenzothiazole in Aqueous Suspension Using Nd^{3+} - TiO_2 Catalysts, *Ind. Eng. Chem. Res.* 45 (2006) 1-7.
- [6] A. Allaoui, M. A. Malouki, P. Wong-Wah-Chung, Homogeneous photodegradation study of 2-mercaptobenzothiazole photocatalysed by sodium decatungstate salts: Kinetics and mechanistic pathways, *Journal of Photochemistry and Photobiology A: Chemistry*. 212 (2010) 153–160.
- [7] H. De Wever, K. De Moor, H. Verachtert, Toxicity of 2-mercaptobenzothiazole towards bacterial growth and respiration, *Appl Microbiol Biotechnol.* 42 (1994) 631-635.
- [8] B. Umamaheswari, Rama Rajaram, Microaerobic degradation of 2-Mercaptobenzothiazole present in industrial wastewater, *Journal of Hazardous Materials*. 321 (2017) 773–781.
- [9] F. B. Li, X.Z. Li, M.F. Hou, Photocatalytic degradation of 2-mercaptobenzothiazole in aqueous La^{3+} - TiO_2 suspension for odor control, *Journal of Applied Catalysis B: Environmental*. 48 (2004) 185–194.

- [10] F. B. Li, X.Z. Li, M.F. Hou, K.W. Cheah, W.C.H. Choy, Enhanced photocatalytic activity of Ce^{3+} -TiO₂ for 2-mercaptobenzothiazole degradation in aqueous suspension for odour control, *Journal of Applied Catalysis A: General*. 285 (2005) 181–189.
- [11] X. Wang, C. Liu, X. Li, F. Li, S. Zhou, Photodegradation of 2-mercaptobenzothiazole in the γ Fe₂O₃/oxalate suspension under UVA light irradiation, *Journal of Hazardous Materials*. 153 (2008) 426–433.
- [12] C. Liu, F. Li, X. Li, G. Zhang, Y. Kuang, The effect of iron oxides and oxalate on the photodegradation of 2-mercaptobenzothiazole, *Journal of Molecular Catalysis A: Chemical*. 252 (2006) 40–48.
- [13] F. Li, C. Liu, C. Liang, X. Li, L. Zhang, The oxidative degradation of 2-mercaptobenzothiazole at the interface of β MnO₂ and water, *Journal of Hazardous Materials*. 154 (2008) 1098–1105.
- [14] R. Andreozzi, V. Caprio, R. Marotta, Oxidation of benzothiazole 2-mercaptobenzothiazole and 2-hydroxybenzothiazole in aqueous solution by means of H₂O₂/UV or photoassisted Fenton systems, *Journal of Chemical Technology and Biotechnology*. 76 (2001) 196–202.
- [15] M. A. Malouki, C. Richard, A. Zertal, Photolysis of 2-mercaptobenzothiazole in aqueous medium Laboratory and field experiments, *Journal of Photochemistry and Photobiology A: Chemistry*. 167 (2004) 121–126.
- [16] A. Bunescu, P. Besse-hoggan, M. Sancelme, A. Cincilei, G. Mailhot, A.M. Delort, Microbial degradation of 2-benzothiazole derivatives: a review, *Environmental Biodegradation Research Trends*, Nova Publishers, New York, 2007.
- [17] A. J. Luna, C. A. O. Nascimento, O. Chiavone-Filho, Photodecomposition of hydrogen peroxide in highly saline aqueous medium, *Brazilian Journal of Chemical Engineering*. 23 (2006) 341–349.
- [18] S. Bahnmuller, C. H. Loi, K. L. Linge, U. V. Gunten, S. Canonica, Degradation rates of benzotriazoles and benzothiazoles under UV-C irradiation and the advanced oxidation process UV/H₂O₂, *Journal of water research*. 74 (2015) 143–154.

- [19] H. D. Burrows, M. Canle L, J. A. Santaballa, S. Steenken, *J Photochem Photobiol B Biol.* 67 (2002) 71–108.
- [20] M. Canle L, J. A. Santaballa, E. Vulliet. *J Photochem Photobiol A Chem.* (2005) 175–192.
- [21] M. Canle, M. I. Fernández Perez, J. A. Santaballa, *Current Opinion in Green and Sustainable Chemistry.* 6 (2017) 101–138.
- [22] T. Katagi, Photoinduced oxidation of the organophosphorus fungicide tolclofos-methyl on clay minerals, *J. Agric. Food Chem.* 38 (1990) 1595–1600.
- [23] D. A. Armstrong, R. E. Huiea , W. H. Koppenola , S. V. Lymara , G. Merényia , P. Netaa , B. Ruscica , D. M. Stanburyb, S. Steenkena, P. Wardman, Standard Electrode Potentials Involving Radicals in Aqueous Solution: Inorganic Radicals, *Pure Appl. Chem.* 87 (2015) 1139–1150.
- [24] E. S. Nweke, E. I. Ugwu, Analysis and Characterization of Clay Soil in Abakaliki, Nigeria, *The Pacific Journal of Science and Technology.* 8 (2007) 190–193.
- [25] J. F. Akinfolarin, O. O. Awopetu, The Effect of Sawdust on the Insulating Effect of Ikere Clay as Refractory Lining, *AU J.T.* 17 (2014) 143–147.
- [26] C. P. Dogan, K. S. Kwong, J. P. Bennet, Improved refractory materials for Slagging coal Gasifiers, in proceedings from the 27th International conference on coal utilization and fuel systems, Clearwater, Florida. 2002.
- [27] R. Loos, B.M. Gawlik, G. Locoro, E. Rimaviciute, S. Contini, G. Bidoglio, EU-wide survey of polar organic persistent pollutants in European river waters, *Environ. Pollut.* 157 (2009) 561–568.
- [28] H. Kirouani-Hanari, Microbial and photolytic degradation of benzothiazoles in water and wastewater. Thèse de l'Université de Berlin, 2003.
- [29] O.G. Vitzthum, P. Werkhoff, P. Hubert, New volatile constituents of black tea aroma, *J. Agric. Food Chem.* 23 (1975) 999–1003.
- [30] K. Anjou, E. Von Sydow, The aroma of cranberries II, *Vaccinium macrocarpon* Ait. *Acta Chem. Scand.* 21 (1967) 2067–2082.

- [31] M.A. Gaja, J.S. Knapp, The microbial degradation of benzothiazoles, *J. Appl. Microbiol.* 83 (1997) 327–334.
- [32] S.J. Choi, H.J. Park, S.K. Lee, S.W. Kim, G. Han, H.Y. Choo, Solid phase combinatorial synthesis of benzothiazoles and evaluation of topoisomerase II inhibitory activity, *Bioorg. Med. Chem.* 14 (2006) 1229–1235.
- [33] S. Hout, N. Azas, A. Darque, M. Robin, C. Di Giorgio, M. Gasquet, J. Galy, P. T. David, Activity of benzothiazoles and chemical derivatives on *Plasmodium falciparum*, *Parasitology.* 129(2004) 525–535.
- [34] H. de Wever, H. Verachter, Biodegradation and toxicity of benzothiazoles, *Water Research.* 31(1997) 2673–2684.
- [35] H. Valdés, C. A. Zaror, Ozonation of benzothiazole saturated-activated carbons: influence of carbon chemical surface properties, *Journal of Hazardous Materials.* 137 (2006) 1042–1048.
- [36] A. Kloepfer, M. Jekel, T. Reemtsma, Occurrence, sources, and fate of benzothiazoles in municipal wastewater treatment plants, *Environ. Sci. Technol.* 39 (2005) 3792–3798.
- [37] T. Reemstma, Determination of 2-substituted benzothiazoles of industrial use from water by liquid chromatography/electrospray ionization tandem mass spectrometry, *Rapid Commun. Mass Spectrom.* 14 (2000) 1612–1618.
- [38] H. De Wever, S. Weiss, T. Reemtsma et al, Comparison of sulfonated and other micropollutants removal in membrane bioreactor and conventional wastewater treatment, *Water Research.* 41 (2007) 935–945.
- [39] O. Fiehn, G. Wegener, J. Jochimsen, M. Jekel, Analysis of the ozonation of 2-mercaptobenzothiazole in water and tannery wastewater using sum parameters, liquid- and gas chromatography and capillary electrophoresis, *Water Res.* 32 (1998) 1075 – 1084.
- [40] F. B. Li, X. Z. Li, K.W. Cheah, Photocatalytic activity of neodymium ion doped TiO₂ for 2-mercaptobenzothiazole degradation under visible light irradiation, *Environ. Chem.* 2 (2005a) 130–137.

- [41] M. H. Habibi, S. Tangestaninejad, I. Mohammadpoor-Baltork, B. Yadollahi, Photocatalytic degradation of wastewater pollutants: titanium dioxide-mediated oxidation of 2-mercaptobenzothiazole, *Pollut. Res.* 20 (2001a) 295–298.
- [42] Q. Bao, L. Chen, J. Tian, J. Wang, Degradation of 2-mercaptobenzothiazole in aqueous solution by gamma irradiation, *Journal of Radiation Physics and Chemistry.* 103 (2014) 198–202.
- [43] D. Ehouman, J. S. Akpa, P. M. Niamien, D. Sissouma, A. Trokourey, Inhibition effect of 2-mercaptobenzothiazole on the corrosion of copper in 2M HNO₃, *Journal of Chemical and Pharmaceutical Research.* 8 (3) (2016) 353–364.
- [44] J. C. Marconato, L. O. Bulhoes, M. L. Temperini, A spectroelectrochemical study of the inhibition of the electrode process on copper by 2-mercaptobenzothiazole in ethanolic solutions, *Electrochimica Acta.* 43(7) (1998) 771–780.
- [45] H. Yang, Y. Sun, J. Ji, W. Song, X. Zhu, Y. Yao, Z. Zhang, 2-Mercaptobenzothiazole monolayers on zinc and silver surfaces for anticorrosion, *Corros. Sci.* 50 (2008) 3160–3167.
- [46] <https://en.wikipedia.org/wiki/Mercaptobenzothiazole>.
- [47] H. L. Bronx, C. A. Clark, Preparation of aminothiols and aminoselenols by improved alkali fusion and their derivatives, US Patent. 1963.
- [48] R. Handte, L. Willms, E. Blume, Process for the preparation of 2-mercaptobenzothiazoles. US Patent. 1984.
- [49] M. Ballabeni, R. Roberto Ballini, F. Bigi, R. Maggi, M. Parrini, G. Giovanni Predieri, G. Sartori, Synthesis of symmetrical N,N'-disubstituted thioureas and heterocyclic thiones from amines and CS₂ over a ZnO/Al₂O₃ composite as heterogeneous and reusable catalyst, *J Org Chem.* 64(1999)1029–1032.
- [50] N. Zhu, F. Zhang, G. Liu, Dynamic covalent chemistry of disulfides offers a highly efficient synthesis of diverse benzofused nitrogen-sulfur heterocycles in one pot, *J Comb Chem.* 12 (2010) 531–540.

- [51] L. Zhu, M. Zhang, Ortho-selective nucleophilic aromatic substitution reactions of polyhaloanilines with potassium/sodium O-ethyl xanthate: A convenient access to halogenated 2(3H)-benzothiazolethiones, *J Org Chem.* 69 (2004) 7371–7374.
- [52] L. Zhu, M. Zhang, M. Dai, A convenient synthesis of 2-mercapto and 2-chlorobenzothiazoles, *J Heterocycl Chem.* 42 (2005) 727–730.
- [53] W. Hung, Y. Tan, M.W. Ding, G. F. Yang, Improved synthesis of 2-(3H)benzothiazolethiones under microwave irradiation, *Synth Commun.* 37 (2007) 369–376.
- [54] H. P. Narkhede, U. B. More, D. S. Dalal, N. S. Pawar, D. H. Moore, P. P. Mahulika, Fly-ash-supported synthesis of 2-mercaptobenzothiazole derivatives under microwave irradiation, *Synth Commun.* 37 (2007) 573–577.
- [55] N.C. Chaudhuri, Convenient strategies for the preparation of modified 2(3H)-benzothiazolethiones, *Synth Commun.* 26(1996) 3783–3790.
- [56] A. Harizi, A. Romdhane, Z. Mighri, Synthesis and reactivity of benzoxa(thia)zol-2-thiones: new route to 2-alkylthiobenzoxa (thia)zoles, *Tetrahedron Lett.* 41(2000) 5833–5835.
- [57] L. Shi, X. Liu, H. Zhang, Y. Jiang, D. Ma. Synthesis of 2-thio-substituted benzothiazoles via a domino condensation/S-arylation/heterocyclization process, *J Org Chem.* 76 (2011) 4200–4204.
- [58] F. Wang, S. Cai, Z. Wang, C. Xi, Synthesis of 2-mercaptobenzothiazoles via DBU-promoted tandem reaction of o-haloanilines and carbon disulfide, *Org Lett.* 13(2011) 3202–3205.
- [59] H. Bujdakova, T. Kuchta, E. Sidoova, A. Gvozdjakova, anti-candida activity of four antifungal benzothiazoles, *FEMS Microbiol. Lett.* 112 (1993) 329–334.
- [60] J. Geier, W. Uter, A. Schnuch, J. Brasch, Diagnostic screening for contact allergy to mercaptobenzothiazole derivatives, *Am. J. Contact Dermat.* 13 (2002) 66–70.
- [61] L. S. Gold, T. H. Slone, B. R. Stern, L. Bernstein, comparison of target organs of carcinogenicity for mutagenic and non-mutagenic chemicals, *Mutat. Res.* 286(1993) 75–100.

- [62] T. Sorahan, Cancer risks in chemical production workers exposed to 2-mercaptobenzothiazole, *Occup Environ Med.* 66 (4) (2009) 269–273.
- [63] C. Graham, Chemical found in babies' dummies and condoms 'probably causes cancer, *The Telegraph*. Retrieved. 2016.
- [64] National Toxicology Program scientists (May 1988). "NTP Toxicology and Carcinogenesis Studies of 2-Mercaptobenzothiazole (CAS No. 149-30-4) in F344/N Rats and B6C3F1 Mice (Gavage Studies)". *Natl Toxicol Program Tech Rep Ser.* 332: 1–172. PMID 12732904
- [65] G. Gannes, S. Tadwalkar, A. Wong, N. Mebuke, British Columbia Fails to Meet the North American Screening Standards: What are the Implications for Workers with Allergic Contact Dermatitis? *Work Safe BC.* (2013).
- [66] H. Neves, J. Eduardo, C. Moncaup, Roberto, Kaufmann, V. W. Filho, *Rev Saude Publica.* 40 (2006)
- [67] T. Norseth, A. Andenen, J. Giltvedt, Cancer incidence in the rubber industry in Norway. *Scand j work environ health.* 9 (1983) 69-71.
- [68] M. H. Whittaker, A. M. Gebhart, T. C. Miller, F. Hammer, *Toxicol Ind Health.* 20 (2004) 149–163.
- [69] M. H. Habibi, S. Tangestaninejad, B. Yadollahi, Photocatalytic mineralisation of mercaptans as environmental pollutants in aquatic system using TiO₂ suspension, *Applied Catalysis B: Environmental.* 33 (2001) 57–63.
- [70] I. Chipinda, J. M. Hettick, R. H. Simoyi, P. D. Siegel, Oxidation of 2-mercaptobenzothiazole in latex gloves and its possible haptention pathway. *Chem. Res. Toxicol.* 20 (2007) 1084–1092.
- [71] D. Devos, H. Dewever, H. Verachtert, Parameters affecting the degradation of benzothiazoles and benzimidazoles in activated-sludge systems. *Appl. Microbiol. Biotechnol.* 39 (1993) 622–626.
- [72] V. I. Repkina, S. A. Dokudovskaya, R. A. Umrikhina, V. A. Samokhina, Maximum permissible concentrations of benzthiazole and 2-mercaptobenzothiazole while drainage water biochemical treatment, *Khimicheskaya Prom.* (1983)598–599

- [73] T. Reemtsma, O. Fiehn, G. Kalnowski, M. Jekel, Microbial transformations and biological effects of fungicide-derived benzothiazoles determined in industrial wastewater, *Environ. Sci. Technol.* 29 (1995) 478–485.
- [74] H. De Wever, P. Besse, H. Verachtert, Microbial transformations of 2-substituted benzothiazoles, *Appl Microbiol Biotechnol.* 57 (2001) 620–625.
- [75] H. De Wever, K. Vereecken, A. Stolz, H. Verachtert, Initial transformations in the biodegradation of benzothiazoles by *Rhodococcus* isolates. *Appl Environ Microbiol.* 64 (1998) 3270-3274.
- [76] P. Besse, B. Combourieu, G. Boyse, M. Sancelme, H. DeWever, A. M. Delort, *Appl Environ Microbiol.* 67(2001)1412–1417.
- [77] N. Haroune, B. Combourieu, P. Besse, M. Sancelme, A. Kloepfer, T. Reemtsma, H. De Wever, A. M. Delort, Metabolism of 2-Mercaptobenzothiazole by *Rhodococcus rhodochrous*, *Applied and environmental microbiology.* (2004) 6315–6319.
- [78] Z. Zajíčková, C. Párkányi, Photodegradation of 2-Mercaptobenzothiazole Disulfide and Related Benzothiazoles. *J. Heterocyclic Chem.* 45 (2008) 303–306.
- [79] M. Serdechnova, V. L. Ivanov, M. R. M. Domingues, D. V. Evtuguin, M. G. S. Ferreira, M. L. Zheludkevich, Photodegradation of 2-mercaptobenzothiazole and 1,2,3-benzotriazole corrosion inhibitors in aqueous solutions and organic solvents, *Journal of The Royal Society of Chemistry.* 2013, DOI: 10.1039/C4CP03867C.
- [80] C. Párkányi, A.O. Abdelhamid, Photodegradation of pesticide: photolysis of 2-mercaptobenzothiazole, *Heterocycle.* 23(1985) 2917–2926.
- [81] H. Valdés, C.A. Zaror, Advanced treatment of benzothiazole contaminated waters: comparison of O₃, AC, and O₃/AC processes, *Wat. Sci. Technol.* 52(2005) 281–288.
- [82] Z. Lu, M. He, L. Yang, Z. Ma, L. Yang, D. Wang, Y. Yan, W. Shi, Y. Liu, Z. Hua, Selective photodegradation of 2-mercaptobenzothiazole by the novel imprinted CoFe₂O₄/MWCNTs photocatalyst, *Journal of RSC Advances.* 2015, DOI: 10.1039/C5RA08795C.

- [83] M. Pera-Titus, V. García-Molina, M. A. Baños, J. Giménez, S. Esplugas, Degradation of chlorophenols by means of advanced oxidation processes: a general review, *Applied Catalysis B: Environmental*. 47 (2004) 219–256.
- [84] Handbook on Advanced Photochemical Oxidation Processes. Cincinnati, Ohio 45268, U.S. Environmental Protection Agency. US.EPA (1998).
- [85] R. Andreozzi, V. Caprio, A. Insola, R. Marotta, Advanced oxidation processes (AOP) for water purification and recovery. *Catalysis Today*. 53 (1999) 51–59.
- [86] J. R. Bolton, K. G. Bircher, W. Tumas, C. A. Tolman, Figures-of-merit for the technical development and application of advanced oxidation processes, *Pure Appl. Chem*. 73(4) (2001) 627–637.
- [87] J. J. Pignatello, Dark and photoassisted Fe^{3+} catalyzed degradation of chlorophenoxy herbicides by hydrogen peroxide, *Environ. Sci. Technol*. 26 (1992) 944–951.
- [88] O. Legrini, E. Oliveros, A. M. Braun, Photochemical Processes for Water Treatment, *Chemical Reviews*. 93 (1993) 671–698.
- [89] S. H. Bossmann, E. Oliveros, S. GÖB, S. Siegwart, E. P. Dahlen, J. R. Payawan, M. Straub, M. Wörner, A. M. Braun, New Evidence against Hydroxyl Radicals as Reactive Intermediates in the Thermal and Photochemically Enhanced Fenton Reactions, *J. Phys. Chem*. 102 (1998) 5542–5550.
- [90] W. Z. Tang, *Physicochemical Treatment of Hazardous Wastes*, CRC Press. 2004
- [91] C. P. Huang, C. Dong, Z. Tang, Advanced chemical oxidation: Its present role and potential future in hazardous waste treatment, *Waste Management*. 13 (1993) 361–377.
- [92] X. Domènech, W. F. Jardim, M. I. Litter, Blesa (para CYTED), 2001.
- [93] D. Mantzavinos, E. Lauer, R. Hellenbrand, A. G. Livingston, I. S. Metcalfe, Wet Oxidation as a Pretreatment Method for Wastewaters Contaminated by Bioresistant Organics, *Water Sci. Technol*. 36(2-3) (1997) 109–116.

- [94] F. J. Rivas, F. Beltrán, F. Carvalho, B. Acedo, B. Gimeno, Stabilized leachates: sequential coagulation–flocculation + chemical oxidation process, *Journal of Hazardous Materials B*. 116 (2004) 95–102.
- [95] M. M. B. Martín, J. A. S. Pérez, J. L. G. Sánchez, L. M. Oca, J. L. C. López, I. Oller, S. M. Rodríguez, Degradation of alachlor and pyrimethanil by combined photo-Fenton and biological oxidation, *Journal of Hazardous Materials*. 155 (2008) 342–349.
- [96] E. Chamarro, A. Marco, S. Esplugas, Use of Fenton reagent to improve organic chemical biodegradability, *Water Research*. 4(35) (2001) 1047–1051.
- [97] J. García-Montaño, L. Pérez-Estrada, I. Oller, M. I. Maldonado, F. Torrades, J. Peral, Pilot plant scale reactive dyes degradation by solar photo-Fenton and biological processes, *Journal of Photochemistry and Photobiology A: Chemistry*. 195 (2008) 205–214.
- [98] M. S. Lucas, A. A. Dias, A. Sampaio, C. Amaral, J. A. Peres, Degradation of a textile reactive Azo dye by a combined chemical–biological process: Fenton’s reagent-yeast, *Water Research*. 41(2007) 1103–1109.
- [99] S. Malato, J. Blanco, M. I. Maldonado, I. Oller, Coupling solar photo-Fenton and biotreatment at industrial scale: Main results of a demonstration plant. *Journal of Hazardous Materials*. 146 (2007) 440–446.
- [100] M. Pérez-Moya, M. Graells, L. J. D. EL Valle, E. Centelles, H. D. Mansilla, Fenton and photo-Fenton degradation of 2-chlorophenol: Multivariate analysis and toxicity monitoring, *Catalysis Today*. 124(2007) 163–171.
- [101] T. Oppenländer, *Photochemical Purification of Water and Air Advanced Oxidation Processes: Principles, Reaction Mechanisms, Reactor Concepts*, Wiley-VCH, Weinheim, 2002.
- [102] S. Canonica, L. Meunier, U. von Gunten, Phototransformation of selected pharmaceuticals during UV treatment of drinking water, *Water Res.* 42 (2008) 121–128
- [103] F.L. Rosario-Ortiz, E.C. Wert, S.A. Snyder, Evaluation of UV/H₂O₂ treatment for the oxidation of pharmaceuticals in wastewater, *Water Res.* 44 (2010) 1440–1448.

- [104] R. Salgado, V. J. Pereira, G. Carvalho, R. Soeiro, V. Gaffney, C. Almeida, V.V. Cardoso, E. Ferreira, M.J. Benoliel, T.A. Ternes, A. Oehmen, M.A.M. Reis, J.P. Noronha, Photodegradation kinetics and transformation products of ketoprofen, diclofenac and atenolol in pure water and treated wastewater, *J. Hazard. Mater.* 244–245 (2013) 516–527.
- [105] S. Cervera, S. Esplugas, *Energía.* 9 (1983)103–107.
- [106] O. M. Alfano, R. J. Brandi, A.E. Cassano, Degradation kinetics of 2,4-D in water employing hydrogen peroxide and UV radiation, *Chemical Engineering Journal.* 82 (2001) 209–218.
- [107] J. L. López, F. S. G. Einschlag, M. C. González, A. L. Capparelli, E. Oliveros, T. M. Hashem, A. M. Braun, Hydroxyl radical initiated photodegradation of 4-chloro-3,5-dinitrobenzoic acid in aqueous solution, *Journal of Photochemistry and Photobiology A: Chemistry.* 137(2000)177–184.
- [108] R. L. Cisneros, A. G. Espinoza, M. I. Litter, Photodegradation of an azo dye of the textile industry, *Chemosphere.* 48 (2002)393–399.
- [109] L. Lunar, D. Sicilia1, S. Rubio, D. Pérez-Bendito, U. Nickel, Degradation of photographic developers by Fenton's reagent: condition optimization and kinetics for metol oxidation, *Water Research.* 34 (6) (2000) 1791–1802.
- [110] W. Z. Tang, R. Z. Chen, Decolorization kinetics and mechanisms of commercial dyes by H₂O₂/Iron powder system, *Chemosphere.* 32(5) (1996) 947–958.
- [111] X. K. Zhao, G. P. Yang, Y. J. Wang, X. C. Gao, Photochemical degradation of dimethyl phthalate by Fenton reagent, *Journal of Photochemistry and Photobiology A: Chemistry.* 161(2004)215–220.
- [112] M. Litter, Introduction to Photochemical Advanced Oxidation Processes for Water Treatment, *Hdb Env. Chem.* 2 (2005) 325–366.
- [113] R. Andreozzi, V. Caprio, A. Insola, G. Longo, Photochemical degradation of benzotriazole in aqueous solution, *J. Chem. Technol. Biotechnol.* 73 (1998) 93–98.

- [114] E. Felis, D. Marciocha, J. Surmacz-Gorska, K. Miksch, Photochemical degradation of naproxen in the aquatic environment, *Water Sci. Technol.* 55 (2007) 281–286.
- [115] E. Borowska, E. Felis, K. Miksch, Degradation of sulfamethoxazole using UV and UV/H₂O₂ processes, *J. Adv. Oxid. Technol.* 18 (2015) 69–77.
- [116] P. R. Gogate, A. B. Pandit, A review of imperative technologies for wastewater treatment II: hybrid methods, *Advances in Environmental Research*.8 (2004b) 553–597.
- [117] K. Barbusinski, *Chem. Dydakt. Ekol. Metrol.* 1 (2009) 111–112.
- [118] H. Fenton, Oxidation of tartaric acid in presence of iron, *J. Chem. Soc. Trans.* 65 (1894) 899–910.
- [119] S. Goldstein, D. Meyerstein, G. Czapski, *Free Radical Biol. Med.*15 (1993) 435–445
- [120] M. Masarwa, H. Cohen, D. Meyerstein, D. L. Hickman, A. Bakac, J. H. Espenson, *J. Am. Chem. Soc.* 110 (1988) 4293–4297.
- [121] P. Wardman, L.P. Candeias, *Radiat. Res.* 145 (1996) 523–531.
- [122] C. P. Huang, C. Dong, Z. Tang, Advanced chemical oxidation: Its present role and potential future in hazardous waste treatment, *Waste Management.* 13(1993) 361–377.
- [123] E. Neyens, J. Baeyens, A review of classic Fenton's peroxidation as an advanced oxidation technique, *Journal of Hazardous Materials B.* 98 (2003)33–50.
- [124] F. Haber, J. J. Weiss, The catalytic decomposition of hydrogen peroxide by iron salts, *Proc Royal Soc London, Ser. A.* 147 (1934) 332–345.
- [125] C. Walling, T. Weil, The ferric ion catalyzed decomposition of hydrogen peroxide in perchloric acid solution, *International Journal of Chemical Kinetics.* 6 (1974)507-516.
- [126] A. Safarzadeh-Amiri, J. R. Bolton, S. R. Cater, Ferrioxalate-mediated photodegradation of organic pollutants in contaminated water, *Water Research.* 31 (4) (1997) 787–798.

- [127] A. Wang, J. Qu, H. Liu, J. Ru, Mineralization of an azo dye Acid Red 14 by photoelectro-Fenton process using an activated carbon fiber cathode, *Applied Catalysis B: Environmental*. 84 (2008) 393–399.
- [128] E. Balanosky, F. Herrera, A. Lopez, J. Kiwi, Oxidative degradation of textile waste water. Modeling reactor performance, *Water Res.* 34(2) (2000) 582–596.
- [129] R. Maciel, G. L. Sant’anna JR, M. Dezotti, Phenol removal from high salinity effluents using Fenton’s reagent and photo-Fenton reactions, *Chemosphere*. 57 (2004) 711–719.
- [130] R. G. Zepp, B. Faust, J. Hoigne, Hydroxyl radical formation in aqueous reactions (pH 3-8) of iron(II) with hydrogen peroxide, The photo-Fenton reaction, *Environ. Sci. Technol.* 26 (1992) 313–319.
- [131] B. C. Faust, J. Hoigné, Photolysis of Fe(III)-hydroxy complexes as sources of OH radicals in clouds, fog and rain, *Atmospheric Environment*. 24A(1)(1990)79–89.
- [132] D. S. Bhatkhande, S. P. Kamble, S. B. Sawant, V. G. Pangarkar, Photocatalytic and photochemical degradation of nitrobenzene using artificial ultraviolet light, *Chemical Engineering Journal*. 102 (2004) 283–290.
- [133] A. L. N. Mota, Desenvolvimento de um reator fotoquímico aplicável no tratamento de efluentes fenólicos presentes na indústria do petróleo, 99f. Dissertação de Mestrado. Programa de Pós-graduação em Engenharia Química da Universidade Federal do Rio Grande do Norte, Natal, 2005.
- [134] J. DE Laat, G. T. Le, B. Legube, A comparative study of the effects of chloride, sulfate and nitrate ions on the rates of decomposition of H_2O_2 and organic compounds by Fe(II)/ H_2O_2 and Fe(III)/ H_2O_2 , *Chemosphere*. 55(2004) 715–723.
- [135] V. Nadtochenko, J. Kiwi, Photo induced mineralization of xylydine by the Fenton reagent. 2. Implications of the precursors formed in the dark, *Environ. Sci. Technol.* 32 (21)(1998) 3282–3285.
- [136] A. Machulek JR, J. E. F. Moraes, C. Vautier-Giongo, C. A. Silverio, L. C. F. Friedrich, C. A. O. Nascimento, M. C. Gonzalez, F. H. Quina, Abatement of the

Inhibitory Effect of Chloride Anions on the Photo-Fenton Process, *Environ. Sci. Technol.* 41(24)(2007) 8459–8463.

[137] J. Blanco, S. Malato, P. Fernández, A. Vidal, A. Morales, P. Trincado, J. C. Oliveira, C. Minero, M. Musci, C. Casalle, M. Brunotte, S. Tratzky, N. Dischinger, K. H. Funken, C. Sattler, M. Vincent, M. Collares-Pereira, J. F. Mendes, C. M. Rangel, Compound parabolic concentrator technology development to commercial solar detoxification applications, *Solar Energy.* 67 (4–6)(1999) 317–330.

[138] R. Dillert, A. E. Cassano, R. Goslich, D. Bahnemann, Large scale studies in solar catalytic wastewater treatment, *Catalysis Today.* 54(1999)267–282.

[139] W. Gernjak, M. Fuerhacker, P. Fernández-Ibañez, J. Blanco, S. Malato, Solar photo-Fenton treatment Process parameters and process control, *Applied Catalysis B: Environmental.* 64(2006)121–130.

[140] M. Kositzki, I. Poullos, S. Malato, J. Cáceres, A. Campos, Solar photocatalytic treatment of synthetic municipal wastewater, *Water Research.* 38 (2004)1147–1154.

[141] S. Malato, J. Blanco, A. Vidal, C. Richter, Photocatalysis with solar energy at a pilot-plant scale: an overview, *Applied Catalysis B: Environmental.* 37(2002)1–15.

[142] S. Malato, J. Blanco, A. Camposa, J. Cáceres, C. Guillard, J. M. Herrmann, A. R. Fernández-Alba, Effect of operating parameters on the testing of new industrial titania catalysts at solar pilot plant scale, *Applied Catalysis B: Environmental.* 42(2003) 349–357.

[143] F. A. A. Momani, A. T. Shawaqfeh, M. S. Shawaqfeh, Solar wastewater treatment plant for aqueous solution of pesticide, *Solar Energy.* 81(10)(2007) 1213–1218.

[144] F. J. Benitez, J. L. Acero, F. J. Real, F. J. Rubio, A. I. Leal, The role of hydroxyl radicals for the decomposition of p-hydroxy phenylacetic acid in aqueous solutions, *Wat. Res.* 35(5) (2001) 1338–1343.

[145] H. Gallard, J. DE Laat, B. Legube, Influence du pH sur la vitesse d'oxydation de composés organiques par Fe(II)/H₂O₂, Mécanismes réactionnels et modélisation. *New J. Chem.* (1998) 263–268.

- [146] S. H. Lin, C. C. Lo, Fenton process for treatment of desizing wastewater, *Water Research*. 31(8)(1997) 2050-2056.
- [147] S. Parra, V Sarria, S, Malato, P. Peringer, C. Pulgarin, Photochemical versus coupled photochemical-biological flow system for the treatment of two biorecalcitrant herbicides: metobromuron and isoproturon, *Appl. Catal. B*. 27 (3) (2000) 153-168.
- [148] A.M.F.M. Guedes, L. M. P. Madeira, R. A. R. Boaventura, C.A.V. Costa, Fenton oxidation of cork cooking wastewater-overall kinetic analysis, *Water Research*. 37 (2003)3061–3069.
- [149] J. H. Ramirez, M. Lampinen, M.A. Vicente, C.A. Costa, L.M. Madeira, Experimental design to optimize the oxidation of Orange II dye solution using a clay-based Fenton-like catalyst *Ind. Eng. Chem. Res.* 47 (2008) 284–294.
- [150] H. Hassan, B.H. Hameed, Fe–clay as effective heterogeneous Fenton catalyst for the decolorization of Reactive Blue 4 *Chem. Eng. J.* 171 (2011) 912–918.
- [151] S. Parra, L. Henao, E. Mielczarski, J. Mielczarski, P. Albers, E. Suvorova, J. Guindet, J. Kiwi, Synthesis, testing, and characterization of a novel Nafion membrane with superior performance in photoassisted immobilized Fenton catalysis, *Langmuir* 20 (2004) 5621–5629.
- [152] M.M. Cheng, W.H. Ma, J. Li, Y.P. Huang, J.C. Zhao, Y.X. Wen, Y.M. Xu, *Environ.Sci. Technol.* 38 (2004) 1569–1575.
- [153] M. Aleksic, H. Kusic, N. Koprivanac, D. Leszczynska, A.L. Bozic, Heterogeneous Fenton Type Processes for the Degradation of Organic Dye Pollutant in Water-The Application of Zeolite Assisted AOPs, *Desalination* 257 (2010) 22–29.
- [154] A. N. Soon, B.H. Hameed, Heterogeneous catalytic treatment of synthetic dyes in aqueous media using Fenton and photo-assisted Fenton process, *Desalination* 269 (2011) 1–16.
- [155] M. Kasiri, H. Aleboyeh, A. Aleboyeh, Degradation of Acid Blue 74 using Fe-ZSM5 zeolite as a heterogeneous photo-Fenton catalyst *Appl. Catal. B: Environ.* 84 (2008) 9–15.

- [156] J.Y. Feng, X.J. Hu, P.L. Yue, H.Y. Zhu, G.Q. Lu, *Chem. Eng. Sci.* 58 (2003) 679–685
- [157] A. Khataee, F. Salahpour, M. Fathinia, B. Seyyedi, B. Vahid, Iron rich laterite soil with mesoporous structure for heterogeneous Fenton-like degradation of an azo dye under visible light, *Journal of Industrial and Engineering Chemistry*. 26 (2015) 129–135.
- [158] J. An, L. Zhu, Y. Zhang, H. Tang, Efficient visible light photo-fenton-like degradation of organic pollutants using in situ surface-modified BiFeO₃ as a catalyst, *J. Environ. Sci.* 25 (2013) 1213–25.
- [159] C.C. Amorim, M. Leão, R.F. Moreira, J.D. Fabris, A.B. Henriques, Performance of Blast Furnace Waste Water Azo Dye Degradation Through Photo-Fenton-Like Process. *Chem. Eng. J.* 224 (2013) 59–66.
- [160] F.L.Y. Lam, X. Hu, A high performance bimetallic catalyst for photo-Fenton oxidation of Orange II over a wide pH range, *Catal. Commun.* 8 (2007) 2125–2129.
- [161] N.N. Fathima, R. Aravindhan, J.R. Rao, B.U. Nair, Dye house wastewater treatment through advanced oxidation process using Cu-exchanged Y zeolite: A heterogeneous catalytic approach, *Chemosphere*. 70 (2008) 1146–1151.
- [162] M. Kasiri, A. Khataee, Photooxidative decolorization of two organic dyes with different chemical structures by H₂O₂/UV process: experimental design. *Desalination* 270 (2011) 151–159.
- [163] E. Garrido-Ramirez, B. Theng, M. Mora, Clays and oxide minerals as catalysts and nanocatalysts in Fenton-like reactions - A review, *Appl. Clay Sci.* 47 (2010) 182–192.
- [164] N. Latifi, A. Marto, A. Eisazadeh, Structural characteristics of laterite soil treated by SH-85 and TX-85 (non-traditional) stabilizers *Electron, J. Geotech. Eng.* 18 (2013) 1707–1718.
- [165] C. Cornu, J. L. Bonardet, S. Casale et al, Identification and location of iron species in Fe/SBA-15 catalysts: interest for catalytic Fenton reaction, *Journal of Physical Chemistry C*. 116(5) (2012)3437–3448.

- [166] C. Walling, Fenton's reagent revisited, *Accounts of Chemical Research*. 8(4) (1975) 125–131.
- [167] A. Bozzi, T. Yuranova, J. Mielczarski, J. Kiwi, Evidence for immobilized photo-Fenton degradation of organic compounds on structured silica surfaces involving Fe recycling, *New Journal of Chemistry*. 28 (4) (2004) 519–526.
- [168] B. Boye, M.M. Dieng, E. Brillas, Degradation of herbicide 4-chlorophenoxyacetic acid by advanced electrochemical oxidation methods. *Environmental Science & Technology*. 36(13)(2002)3030–3035.
- [169] E. Brillas, M. A. Baños, and J. A. Garrido, Mineralization of herbicide 3,6-dichloro 2-methoxybenzoic acid in aqueous medium by anodic oxidation, electro-Fenton and photoelectro-Fenton, *Electrochimica Acta*. 48(12) (2003)1697–1705.
- [170] N. Bouziane, Elimination du 2-MBT Par voies Photochimique et Par Adsorption sur la Bentonite et le charbon actif en Poudre, *Mémoire du magister, Université Mentouri de Constantine*. 2007.
- [171] P. Jing, M. Hou, P. Zhao, X. Tang, H. Wan, Adsorption of 2-mercaptobenzothiazole from aqueous solution by organo-bentonite, *Journal of Environmental Sciences*. 25(6) (2013) 1139–1144.
- [172] A. Aarfane, A. Salhi, M. El Krati, S. Tahiri, M. Monkade, E.K. Lhadi, M. Bensitel, Etude cinétique et thermodynamique de l'adsorption des colorants Red195 et Bleu de méthylène en milieu aqueux sur les cendres volantes et les mâchefers (Kinetic and thermodynamic study of the adsorption of Red195 and Methylene blue dyes on fly ash and bottom ash in aqueous medium), *J. Mater. Environ. Sci.* 5 (6) (2014) 1927–1939.
- [173] K. Lal, A. Garg, Utilization of Dissolved Iron as Catalyst During Fenton-Like Oxidation of Pretreated Pulp Mill Effluent, *Process Safety and Environment Protection*. DOI: <http://dx.doi.org/10.1016/j.psep.2017.09.005>.
- [174] S. K. Cole, W. J. Cooper, R. V. Fox, P. R. Gardinali, S. P. Mezyk, B. J. Mincher, K. E. O'Shea, Free radical chemistry of disinfection byproducts. 2. Rate constants and degradation mechanisms of trichloronitromethane (chloropicrin), *Environmental Science and Technology*. 41(2007) 863–869.

- [175] C. W. Yang, D. Wang, Q. Tang, The synthesis of NdFeB magnetic activated carbon and its application in degradation of azo dye methyl orange by Fenton-like process, *J. Taiwan Inst. Chem. Eng.* 45 (2014) 2584–2589.
- [176] Y. Sun, J. J. Pignatello, Chemical treatment of pesticide wastes. Evaluation of iron(III) chelates for catalytic hydrogen peroxide oxidation of 2,4-D at circumneutral pH. *J. Agric. Food Chem.* 40 (1992) 322–327.
- [177] Y. Sun, J. J. Pignatello, Organic intermediates in the degradation of 2,4 dichlorophenoxyacetic acid by iron(3+)/hydrogen peroxide and iron(3+)/hydrogen peroxide/UV. *J. Agric. Food Chem.* 41 (1993a) 1139–1142.
- [178] Y. Sun, J. J. Pignatello, Photochemical reactions involved in the total mineralization of 2,4-D by $\text{Fe}^{3+}/\text{H}_2\text{O}_2/\text{UV}$, *Environ. Sci. Technol.* 27 (1993b) 304–310.
- [179] M. R. A. Silva, A. G. Trovó, R. F. P. Nogueira, Degradation of the herbicide tebuthiuron using solar photo-Fenton process and ferric citrate complex at circumneutral pH, *J. Photochem. Photobiol. A* 191(2007) 187–192.
- [180] N. Wanga, T. Zheng, G. Zhang, P. Wang, A review on Fenton-like processes for organic wastewater treatment, *Journal of Environmental Chemical Engineering.* 4 (2016) 762–787.
- [181] R. A. Torres, C. Petrier, E. Combet, F. Moulet, C. Pulgarin, Bisphenol A mineralization by integrated ultrasound-UV-iron (II) treatment, *Environ. Sci. Technol.* 41 (2006) 297–302.
- [182] E. M. Rodriguez, B. Nunez, G. Fernandez, F. J. Beltran, Effects of some carboxylic acids on the Fe(III)/UVA photocatalytic oxidation of muconic acid in water, *Applied Catalysis B: Environmental.* 89 (2009) 214–222.
- [183] M. Taxiarchou, D. Panyas, I. Douni, I. Paspaliaris, A. Kontopoulos, Removal of iron from silica sand by leaching with oxalic acid, *Hydrometallurgy.* 46 (1997) 215–227.
- [184] M. A. Blesa, H. A. Marinovich, E. C. Baumgartner, A. J. G. Maroto, Mechanism of dissolution of magnetite by oxalic acid–ferrous ion solutions, *Inorg. Chem.* 26 (1987) 3713–3717.

- [185] Z. Zajíčková, C. Zajíčková, Monitoring of Photodegradation Process of Various Benzothiazoles by HPLC and UV Spectrometry: Application of LC-MS in Photoproduct Identification, *Journal of Liquid Chromatography & Related Technologies*. 32 (2009)1032–1043.
- [186] E. Borowska, E. Felis, J. Kalka, Oxidation of benzotriazole and benzothiazole in photochemical processes: Kinetics and formation of transformation products, *Chemical Engineering Journal*. 304 (2016) 852–863.
- [187] N. Jamil, N. Ahsan, M.A. Munawar, J. Anwar, U. Shafique, Removal of toxic dichlorophenol from water by sorption with chemically activated carbon of almond shells: a green approach, *J Chem Soc Pak*. 33 (2011) 640–645.
- [188] K. Kuśmierk, A. Świątkowski, The influence of different agitation techniques on the adsorption kinetics of 4-chlorophenol on granular activated carbon, *Reac Kinet Mech Cat*. 116 (2015) 261–271.
- [189] S. Fan, Y. Wang, Z. Wang, J. Tang, J. Tang, X. Li, Removal of methylene blue from aqueous solution by sewage sludge-derived biochar: Adsorption kinetics, equilibrium, thermodynamics and mechanism, *JECE* 1378. <http://dx.doi.org/doi:10.1016/j.jece.2016.12.019>.
- [190] L. Liu, Y. Lin, Y. Liu, H. Zhu, Q. He, Removal of methylene blue from aqueous solutions by sewage sludge based granular activated carbon: Adsorption equilibrium, kinetics, and thermodynamics, *J. Chem. Eng. Data*. 58 (2013) 2248–2253.
- [191] X. Guan, H. Fan, S. Yan, J. Chang, Chromium(VI) concurrent detoxification and immobilization by gallate: kinetics, equilibrium, thermodynamics, and mechanism studies, *JECE* 1917. <https://doi.org/10.1016/j.jece.2017.10.007>.
- [192] A. B. Pérez Marín, M.I. Aguilar, V.F. Meseguer, J.F. Ortuño, J. Sáez, M. Lloréns, Biosorption of chromium (III) by orange (*Citrus cinensis*) waste: Batch and continuous studies, *Chem. Eng. J*. 155 (2009) 199–206.
- [193] A. Khataee, F. Salahpour, M. Fathinia, B. Seyyedi, B. Vahid, Iron rich laterite soil with mesoporous structure for heterogeneous Fenton-like degradation of an azo dye under visible light, *Journal of Industrial and Engineering Chemistry*. 26 (2015) 129–135.

- [194] F. V. F. Araujo, L. Yokoyama, L. A. C. Teixeira, J. C. Campos, Heterogeneous Fenton process using the mineral hematite for the discolouration of a reactive dye solution, *Brazilian Journal of Chemical Engineering*. 28 (04) (2011) 605 – 616.
- [195] S. Kong, R. Watts, J. Choi, Treatment of petroleum contaminated soils using iron mineral catalyzed hydrogen peroxide, *Chemosphere*. 37 (1998) 1473–1482.
- [196] W. Huang. M. Brigante. F. Wu. K. Hanna. G. Mailhot, Effect of ethylenediamine-N,N'-disuccinic acid on Fenton and photo-Fenton processes using goethite as an iron source: optimization of parameters for bisphenol A degradation, *Environ Sci Pollut Res*. 20 (2013) 39–50.
- [197] D. M. Sherman and T. D. Waite. Electronic spectra of Fe³⁺ oxides and oxide hydroxides in near IR to near UV, *American Mineralogist*. 70 (1985) 1262–1269.
- [198] C. Martinez, M. Canle L, M. I. Fernandez, J. A. Santaballa , J. Faria, Kinetics and mechanism of aqueous degradation of carbamazepine by heterogeneous photocatalysis using nanocrystalline TiO₂, ZnO and multi-walled carbon nanotubes–anatase composites, *Appl Catal B Environ*. 102 (2011) 563–571.

PUBLISHED PAPER



Simulated sunlight photodegradation of 2-mercaptobenzothiazole by heterogeneous photo-Fenton using a natural clay powder

Z. Redouane-Salah^{a,b,**}, M.A. Malouki^b, B. Khennaoui^a, J.A. Santaballa^c, M. Canle^{c,*}

^a Laboratoire des Techniques Innovantes de Préservation de l'Environnement, Université Constantine 1, Algeria

^b Département des Sciences de la Matière, Center Universitaire de Tamanrasset, Algeria

^c Chemical Reactivity & Photoreactivity Group (REACTI), Department of Chemistry, Faculty of Sciences & CICA, University of A Coruña, E-15071 A Coruña, Spain

ARTICLE INFO

Keywords:

MBT
Heterogeneous photo-Fenton process
Natural clay powder (NCP)
Photodegradation
Hydroxyl radical
Reaction mechanism

ABSTRACT

The efficiency of 2-mercaptobenzothiazole (MBT) degradation by heterogeneous photo-Fenton process using local natural clay powder (NCP) is described. Experiments were conducted at natural pH with a batch reactor equipped with a medium-pressure Hg lamp emitting mainly at 366 nm. The natural clay was characterized by SEM-EDS, UV-vis diffuse reflectance spectroscopy, XRF and XRD analysis. The specific BET surface area of the clay was $30.2 \text{ m}^2 \text{ g}^{-1}$. The photodegradation of MBT follows first order (for direct photolysis) and pseudo-first order kinetics (for photocatalysis). Direct photolysis of MBT showed a negligible effect both upon 254 and 365 nm irradiation, while 42.5% and 62% of MBT was eliminated in three hours under 310 nm irradiation in the presence of H_2O_2 and under sunlight irradiation (using NCP), respectively. Kinetic runs carried out with $5.0 \cdot 10^{-5} \text{ M}$ MBT and 0.5 g L^{-1} clay showed both higher MBT conversion and photodegradation rate at basic pH (10) and in oxygen saturated media. The presence of oxalic acid and H_2O_2 significantly enhanced MBT photodegradation. The photodegradation of MBT is mainly attributed to reaction with $\text{HO}\cdot$, leading to different intermediates that have been identified by HPLC-MS. A reaction mechanism is proposed. The highest TOC removals were obtained using UVA at low pHs (2.6), and in the absence of O_2 with 68% and 65% TOC removal respectively in two hours, whereas MBT transformation is faster ($t_{1/2} = 7 \text{ min}$) and higher (90%) at pH = 10. The obtained results strongly support the use of natural clay rich in iron oxides as inexpensive, clean and efficient photocatalysts for water pollutants abatement using heterogeneous photo-Fenton process.

1. Introduction

2-Mercaptobenzothiazole or benzothiazolethiol (MBT) is one of the most important members of the benzothiazoles family [1]. This synthetic xenobiotic, found as the corresponding sodium, potassium and zinc salts, is used as biocide. MBT is also an important chemical additive, used as a vulcanization accelerator in the tire industry [2], and widely used in the synthesis of a variety of products, such as antibiotics or rubber [3], but also as a preservative or as anticorrosion agent for copper [4], zinc or silver [5].

MBT is an odorous, toxic and poorly biodegradable chemical [6]. It has been detected in wastewater effluents, sewage treatment plants, road drainage and surface waters [7]. A number of studies have confirmed that MBT shows toxic effects on aquatic organisms, and is an allergen and potential mutagen for humans [6], with a non-negligible impact on the environment [8].

The photocatalytic degradation of MBT in aqueous solution using:

$\text{La}^{3+}\text{-TiO}_2$, $\text{Ce}^{3+}\text{-TiO}_2$ and $\gamma\text{-Fe}_2\text{O}_3/\text{Oxalate}$ under UV irradiation has been reported by Li et al. [9,10] and Wang et al. [11], respectively. The effect of iron oxides and oxalate on the photodegradation of MBT has been studied by Chengshuai Liu et al. [12]. The oxidative degradation of MBT at the interface of $\beta\text{-MnO}_2$ and water was reported by Fangbai Li et al. [13], the results showing that MBT was effectively degraded and mineralized into SO_4^{2-} and NO_3^- by $\beta\text{-MnO}_2$. Andreozzi et al. reported the oxidation of MBT in aqueous solution using $\text{H}_2\text{O}_2/\text{UV}$ and Fe^{3+} -photoassisted Fenton techniques in the pH range 3.0–8.0 [14]. Malouki et al. [2] found that the deprotonated form of MBT is 10 times more reactive than its molecular form toward direct photolysis at 313 nm. MBT was photoconverted into benzothiazole (BT) and 2-hydroxybenzothiazole (2-HOBT) when irradiated in aerated medium, with a photoconversion yield of 0.02. Moreover, the authors compared the disappearance of MBT in Milli-Q water at pH = 8 and lake water, finding that the disappearance of MBT was four times faster in natural water, showing the synergistic effect of the matrix [2,15]. Recently,

* Corresponding author.

** Corresponding author at: Département des Sciences de la Matière, Center Universitaire de Tamanrasset, Algeria.

E-mail addresses: z.rsalah@umc.edu.dz (Z. Redouane-Salah), mcanle@udc.es (M. Canle).

<https://doi.org/10.1016/j.jece.2018.02.011>

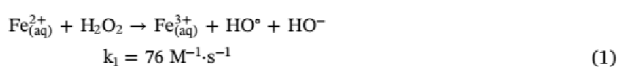
Received 15 October 2017; Received in revised form 3 February 2018; Accepted 8 February 2018

Available online 13 February 2018

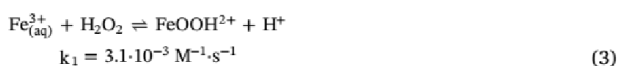
2213-3437/ © 2018 Elsevier Ltd. All rights reserved.

Allaoui et al. [8] studied the homogeneous photochemical degradation of MBT in the presence of decatungstate anion (DTA) in aqueous solution, observing an increase of photodegradation, in the presence of DTA, by a factor of six as compared to direct photolysis.

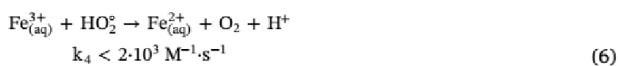
Considering the persistence of MBT in the environment, its confirmed toxicity and low biodegradability, we focused our study on the ability of simulated sunlight to degrade it in the presence of natural clay – as a source of iron – and of hydrogen peroxide. This type of reaction, known as heterogeneous photo-Fenton process, has demonstrated remarkable performance in the treatment of wastewater containing toxic or non-biodegradable organic compounds [16]. The core of the process is the production of hydroxyl radical (HO·) by interaction between iron species and UV light. This radical species is well-known as highly effective and unselective in the degradation of persistent organic pollutants [17–20]. H₂O₂/Fe²⁺ mixtures show very powerful oxidizing properties in acidic medium, which is generally explained in terms of the generation of hydroxyl radicals, as in Eqs. (1)–(4): [21,22]



Under appropriate acidity conditions (pH ca. 2.7–2.8) Fe³⁺ is regenerated:



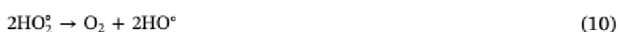
And HO₂· can also produce Fe²⁺:



In the presence of light (λ ≥ 300 nm), Fe³⁺ complexes can regenerate Fe²⁺:



On the other hand, UVA irradiation of clays may also yield different reactive oxygen species (ROS), as in Eqs. (8)–(12) [23].



The different generated ROS, and specially HO·, the strongest oxidant possibly found in aqueous environment (E°(HO·, H⁺/H₂O) = 2.73 V vs. NHE) [24], are highly oxidative and may react with essentially any persistent organic pollutant, due to their high oxidation potential.

Clays are abundant fine-grained components of geological materials, produced by the weathering and disintegration of granite and feldspathic rocks [25]. These anhydrous complex compounds are composed of alumina (Al₂O₃) and silica (SiO₂), and contain varied amounts of impurities of iron, organic matters and residual minerals [26,27]. Clays usually have diameters ranging from a few microns to a few hundredths of a micron, and tend to show large surface areas and adsorption capacities.

To the best of our knowledge detailed studies on UV/H₂O₂/clay processes using natural clays as heterogeneous photocatalysts for degradation of MBT have not been reported. The aim of this work is to assess the potential of the heterogeneous photo-Fenton process [28] for the removal of MBT from aqueous media using a cheap and abundant natural resource as a photocatalyst in the presence of hydrogen peroxide under simulated sunlight irradiation.

2. Experimental

2.1. Materials

All chemicals used in this study were of the highest quality commercially available and used without any further purification. 2-Mercaptobenzothiazole (MBT, benzothiazolethiol, m.p. 178–181 °C) was purchased from *Fluka* (99% purity). *tert*-Butanol (99.5% purity) from *Janssen Chimica*. Hydrogen peroxide 33% (w/v) and potassium hydroxide (85%) were purchased from *Panreac*, and perchloric acid (65%) from *Carlo Erba*. Natural clay was obtained from El-Hoggar region, city of Tamanghasset in the south of Algeria, and used without any previous chemical treatment except for appropriate grinding and sieving (80 meshes of diameter sieve). Milli-Q water was obtained from a Millipore device with a resistivity of 18.2 MΩ cm at 298 K, used for HPLC analyses. Solutions were prepared with distilled water. pH was adjusted by adding KOH or HClO₄ solution and controlled using a *Hanna* pH-meter. De-oxygenation of solutions was performed by bubbling Argon gas was ALPHAGAZ™ 1 brand from Air Liquide with a maximum impurity level of H₂O < 3, C_nH_m < 0.5 (both in 140 ppm vol.) and O₂ < 2 ppm vol. Ar gas is N50 compliant, which guarantees a minimum purity of 99.9992% (mol); it was used during all irradiation time, at room temperature, ca. 298.0 ± 0.1 K.

2.2. Characterisation of the natural clay

The natural clay mineral, with a yellowish-brownish colour was crushed into small particles (powder) of less than 80 mesh, and then micrographed by scanning electron microscopy (SEM) to verify its morphology. Some random areas were analysed by energy dispersive X-ray spectroscopy (EDS) for quantitative chemical composition analysis of the surface. The chemical composition of the clay was determined by X-ray fluorescence (XRF) analysis; data were obtained using a 4 kW wavelength dispersion X-ray fluorescence spectrometer, model S4 Pioneer (Bruker-AXS). The evaluation of results was done using SpectraPlus software v. 1.70 (Socabim). X-ray diffraction spectra measurements were performed using a Siemens-Bruker D5000 diffractometer, with Bragg-Brentano geometry and Theta/2-Theta configuration, equipped with graphite monochromator, and a scintillation counter detector. Data collection was carried out from 5 to 80° with a step size of 0.05° and an acquisition time of 2.5 s. Data processing software was DiffracPlus v. 8.0.0.2 (Socabim).

The optical properties of the natural clay mineral were determined by UV–vis diffuse reflectance spectroscopy using Evolution 260 Bio Thermo Scientific spectrophotometer. The sample was dispersed in distilled water at neutral pH to give a colloidal suspension, and the spectra were obtained using a 1 cm path length quartz cell.

The BET specific surface area and pore distribution of the sample were determined by N₂ adsorption-desorption isotherms using a Micromeritics TriStar II Plus instrument at the temperature of liquid nitrogen (77.4 K). The control, acquisition and data processing software was Microactive for Tristar II Plus, v. 2.03 (Micromeritics).

2.3. Irradiation experiments

Irradiation experiments were carried out in a Pyrex glass photo-reactor (200 mL), as shown in Fig. 1, open to the air. The light source was a Heraeus medium-pressure Hg lamp TQ 150, cooled by water

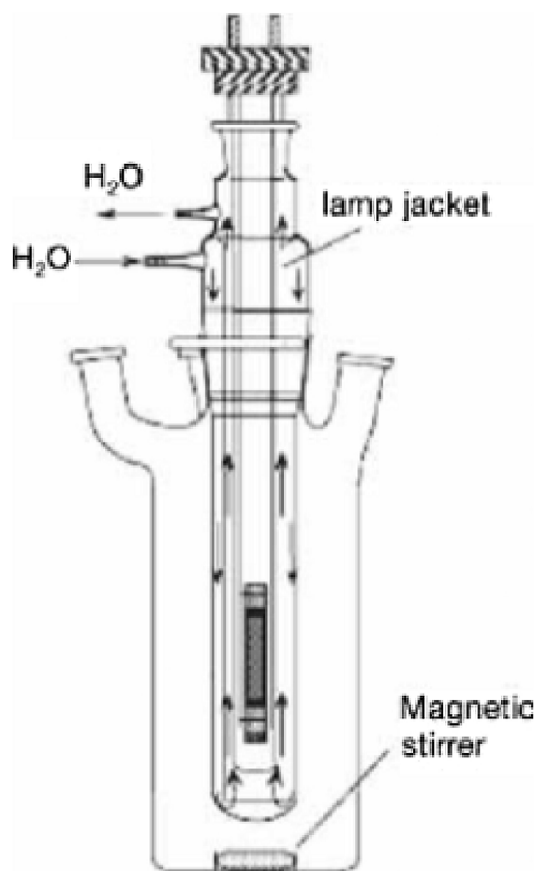


Fig. 1. Photoreactor configuration.

circulation to 298.0 ± 0.1 K. The irradiation spectrum was cut off below 366 nm using a Duran 50 glass jacket. The photon flux at 366 nm was $2.38 \cdot 10^{-6}$ Einstein s^{-1} .

In the degradation experiments, 0.5 g L^{-1} of the natural clay powder (NCP) were added to a $5.0 \cdot 10^{-5} \text{ M}$ (8.36 mg L^{-1}) MBT solution and stirred magnetically for 15 min to allow for the adsorption–desorption equilibrium to be established. The lamp was warmed up before inserting it in the reaction medium and starting the photodegradation experiment. The first sample was taken at the end of the dark adsorption period, just before the lamp was inserted, in order to determine the starting concentration of the compound in solution, which was taken as C_0 for each experiment. Then, the suspensions were irradiated at constant stirring speed. During the irradiation, discrete samples of the suspension were collected at regular times for analysis. To remove the suspended clay, the samples were centrifuged at 16,000 rpm for five min using a Nahita centrifuge. The effect of the main operational parameters, including MBT and H_2O_2 concentration, initial pH and clay dosage on the degradation rate were investigated.

2.4. Analytical procedure

2.4.1. UV–visible spectroscopy analysis

After centrifugation of the sample, the clean transparent solutions were analysed. The photodegradation process was monitored by the change in concentration of MBT, following the UV/vis change in the characteristic bands of MBT as a function of irradiation time. Absorption spectra were registered using a double beam UV–vis spectrophotometer (Libra Biochrom) covering 190–1100 nm. Measurements were made at $\lambda_{\text{max}} = 320$ nm of MBT solution at natural pH, using

quartz cells of 1 cm optical path length.

2.4.2. HPLC analysis

MBT was also monitored using HPLC instrument with P4000 pump, AS3000 Auto Sampler and spectra system UV6000LP detector. The mobile phase was MeOH/Milli-Q water 60:40 ratio, the detection wavelengths were at $\lambda = 280$ and 320 nm. Separation was carried out using KROMAPHASE C18 column ($150 \times 4.6 \text{ mm} \times 5 \mu\text{m}$) at a flow rate of 1 mL min^{-1} .

2.4.3. HPLC–MS analysis

Identification of photoproducts was carried out by HPLC–MS, using a Thermo Scientific, LTQ Orbitrap Discovery apparatus, equipped with an electrospray interface operating in positive ion mode (ESI+). A Phenomenex Kinetex XB-C18 ($100 \text{ mm} \times 2.10 \text{ mm}$, $2.6 \mu\text{m}$) column was used. The analyses were carried out using full-scan data dependent MS scanning from m/z 50 to 400. The structures of the photoproducts were proposed by interpretation of their corresponding MS spectra.

2.4.4. TOC analysis

Total organic carbon (TOC) was quantified using a Shimadzu TOC-5000 Analyzer. TOC removal efficiency was calculated based on its initial value.

3. Results and discussion

3.1. Characterization of the natural clay

3.1.1. SEM-EDS

The morphology of the clay sample as revealed by SEM shows irregular shapes, with agglomerates of ca. $1 \mu\text{m}$, composed of fine long crystal nanometric needles, observed with typical size 200 nm length \times 20 nm width, as shown in Fig. 2 (Fig. S1, Supporting information). The observed edges are compatible with orthorhombic crystals.

Randomly taken EDS analyses of the raw sample indicate the presence of aluminium (6.83%), silicon (8.38%), calcium (1.38%), titanium (0.63%) phosphorus (0.36%), oxygen (34.3%) and iron (48.1%). The amount of Fe and O could suggest the clay may be composed of either iron oxide Fe_2O_3 or iron hydroxide $-\text{FeOOH}$. The Si/Al ratio ca. 1.2 points to a rather weathered clay, reflecting a high Si-loss, which is in agreement with goethite ($\alpha\text{-FeOOH}$) or hematite ($\alpha\text{-Fe}_2\text{O}_3$).

3.1.2. BET

BET isotherms showed a specific surface area of ca. $30.2 \text{ m}^2 \text{ g}^{-1}$, and an average particle size of $0.1985 \mu\text{m}$, in good agreement with the size of the agglomerates observed by SEM; whereas the BJH pore volume and size were: $0.051 \text{ cm}^3 \text{ g}^{-1}$ and 70.3 \AA respectively.

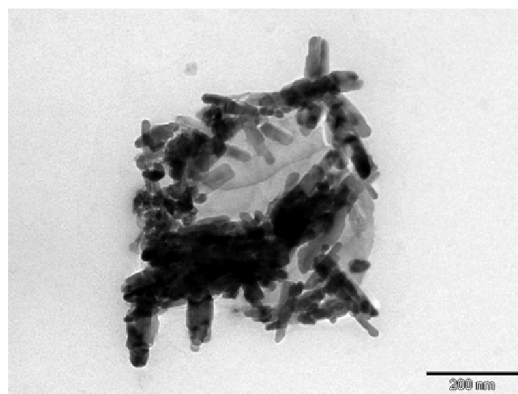


Fig. 2. SEM image of a randomly taken representative sample of the NCP.

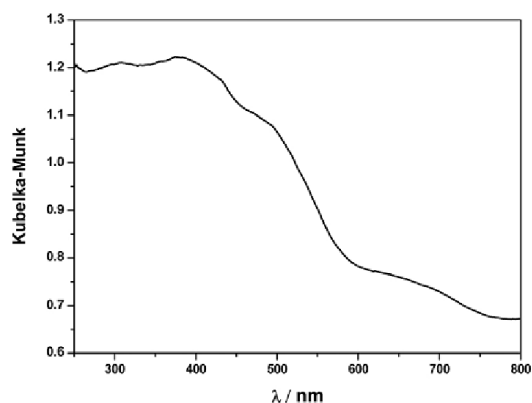


Fig. 3. UV-vis diffuse reflectance spectrum of NCP.

3.1.3. XRF

XRF results, expressed as% in oxides, confirmed that the clay is rich mainly in Fe_2O_3 , which represents 77.7% of the total composition, followed by SiO_2 (11.5%), Al_2O_3 (6.5%) and CaO (1.3%), respectively. Other components are also present although in very low percentages, not exceeding 1% (see Table S1 of Supporting information).

3.1.4. UV-vis DRS

A broad and intense band in the region 250–600 nm of the UV/vis diffuse reflectance spectrum was observed for suspensions of NCP (Fig. 3), with a maximum at around 380 nm. The reflectance was also significant in all the range between 600 and 800 nm, primarily associated to iron and the presence of iron oxide. The intense reflectance in the range 250–600 nm results mainly from ligand to metal charge transfer transition (LMCT) from $\text{O}^{2-} \rightarrow \text{Fe}^{3+}$. However, the Vis absorption edge, which gives the iron oxides their red to yellow colours, does not result from LMCT transitions, but is the consequence of very intense Fe^{3+} ligand field $\text{Fe}^{3+} \rightarrow \text{L}$ pair transitions. The UV/vis spectrum of the sample suggests the presence of goethite [29].

3.1.5. XRD

XRD of the clay (Fig. 4) showed a diffraction pattern that is undoubtedly attributed to the presence of goethite, quartz and kaolinite (JCPDS files 29-0713, 46-1045 and 14-0164, respectively), with goethite ($\text{FeO}(\text{OH})$) as the most dominant component of the clay. This is in agreement with SEM-EDS observations and confirms, out of doubt, that the natural clay is rich in Fe^{3+} and therefore useful for the heterogeneous photo-Fenton process.

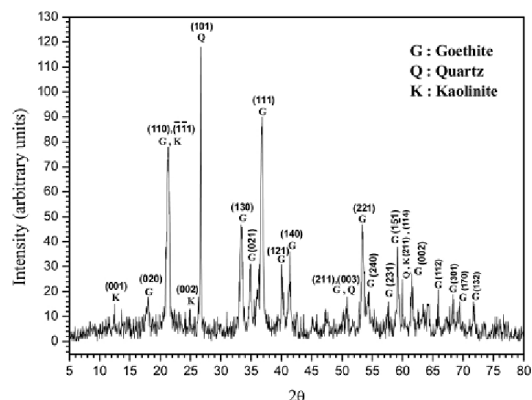
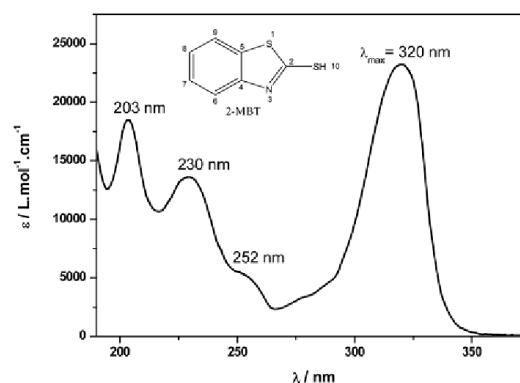


Fig. 4. X-ray diffractogram of the natural clay.

Fig. 5. UV-vis spectrum of aqueous $5.0 \cdot 10^{-5}$ M MBT, (natural pH ca. 6.3).

3.2. UV-vis analysis of MBT solution

The UV-vis spectrum of the molecular form of $5.0 \cdot 10^{-5}$ M aqueous MBT (Fig. 5) showed three characteristic maxima: 320 nm ($\epsilon = 23287 \text{ M}^{-1} \text{ cm}^{-1}$), 230 nm ($\epsilon = 13657 \text{ M}^{-1} \text{ cm}^{-1}$) and 203 nm ($\epsilon = 18677 \text{ M}^{-1} \text{ cm}^{-1}$). Moreover, the spectrum shows a shoulder at 252 nm ($\epsilon = 5364 \text{ M}^{-1} \text{ cm}^{-1}$). Molar absorptivity values were calculated either according to the law of Beer-Lambert or directly from the UV-vis spectrum.

These spectral features, $n \rightarrow \pi^*$ and $\pi \rightarrow \pi^*$ electronic transitions, represent a significant overlap with the sunlight emission in the region above 300 nm. Thus, MBT is likely to undergo photo-oxidation under natural or simulated sunlight irradiation. On the other hand, a significant hypsochromic effect (blue shift) to 308 nm, in addition to a hypochromic effect, is observed when $\text{pH} > 7$.

3.3. Kinetics of degradation

Kinetics were monitored at the maximum wavelength of MBT (see above), at 298 K and at the natural pH of the solution (ca. 6.3), produced by the mixture of dissolved reagents and suspension of NCP particles. Direct photolysis and adsorption kinetics were routinely treated according to either a first order or a pseudo-first order kinetic model, Eq. (13):

$$r = k_{\text{obs}} \cdot C \quad (13)$$

where r is the reaction rate and, $k_{\text{obs}} \approx k_{\text{LH}} K_{\text{LH}}$, k_{obs} the limiting pseudo-first order kinetic rate constant. UV-vis photocatalytic degradation processes are usually adequately described by the Langmuir-Hinshelwood kinetic model [30] as in Eq. (14):

$$r = k_{\text{LH}} \cdot \Theta = k_{\text{LH}} \cdot \frac{K_{\text{LH}} \cdot C}{1 + K_{\text{LH}} \cdot C} \quad (14)$$

where C is the MBT concentration once the adsorption-desorption equilibrium has been established, $k_{\text{LH}} (\text{mol s}^{-1} \text{ cm}^{-2})$ is an apparent kinetic rate constant per unit of surface area, and $\Theta (\text{cm}^2)$ accounts for the coverage of catalyst surface by MBT. K_{LH} is the Langmuir-Hinshelwood adsorption constant. Assuming $K_{\text{LH}} C \ll 1$, Eq. (14) reduces to Eq. (13).

3.4. MBT adsorption onto NCP

Before starting the photodegradation experiments, an estimation of the adsorption of MBT on the surface of natural clay powder was investigated during 150 min in the dark, with $[\text{MBT}] = 5.0 \cdot 10^{-5}$ M and 0.5 g L^{-1} NCP. The results showed a very fast adsorption in the first 15 min, estimated about 11%, i.e. $5.5 \cdot 10^{-6}$ M of the initial MBT concentration. Under these conditions, and at $T = 298 \text{ K}$, the adsorption-

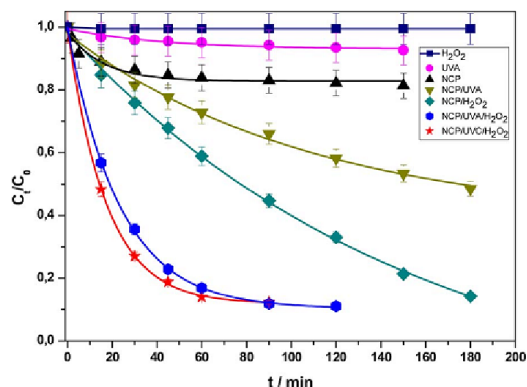


Fig. 6. Degradation of MBT under different experimental conditions. $[MBT] = 5.0 \cdot 10^{-5} M$, $[H_2O_2]_0 = 1.0 \cdot 10^{-3} M$, $[NCP] = 0.5 g L^{-1}$, (natural pH ca. 6.3), $T = 298.0 K$.

Table 1

Rate constants obtained for the degradation of MBT under different conditions. $[MBT] = 5.0 \cdot 10^{-5} M$ (natural pH ca. 6.3), $T = 298.0 K$.

Experimental conditions	k_{obs}/min^{-1}
$0.5 g L^{-1}$ NCP (adsorption in dark)	0.06 ± 0.01
$1 mM H_2O_2$	No reaction
UVA	0.024 ± 0.007
$0.5 g L^{-1}$ NCP/ $1 mM H_2O_2$	0.0067 ± 0.0007
$0.5 g L^{-1}$ NCP/UVA	0.009 ± 0.001
$0.5 g L^{-1}$ NCP/UVA/ $1 mM H_2O_2$	0.0431 ± 0.0006
$0.5 g L^{-1}$ NCP/UVC/ $1 mM H_2O_2$	0.058 ± 0.001

desorption equilibrium is reached in ca. three hours, with ca. 20% adsorption and an adsorption rate constant $k_{ads} = (0.06 \pm 0.01) min^{-1}$ (see Fig. 6 and Table 1).

When the amount of NCP was doubled to $1.0 g L^{-1}$, much higher adsorption, ca. 28% of MBT, was observed within 10 first min of contact under the same conditions. For the sake of simplicity, we decided to use $0.5 g L^{-1}$ as load of NCP in the rest of experiments and assume the Langmuir model, i.e. a true adsorption-desorption equilibrium forming a single layer of MBT onto a homogeneous surface of NCP with equivalent and homogeneously distributed adsorption sites through all the surface. Alterations of the adsorption properties of the NCP or of the adsorption-desorption equilibrium are considered negligible once the solution started to be irradiated.

3.5. Degradation of MBT under different conditions

Preliminary studies were carried out to investigate the degradation efficiency of $5.0 \cdot 10^{-5} M$ MBT under different conditions. Fig. 6 shows a very small effect of UVA-Vis irradiation on MBT degradation when irradiation was used alone. Introduction of NCP while the sample is irradiated with UVA leads to MBT degradation, ca. 51.5% within 180 min. Addition of H_2O_2 significantly improves the degradation process, reaching 67% of degradation extent in 120 min. Replacement of the UVA-vis source by 254 nm (UVC) enhanced the oxidizing power of the system, and increased MBT degradation from 78% to 88% in less than 90 min. Such increase can be explained on the basis of the enhanced generation of highly reactive oxygen species (ROS), especially $HO\cdot$, from H_2O_2/Fe^{2+} mixtures in acidic medium [22].

Table 1 compiles the observed first-order or pseudo-first order rate constants obtained under different experimental conditions. The obtained results show that H_2O_2 alone does not react with MBT, and UVA photolysis is highly ineffective, with just ca. 7% transformation of MBT in 2.5 h, presumably due to the existence of alternative photophysical

deactivation pathways for the generated excited states.

The Fenton process (NCP/ H_2O_2) is relatively effective with ca. 86% of MBT conversion in three hours (lifetime $t_{1/2} = 103$ min). The combination NCP/UVA, that initiates the photo-Fenton process, improves slightly the reaction rate, with a lifetime $t_{1/2} = 77$ min, but is less effective from the point of view of transformation efficiency, reaching only ca. 49%. The synergistic combination of Fenton and photo-Fenton processes, NCP/UVA/ H_2O_2 yields best results, improving both the reaction rate ($t_{1/2} = 16$ min) and conversion (ca. 90% in 2 h). Finally, the use of higher energy radiation, i.e. NCP/UVC/ H_2O_2 , contributes to reduce slightly the transformation lifetime to $t_{1/2} = 12$ min, almost without change in MBT conversion, ca. 88%.

3.6. Role of the hydroxyl radical

An indirect method was used to confirm the role of $HO\cdot$ radicals and to what extent they might be involved in the degradation of MBT in aqueous solution by heterogeneous photo-Fenton process. *tert*-BuOH ($1.0 \cdot 10^{-2} M$) was added to the solution under the same experimental conditions. The results, shown in Fig. 7, revealed an inhibition of ca. 19% in the MBT degradation after 120 min of irradiation ($k = 0.008 \pm 0.001 s^{-1}$, $t_{1/2} = 86$ min, 71% transformation, 86% reduction in the reaction rate) as compared with the process in the absence of *tert*-BuOH ($k = 0.0431 \pm 0.0006 s^{-1}$, $t_{1/2} = 16$ min, 90% transformation).

Though this result clearly shows the involvement of $HO\cdot$ radicals, it also implies they are not the only reactive species involved in the process; otherwise, the 200-fold excess of *tert*-BuOH would completely hinder the reaction. Hence, besides direct photolysis and since at the working acidity conditions $O_2\cdot^-$ would be fully protonated, $HO_2\cdot$ might participate as described in Eqs. (6)–(8).

3.7. Effect of operational parameters

The effect of different operational parameters (pH, H_2O_2 concentration, catalyst dosage and substrate concentration) has been studied, all of which play a significant role on the efficiency and rate of degradation both for homogeneous and heterogeneous photo-Fenton processes.

3.7.1. Effect of pH

Acidity is the main influencing factor for the precipitation of iron oxides, and also determines the adsorption onto the surface of the catalyst. There have been different reports on the optimal pH for wastewater treatment efficiency ranging from pH 2,8–4 to natural or even alkaline medium [31].

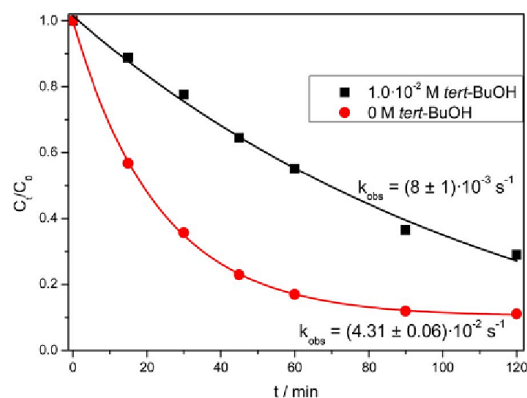


Fig. 7. Effect of *tert*-BuOH on the rate of degradation of aqueous MBT. $[MBT] = 5.0 \cdot 10^{-5} M$, $[H_2O_2]_0 = 1.0 \cdot 10^{-3} M$, $[NCP] = 0.5 g L^{-1}$ upon UVA/Vis irradiation, (natural pH ca. 6.3), $T = 298.0 K$.

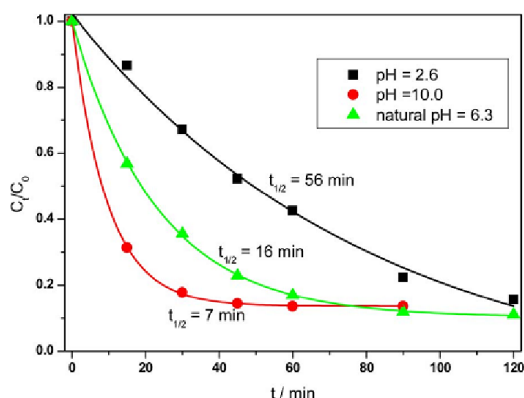


Fig. 8. Effect of pH on the heterogeneous photodegradation of aqueous MBT [MBT] = $5.0 \cdot 10^{-5}$ M, $[H_2O_2]_0 = 1.0 \cdot 10^{-3}$ M, [NCP] = 0.5 g L^{-1} upon UVA/vis irradiation. T = 298.0 K.

Fig. 8 shows the effect of the pH on the efficiency of degradation of aqueous MBT in acidic, neutral and alkaline media. The highest reactivity was observed at pH = 10 ($k_{\text{pH}=10} = 0.105 \pm 0.001 \text{ s}^{-1}$, $t_{1/2} = 7 \text{ min}$), followed by natural pH (ca. 6.3) ($k_{\text{pHca.6.3}} = 0.0431 \pm 0.0006 \text{ s}^{-1}$, $t_{1/2} = 16 \text{ min}$), and pH 2.6 ($k_{\text{pH}=2.6} = 0.012 \pm 0.002 \text{ s}^{-1}$, $t_{1/2} = 56 \text{ min}$). The observed efficiency of the process, in terms of MBT transformation, was approximately the same, ca. 90% in 2 h for the three pH values. Agglomeration of ferric species was observed at pH = 2.6, an indication of the instability of the participating iron species in acidic pH. These results are in good agreement with previous reports: since iron can form complexes with several Lewis bases, it has been suggested that in the presence of complexing agents the need for acidification could be circumvented [32–35]. The fact that the rate of degradation of MBT is higher in alkaline medium is probably due to the important solubility of iron species at this pH and the increase in the availability of active sites on the catalyst surface.

3.7.2. Effect of MBT concentration

Fig. 9 shows the effect of the MBT concentration on its photo-Fenton heterogeneous degradation upon UVA–vis irradiation ($\lambda \geq 366 \text{ nm}$) (see also Table S2–Supporting information). Within experimental error, the observed rate constants were the same: $k_{\text{obs}} = 0.041 \pm 0.001$, 0.0431 ± 0.0006 and $0.038 \pm 0.002 \text{ M}^{-1} \text{ s}^{-1}$, for initial MBT concentrations $2.5 \cdot 10^{-5}$, $5.0 \cdot 10^{-5}$ and $7.5 \cdot 10^{-5} \text{ M}$, respectively. The same was observed for MBT transformation efficiency (ca. 90%). This

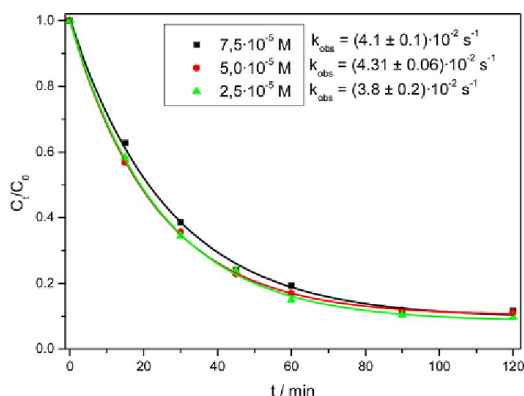


Fig. 9. Effect of MBT concentration on its photo-Fenton heterogeneous degradation [MBT] = $5.0 \cdot 10^{-5}$ M, $[H_2O_2] = 1.0 \cdot 10^{-3}$ M, [NCP] = 0.5 g L^{-1} upon UVA/vis irradiation, (natural pH ca. 6.3), T = 298.0 K.

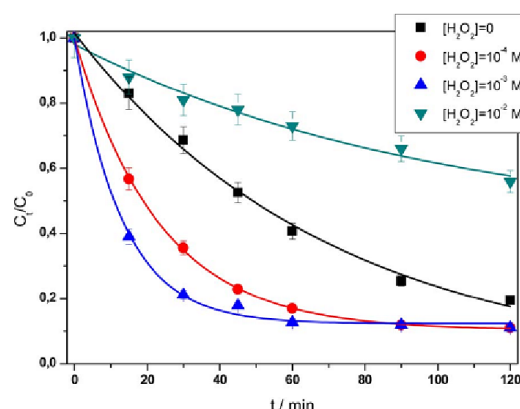


Fig. 10. Effect of H_2O_2 on the heterogeneous photo-Fenton degradation of aqueous MBT [MBT] = $5.0 \cdot 10^{-5}$ M, [NCP] = 0.5 g L^{-1} upon UVA/vis irradiation (natural pH ca. 6.3), T = 298.0 K.

indicates that, at the studied MBT concentrations, there are still active sites available for adsorption onto the surface of the NCPs. There is no doubt that, like in other photocatalysis studies, the MBT photodegradation rate should vary when its initial concentration be in the milli molar range.

3.7.3. Effect of H_2O_2 concentration

The effect of H_2O_2 concentration on the removal of MBT from aqueous solution is shown in Fig. 10, and the corresponding pseudo-first order rate constants collected in Table 2.

k_{obs} increases with H_2O_2 concentration, but not linearly, less as the concentration increases; and a reduction in the extent of transformation is also observed as the concentration of H_2O_2 increases. Therefore $1.0 \cdot 10^{-3} \text{ M}$ was the selected H_2O_2 concentration for the rest of experiments. Both the tendency observed for the reaction rate and for the extent of reaction point to the inhibition of the process at higher H_2O_2 concentrations, which is explained in terms of the $HO\cdot$ radical scavenging effect caused by H_2O_2 .

3.7.4. Effect of the load of NCP

Fig. 11 shows the effect of the load of NCP on the heterogeneous photo-Fenton degradation of MBT and Table 3 summarizes the corresponding rate constants.

The degradation rate increases linearly with growing concentrations of NCP, as shown in the inset of Fig. 11. The direct proportionality observed shows the experimental conditions correspond to a true photocatalytic regime and, as pointed out previously for the dependence with the MBT concentration, there are enough active sites available for adsorption on the surface of the NCPs. Under these conditions, the efficiency in the use of light by the photocatalyst is optimal.

3.7.5. Effect of oxygen

The effect of the partial pressure of oxygen was studied and the

Table 2
Effect of H_2O_2 concentration on the rate constant for heterogeneous photo-Fenton degradation of aqueous MBT. [MBT] = $5 \cdot 10^{-5} \text{ M}$, [NCP] = 0.5 g L^{-1} , UVA/vis irradiation, natural pH, T = 298.0 K.

$[H_2O_2]/\text{M}$	$k_{\text{obs}}/\text{min}^{-1}$
0	0.010 ± 0.003
1.0310^{-4}	0.009 ± 0.001
$1.0 \cdot 10^{-3}$	0.0431 ± 0.0006
$1.0 \cdot 10^{-2}$	0.077 ± 0.004

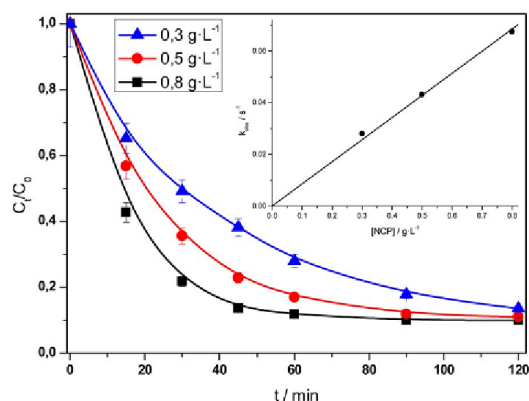


Fig. 11. Effect of the load of NCP on the rate of heterogeneous photo-Fenton degradation of MBT [MBT] = $5.0 \cdot 10^{-5}$ M, $[\text{H}_2\text{O}_2] = 1.0 \cdot 10^{-3}$ M, UVA/vis irradiation, (natural pH ca. 6.3), T = 298.0 K. Inset: dependence k_{obs} vs. [NCP].

Table 3

Effect of the load of NCP on the rate constant for the heterogeneous photo-Fenton degradation of aqueous MBT. [MBT] = $5.0 \cdot 10^{-5}$ M, $[\text{H}_2\text{O}_2] = 1.0 \cdot 10^{-3}$ M, UVA/vis irradiation, (natural pH ca. 6.3), T = 298.0 K.

[NCP]/g L ⁻¹	$k_{\text{obs}}/\text{M}^{-1} \text{min}^{-1}$
0.3	0.028 ± 0.002
0.5	0.0431 ± 0.0006
0.8	0.0675 ± 0.0007

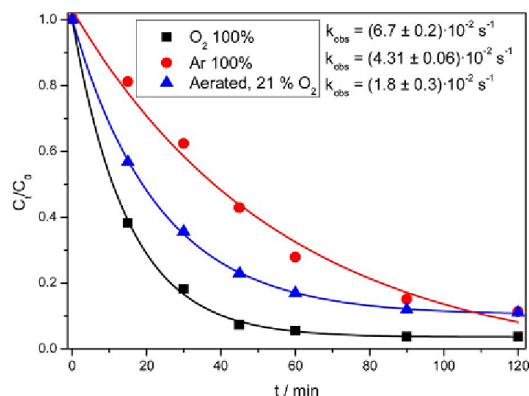


Fig. 12. Effect of the concentration of dissolved O_2 on the rate of degradation of MBT by heterogeneous photo-Fenton process. [MBT] = $5.0 \cdot 10^{-5}$ M, [NCP] = 0.5 g L^{-1} upon UVA/vis irradiation, $[\text{H}_2\text{O}_2] = 1.0 \cdot 10^{-3}$ M, (natural pH ca. 6.3), T = 298 K.

results are shown in Fig. 12. Oxygen concentration in solution was controlled by diluting $\text{O}_2(\text{g})$ in Ar gas before saturation. The extent of reaction is approximately the same after 2 h, while the reaction rate increases with the concentration of oxygen in solution, a clear indication of the relevance of ROS in the heterogeneous photo-Fenton process.

The observed increase in k_{obs} is, however, not linear, which points to the participation of different ROS in the process, that are generated at different rates and with different yields. Torres et al. [36] investigated the reactivity of Bisphenol A (BPA) with $\text{HO}\cdot$ in UV- Fe^{3+} treatment, hypothesizing that monohydroxylated BPA products could be formed via $\text{HO}\cdot$ attack followed by reaction with O_2 to form peroxy radicals ($\text{ROO}\cdot$). Finally, important reactivity is still observed in the absence of O_2 , which reveals the relevance of the Fenton and photo-Fenton processes described above on the MBT degradation.

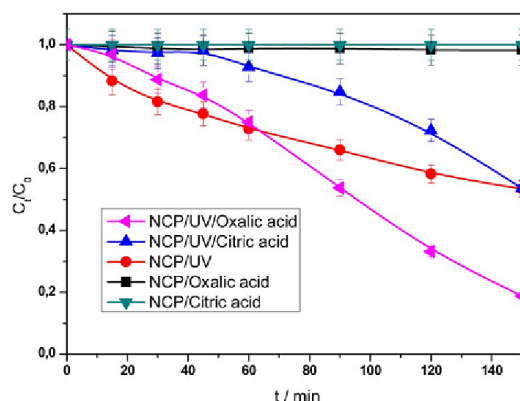


Fig. 13. Effect of oxalic acid and citric acid on the heterogeneous photo-Fenton degradation of aqueous MBT. [Oxalic acid] = $1.0 \cdot 10^{-3}$ M, [Citric acid] = $1.0 \cdot 10^{-3}$ M, [MBT] = $5.0 \cdot 10^{-5}$ M, [NCP] = 0.5 g L^{-1} upon UVA/vis irradiation, $[\text{H}_2\text{O}_2] = 1.0 \cdot 10^{-3}$ M, $\text{pH}_0 = 6.8$, T = 298.0 K.

Table 4

Effect of different operational parameters on TOC removal from MBT solutions [MBT]₀ = 7.75 mg L^{-1} , $[\text{H}_2\text{O}_2]_0 = 1.0 \cdot 10^{-3}$ M, [NCP] = 0.5 g L^{-1} , T = 298.0 K.

Experimental conditions	TOC/mg L ⁻¹	% TOC removal
pH = 2.6, UVA	2.48	68
Natural pH, UVA	3.79	51
Natural pH, UVC	4.63	40
pH = 10, UVA	5.12	34
Ar-saturation, UVA	2.73	65
O_2 -saturation, UVA	4.63	40

3.7.6. Effect of oxalic and citric acids

The effect of oxalic and citric acids on the UVA-Vis heterogeneous photo-Fenton degradation efficiency of MBT from aqueous solution has been studied in the absence of H_2O_2 . As shown in Fig. 13, oxalic and citric acids show no thermal effect in the absence of UVA-Vis irradiation within 150 min. When the solutions were irradiated, the same efficiency of degradation obtained for the process in the NCP/UVA (absence of carboxylic acids) was observed after 60 min in the case of oxalic acid and 150 min for citric acid. The shape of the (C_t/C_0) vs. t dependence was quite similar in both cases: the observed dependence could be regarded as an induction period (longer for citric acid) followed by a decay, that is not fitted by a first order kinetic model in any of both cases.

The higher efficiency observed of oxalic acid is probably due to the formation of iron complexes with carboxylate ions (Fe^{3+} -carboxylate), which increases the solubility of iron oxides present in the mineral matrix. This hypothesis may explain also the observed induction period: the complexation equilibrium must be reached before Fe^{3+} can be made available. Fe^3 -carboxylate complexes differ in stability and photoreactivity toward the studied compound. Therefore, the lower reactivity of citric acid can be related to the lower quantum yield of Fe^3 -citric toward formation of Fe^{2+} ($\Phi = 0.59$) as compared to the quantum yield of Fe^3 -oxalic acid ($\Phi = 1.0$ – 1.2) [37]. The profiles with carboxylic acids resemble the typical profiles of autocatalyzed processes. The overall degradation at the end of the experiment with oxalic acid was around 82% after 2.5 h, and 47% for citric acid (the same extent of reaction reached with NCP/UV treatment). The observed behavior can be explained by the fact that the formation of Fe^{3+} -oxalate complexes, according to Eq. (15), initially limits the photoreduction of Fe^{3+} , but then improves the dissolution of iron, which leads to the observed increase of degradation.

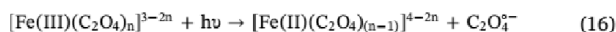
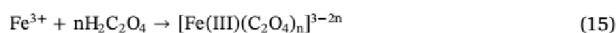
Under UV-vis light irradiation, these complexes could be excited and transformed to Fe^{2+} -oxalate complexes and $\text{C}_2\text{O}_4^{\cdot -}$, as in Eq. (16):

Table 5
Identified photoproducts and comparison with others reported in the literature.

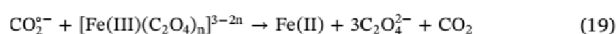
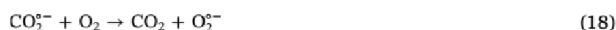
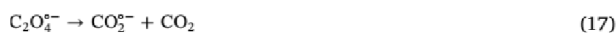
Compound	Method and reference
	<i>This study</i> (NCP/H ₂ O ₂ /UVA-vis) Direct photolysis [2,40] Nd ³⁺ -TiO ₂ /UV _{365nm} [9]
	Direct photolysis [40]
	<i>This study</i> (NCP/H ₂ O ₂ /UVA-vis) Direct photolysis [2,40]
	Nd ³⁺ -TiO ₂ /UV _{365nm} [7]
	Direct photolysis [2]
	<i>This study</i> (NCP/H ₂ O ₂ /UVA-vis)
	Nd ³⁺ -TiO ₂ /UV _{365nm} [7]
	<i>This study</i> (NCP/H ₂ O ₂ /UVA-vis) Direct photolysis [40] DTA/UV _{365nm} [8]
	Direct photolysis [2]
	<i>This study</i> (NCP/H ₂ O ₂ /UVA-vis)
	DTA/UV _{365nm} [8]
	Direct photolysis [2]
	<i>This study</i> (NCP/H ₂ O ₂ /UVA-vis)
	Direct photolysis [2,40]
	Nd ³⁺ -TiO ₂ /UV _{365nm} [7]
	Nd ³⁺ -TiO ₂ /UV _{365nm} [7]
	<i>This study</i> (NCP/H ₂ O ₂ /UVA-Vis)

Table 5 (continued)

Compound	Method and reference
	Direct photolysis [40]
	Direct photolysis [40]
	Direct photolysis [40] DTA/UV _{365nm} [8]
Dimer (disulfide form) (m/z = 332)	



The so-formed oxalate radical anion $\text{C}_2\text{O}_4^{\cdot-}$ decomposes to a carbon dioxide radical anion ($\text{CO}_2^{\cdot-}$) and CO_2 , Eq. (17). The $\text{CO}_2^{\cdot-}$ radical anion may react with dissolved oxygen, Eq. (18) and ferrioxalate complexes, Eq. (19), regenerating Fe^{2+} .

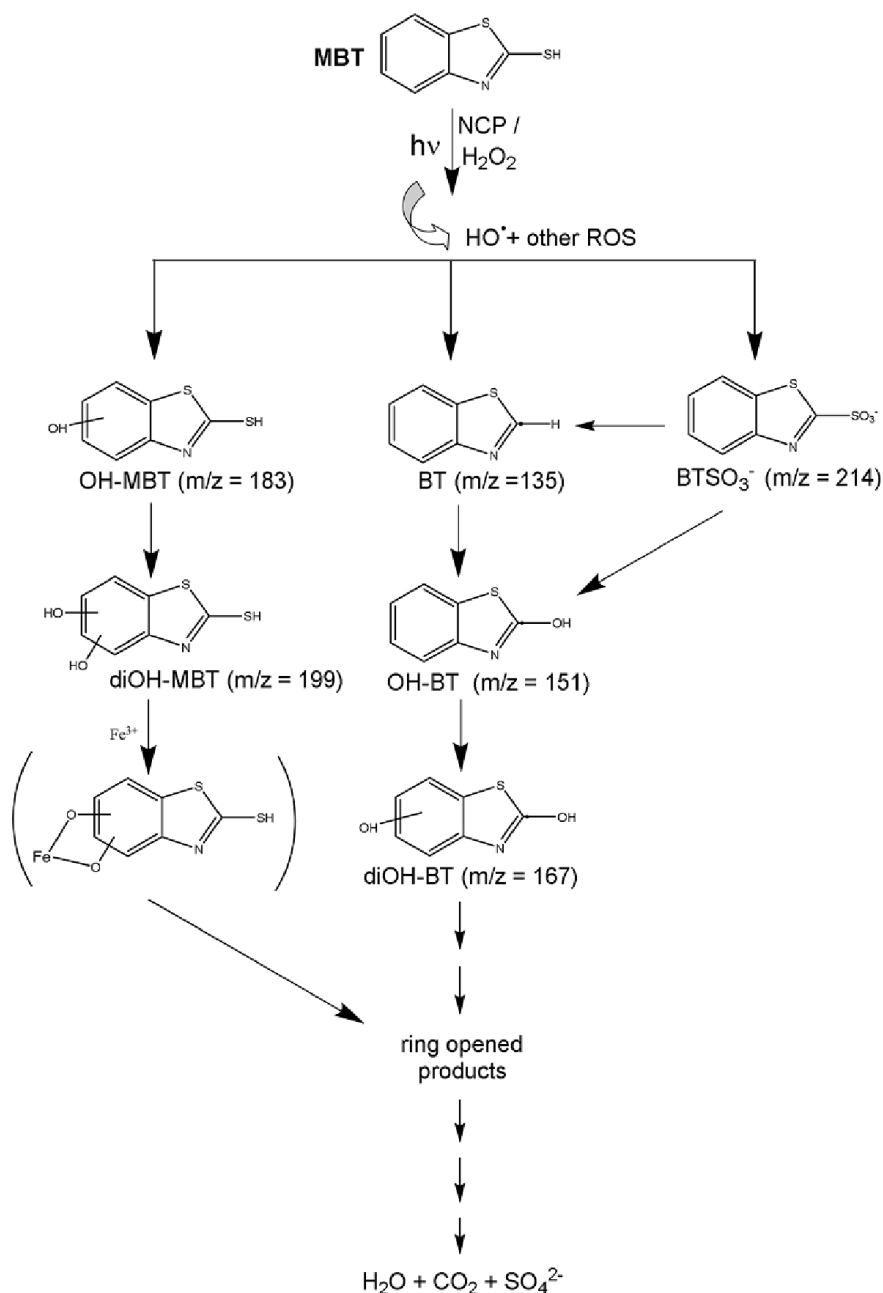


Oxalic acid reacts simultaneously as a donor of proton and ligand, and the dissolution of iron is assumed to take place via an electrochemical photoreduction process [38,39]. Charge transfer processes between the predominant oxalate species, namely ferric oxalate $[\text{Fe(III)}(\text{C}_2\text{O}_4)_n]^{3-2n}$, and ferrous oxalate $[\text{Fe(II)}(\text{C}_2\text{O}_4)_{(n-1)}]^{4-2n}$, and oxalate take place on the surface of NCP, introducing additional complexity on the observed heterogeneous photo-Fenton process.

3.8. Mineralization efficiency

To determine the degree of mineralization reached upon treatment, duplicated samples were collected at the beginning of the experiment and after 2 h of photo irradiation under different conditions, and then analyzed for TOC concentration. Table 4 compiles the TOC removal results under different conditions. % TOC removal was calculated once [MBT] did not show any further change, typically after 2 h of reaction.

The obtained results show mineralization is not reached within typical MBT transformation time, i.e.: it leads to a number of reaction intermediates and/or products that are relatively persistent. Lower pH values lead to increased TOC removals, in agreement with the possibility of Fe^{3+} is regeneration under appropriate acidity conditions (pH ca. 2.7–2.8), as described by Eqs. (3)–(4) in the introduction. The presence of O_2 seems to worsen the mineralization, which could be associated to the generation of less reactive intermediates, possibly through peroxidation and/or hydroperoxidation processes. Finally, while UVC leads to a faster transformation of MBT than UVA, the process is more efficient for UVA in terms of TOC removal, which must be attributed to the generation of more persistent, less reactive intermediates. In summary, the best operational conditions to attain a high TOC removal are the use of UVA in combination with low pH values and absence or low concentrations of O_2 .



Scheme 1. Mechanism proposed for MBT photodegradation in aqueous solution in the presence of NCP under simulated sunlight irradiation at 366 nm (in brackets: hypothesized, undetected structure).

3.9. Identification of intermediates and reaction mechanism

Irradiated MBT solutions were analysed by LC-ESI-MS in positive mode ionisation in order to identify the main photoproducts after 60 min of irradiation. The obtained results are compiled in Table 5 and compared to published data [2,7,8,40–44]. Very similar chromatograms (as shown in Supporting information S2 and S4) were obtained from solutions of aqueous $5.0 \cdot 10^{-5}$ M MBT and NCP for the different operational conditions described above. Only the main peaks were identified, and appropriate structures proposed, considering the observed (m/z) ratios. The main photoproducts found were benzothiazole

(BT) and 2-benzothiazolesulfonate. The oxidation of MBT is mainly accomplished by reaction with HO^\bullet photogenerated at the surface of NCP in the presence of H_2O_2 . Detection of polyhydroxylated photoproducts is indicative of ongoing further degradation.

Considering the different photoproducts identified, we have proposed a mechanism (Scheme 1) for MBT heterogeneous photo-Fenton degradation in the presence of NCP. The observed extent of MBT disappearance was ca. 95%. The generated reactive oxygen species (ROS) by photo-Fenton reaction, mainly HO^\bullet radical, react with the MBT molecules adsorbed onto the clay. Some of the main reaction pathways observed are: i) hydroxylation of the benzene ring, ii) hydroxylation of

the carbon in thiazole ring, iii) loss of the –SH group and iv) S-oxidation. These transformations are expected to lead to the opening of the benzene ring and complete mineralization of the product.

4. Conclusions

This paper reports the research on the efficiency of heterogeneous photo-Fenton process on the photodegradation of MBT in aqueous solutions using inexpensive natural clay powder (NCP) and under simulated sunlight (UVA–vis) irradiation. The characterisation analyses of NCP showed an irregular shape of agglomerates of ca. 1 µm, composed of fine long crystal nanometric needles, with 30.2 m² g⁻¹ BET specific surface area, XRF and XRD results indicated the presence of an important amount of Fe³⁺ as an iron oxide goethite. The photodegradation of MBT follows pseudo-first order kinetics. Replacement of the UVA-Vis source by 254 nm (UVC) enhanced the oxidizing power of the system, and increased MBT degradation from 78% to 88% in less than 90 min. The species responsible for the photo-degradation of MBT was found to be mainly HO·, as the presence of *tert*-BuOH notably slowed down MBT photodegradation rate and reduced the percentage of MBT conversion. The kinetic study revealed that the photodegradation rate was strongly affected by dissolved O₂, pH, H₂O₂ and NCP dose. The MBT degradation in the presence of oxalic acid was found to be much more relevant than that of citric acid. The formation of carboxylic acids-iron complexes slows down the process during the first 60 min, and then speeds it up by dissolving solid iron species. The photo-products identified by LC–MS point to the formation of BT followed by 2-benzothiazolesulfonate and polyhydroxylated products. The highest TOC removals were obtained using UVA at low pHs (68%, pH 2.6), in the absence of O₂ (65%), whereas largest (90%) and fastest (t_{1/2} = 7 min) MBT disappearance takes place at alkaline pH (10) and oxygen saturated aqueous solution. The obtained results strongly support the use of NCPs rich in iron oxides as inexpensive, clean and efficient photocatalysts for the abatement of persistent organic micro-pollutants in water using heterogeneous photo-Fenton process.

Acknowledgements

Z. Redouane-Salah acknowledges the *Université Constantine 1* (Algeria) and *Centre Universitaire de Tamansrasset* (Algeria) for a training leave at the Univ. of A Coruña. This research was partially supported by the Group of Chemical Reactivity & Photoreactivity (REACT!) at University of A Coruña, with financial support from *Ministerio de Economía y Competitividad* (Spain) through project CTQ2015-71238-R (MINECO/FEDER).

Appendix A. Supplementary data

Supplementary data associated with this article can be found, in the online version, at <https://doi.org/10.1016/j.jece.2018.02.011>.

References

- M.A. Gaja, J.S. Knapp, Removal of 2-mercaptobenzothiazole by activated sludge: a cautionary note, *J. Water Res.* 32 (1998) 3786–3789.
- M.A. Malouki, C. Richard, A. Zertal, Photolysis of 2-mercaptobenzothiazole in aqueous medium laboratory and field experiments, *J. Photochem. Photobiol. A: Chem.* 167 (2004) 121–126.
- Q. Bao, L. Chen, J. Tian, J. Wang, Degradation of 2-mercaptobenzothiazole in aqueous solution by gamma irradiation, *J. Radiat. Phys. Chem.* 103 (2014) 198–202.
- D. Ehouman, J.S. Akpa, P.M. Niamien, D. Sissouma, A. Trokourey, Inhibition effect of 2-mercaptobenzothiazole on the corrosion of copper in 2 M HNO₃, *J. Chem. Pharm. Res.* 8 (3) (2016) 353–364.
- H. Yang, Y. Sun, J. Ji, W. Song, X. Zhu, Y. Yao, Z. Zhang, 2-Mercaptobenzothiazole monolayers on zinc and silver surfaces for anticorrosion, *Corros. Sci.* 50 (2008) 3160–3167.
- J. Dercó, A. Kassai, M. Melicher, J. Dudas, Removal of the 2-mercaptobenzothiazole from model wastewater by ozonation, *J. Hindawi Publ. Corp.* 2014 (2014), <http://dx.doi.org/10.1155/2014/173010> (Article ID 173010, 7 pages).
- F.B. Li, X.Z. Li, K.H. Ng, Photocatalytic degradation of an odorous pollutant: 2-mercaptobenzothiazole in aqueous suspension using Nd³⁺-TiO₂ catalysts, *Ind. Eng. Chem. Res.* 45 (2006) 1–7.
- A. Allaoui, M.A. Malouki, P. Wong-Wah-Chung, Homogeneous photodegradation study of 2-mercaptobenzothiazole photocatalysed by sodium decatungstate salts: kinetics and mechanistic pathways, *J. Photochem. Photobiol. A: Chem.* 212 (2010) 153–160.
- F.B. Li, X.Z. Li, M.F. Hou, Photocatalytic degradation of 2-mercaptobenzothiazole in aqueous La³⁺-TiO₂ suspension for odor control, *J. Appl. Catal. B: Environ.* 48 (2004) 185–194.
- F.B. Li, X.Z. Li, M.F. Hou, K.W. Cheah, W.C.H. Choy, Enhanced photocatalytic activity of Ce³⁺-TiO₂ for 2-mercaptobenzothiazole degradation in aqueous suspension for odour control, *J. Appl. Catal. A: Gen.* 285 (2005) 181–189.
- X. Wang, C. Liu, X. Li, F. Li, S. Zhou, Photodegradation of 2-mercaptobenzothiazole in the γFe₂O₃/oxalate suspension under UVA light irradiation, *J. Hazard. Mater.* 153 (2008) 426–433.
- C. Liu, F. Li, X. Li, G. Zhang, Y. Kuang, The effect of iron oxides and oxalate on the photodegradation of 2-mercaptobenzothiazole, *J. Mol. Catal. A: Chem.* 252 (2006) 40–48.
- F. Li, C. Liu, C. Liang, X. Li, L. Zhang, The oxidative degradation of 2-mercaptobenzothiazole at the interface of βMnO₂ and water, *J. Hazard. Mater.* 154 (2008) 1098–1105.
- R. Andreozzi, V. Caprio, R. Marotta, Oxidation of benzothiazole 2-mercaptobenzothiazole and 2-hydroxybenzothiazole in aqueous solution by means of H₂O₂/UV or photoassisted Fenton systems, *J. Chem. Technol. Biotechnol.* 76 (2001) 196–202.
- A. Bunescu, P. Besse-hoggan, M. Sancelme, A. Cincilei, G. Mailhot, A.M. Delort, Microbial Degradation of 2-Benzothiazole Derivatives: A Review, *Environmental Biodegradation Research Trends*, Nova Publishers, New York, 2007.
- A.J. Luna, C.A.O. Nascimento, O. Chivone-Filho, Photodecomposition of hydrogen peroxide in highly saline aqueous medium, *Braz. J. Chem. Eng.* 23 (2006) 341–349.
- S. Bahnmüller, C.H. Loi, K.L. Linge, U.V. Gunten, S. Canonica, Degradation rates of benzotriazoles and benzothiazoles under UV-C irradiation and the advanced oxidation process UV/H₂O₂, *J. Water Res.* 74 (2015) 143–154.
- H.D. Burrows, M. Canle, J.A. Santaballa, S. Steenkens, Reaction pathways and mechanisms of photodegradation of pesticides, *J. Photochem. Photobiol. B: Biol.* 67 (2002) 71–108.
- M. Canle, J.A. Santaballa, E. Vulliet, On the Mechanism of TiO₂-Photocatalyzed Degradation of Aniline Derivatives, *J. Photochem. Photobiol. A: Chem.* (2005) 175–192.
- M. Canle, M.I. Fernández Perez, J.A. Santaballa, Photocatalyzed degradation / abatement of endocrine disruptors, *Curr. Opin. Green Sustain. Chem.* 6 (2017) 101–138.
- J.J. Pignatello, E. Oliveros, A. MacKay, Advanced oxidation processes for organic contaminant destruction based on the fenton reaction and related chemistry, *Crit. Rev. Environ. Sci. Technol.* 36 (2006) 1–84.
- R. Andreozzi, V. Caprio, A. Insola, R. Marotta, Advanced oxidation processes (AOP) for water purification and recovery, *Catal. Today* 53 (1999) 51–59.
- T. Katagi, Photoinduced oxidation of the organophosphorus fungicide tolclofos-methyl on clay minerals, *J. Agric. Food Chem.* 38 (1990) 1595–1600.
- D.A. Armstrong, R.E. Huiea, W.H. Koppenola, S.V. Lymara, G. Merényia, P. Netaa, B. Ruscica, D.M. Stanbury, S. Steenkens, P. Wardman, Standard electrode potentials involving radicals in aqueous solution: inorganic radicals, *Pure Appl. Chem.* 87 (2015) 1139–1150.
- E.S. Nweke, E.I. Ugwu, Analysis and characterization of clay soil in Abakaliki, Nigeria, *Pac. J. Sci. Technol.* 8 (2007) 190–193.
- J.F. Akinfolarin, O.O. Awopetu, The effect of sawdust on the insulating effect of Ikere clay as refractory lining, *AU J.T.* 17 (2014) 143–147.
- C.P. Dogan, K.S. Kwong, J.P. Bennet, Improved refractory materials for slagging coal gasifiers, Proceedings from the 27th International Conference on Coal Utilization and Fuel Systems, Clearwater, Florida, 2002.
- B. Khennaoui, M.A. Malouki, M. Canle, F. Zehani, N. Boutaoui, Z. Redouane-Salah, A. Zertal, Heterogeneous photo-Fenton process for degradation of azo dye: methyl orange using a local cheap material as a photocatalyst under solar light irradiation, *Optik* 137 (2017) 6–16.
- D.M. Sherman, T.D. Waite, Electronic spectra of Fe³⁺ oxides and oxide hydroxides in near IR to near UV, *Am. Mineral.* 70 (1985) 1262–1269.
- C. Martínez, M. Canle, L.M.I. Fernández, J.A. Santaballa, J. Faria, Kinetics and mechanism of aqueous degradation of carbamazepine by heterogeneous photocatalysis using nanocrystalline TiO₂, ZnO and multi-walled carbon nanotubes–nanatase composites, *Appl. Catal. B: Environ.* 102 (2011) 563–571.
- C.W. Yang, D. Wang, Q. Tang, The synthesis of Nd/FeB magnetic activated carbon and its application in degradation of azo dye methyl orange by Fenton-like process, *J. Taiwan Inst. Chem. Eng.* 45 (2014) 2584–2589.
- Y. Sun, J.J. Pignatello, Chemical treatment of pesticide wastes. Evaluation of iron (III) chelates for catalytic hydrogen peroxide oxidation of 2,4-D at circumneutral pH, *J. Agric. Food Chem.* 40 (1992) 322–327.
- Y. Sun, J.J. Pignatello, Organic intermediates in the degradation of 2,4-dichlorophenoxyacetic acid by iron(3+)/hydrogen peroxide and iron(3+)/hydrogen peroxide/UV, *J. Agric. Food Chem.* 41 (1993) 1139–1142.
- Y. Sun, J.J. Pignatello, Photochemical reactions involved in the total mineralization of 2,4-D by Fe³⁺/H₂O₂/UV, *Environ. Sci. Technol.* 27 (1993) 304–310.
- M.R.A. Silva, A.G. Trovó, R.F.P. Nogueira, Degradation of the herbicide tebutiuron using solar photo-Fenton process and ferric citrate complex at circumneutral pH, *J. Photochem. Photobiol. A* 191 (2007) 187–192.

- [36] R.A. Torres, C. Petrier, E. Combet, F. Moulet, C. Pulgarin, Bisphenol A mineralization by integrated ultrasound-UV-iron (II) treatment, *Environ. Sci. Technol.* 41 (2006) 297–302.
- [37] E.M. Rodriguez, B. Nunez, G. Fernandez, F.J. Beltran, Effects of some carboxylic acids on the Fe(III)/UVA photocatalytic oxidation of muconic acid in water, *Appl. Catal. B: Environ.* 89 (2009) 214–222.
- [38] M. Taxiarchou, D. Panias, I. Douni, I. Paspaliaris, A. Kontopoulos, Removal of iron from silica sand by leaching with oxalic acid, *Hydrometallurgy* 46 (1997) 215–227.
- [39] M.A. Blesa, H.A. Marinovich, E.C. Baumgartner, A.J.G. Maroto, Mechanism of dissolution of magnetite by oxalic acid–ferrous ion solutions, *Inorg. Chem.* 26 (1987) 3713–3717.
- [40] Z. Zajíčková, C. Párkányi, Photodegradation of 2-mercaptobenzothiazole disulfide and related benzothiazoles, *J. Heterocycl. Chem.* 45 (2008) 303–306.
- [41] Z. Zajíčková, C. Zajíčková, Monitoring of photodegradation process of various benzothiazoles by HPLC and UV spectrometry: application of LC-MS in photo-product identification, *J. Liq. Chromatogr. Relat. Technol.* 32 (2009) 1032–1043.
- [42] E. Borowska, E. Felis, J. Kalka, Oxidation of benzotriazole and benzothiazole in photochemical processes: kinetics and formation of transformation products, *Chem. Eng. J.* 304 (2016) 852–863.
- [43] N. Haroune, B. Combourieu, P. Besse, M. Sancelme, A. Kloepfer, T. Reemtsma, H. De Wever, A.M. Delort, Metabolism of 2-mercaptobenzothiazole by *Rhodococcus rhodochrous*, *Appl. Environ. Microbiol.* 70 (2004) 6315–6319.
- [44] M. Serdechnova, V.L. Ivanov, M.R.M. Domingues, D.V. Evtuguin, M.G.S. Ferreira, M.L. Zheludkevich, Photodegradation of 2-mercaptobenzothiazole and 1,2, 3-benzotriazole corrosion inhibitors in aqueous solutions and organic solvents, *Phys. Chem. Chem. Phys.* 16 (2014) 25152–25160, <http://dx.doi.org/10.1039/C4CP03867C> 2013.

Curriculum Vitae

Zakaria REDOUANE-SALAH

Marital Status: married
Date of birth: 19/12/1984 at Constantine
Nationality: Algerian
Home address: City 11/12/60-61 N°339 Djebel-Ouahch Constantine, Algeria
Mobile: +213 792 079 274
E-mail: z.rsalah@umc.edu.dz

Full-time assistant lecturer at the University Center of Tamanrasset in Algeria, Since 2012

Permanent member in:

1. Laboratoire des Techniques innovantes de preservation de l'environnement (University of constantine 1, Algeria)

EDUCATIONAL BACKGROUND

July 2018 University of Constantine 1, Algeria

✚ **PhD in Science.**

Thesis: "Simulated sunlight photodegradation of an organic pollutant by heterogeneous photo-Fenton-like processes: case of 2-mercaptobenzothiazole using a local natural clay powder"

- Very honored by the jury and highly appreciated.

November 2010 University of Constantine 1, Algeria

✚ **Magister's Degree in Analytical and Physical Chemistry.**

Title: «Removal of organic pollutant by photo-degradation via photo-inductors in homogenous and heterogeneous phase»

French title: (Elimination d'un polluant organique par photodégradation par des photo-inducteurs en phase homogène et hétérogène)

- Honored by jury and highly appreciated.

June 2008 University of Constantine 1, Algeria

✚ **BS in Chemistry (4 years study at the university).**

June 2003

- ✚ **Baccalaureate Certificate at High School, Branch: Chemistry, and appreciation: Very good.**

RESEARCH INTEREST

I am interested in photochemistry applied to the environment:

- ✓ Photodegradation in homogeneous and heterogeneous phases.
- ✓ Adsorption on natural or commercial inorganic supports.

SCIENTIFIC ACTIVITIES

I. RESEARCH PAPER

- **Simulated sunlight photodegradation of 2-mercaptobenzothiazole by heterogeneous photo-Fenton using a natural clay powder.**
Z. Redouane-Salah, M.A. Malouki, B. Khennaoui, J.A. Santaballa, M. Canle, Journal of Environmental Chemical Engineering 6 (2018) 1783–1793.
- **Homogeneous Photodegradation of Azo Dye (Methyl Orange) by Decatungstates of Sodium.** Khennaoui Badis, Moulay Abderrahmane Malouki **Zakaria SALAH REDOUANE** and Abdennour Zertal. Journal of Environmental Science and Engineering A 1, (2012) 844-852.

II. INTERNATIONAL CONFERENCES

1. **Z. Redouane Salah**, M. A. Malouki, B. Khennaoui, and A. Zertal.

“Advanced oxidation processes: new and efficient processes for water treatment from azo dyes” 5^{ème} édition du congrès international Eaux, Déchets et Environnement Un déficit millénaire (EDE5)» Université Hassan 1^{er} **Maroc** Les 24-26 Novembre 2015

2. **Zakaria REDOUANE-SALAH**, Moulay Abderrahmane MALOUKI, B.Khennaoui and Abdennour ZERTAL

“Decatungstate anions ($W_{10}O_{32}^{4-}$): A new and promising photocatalyst for dyes elimination” International Days of Kinetics, Catalysis and Calorimetry JI3C, **Algiers**, May 2 - 4, **2015**

3. B. Khennaoui, M. A. Malouki, **Z. Redouane Salah** et A. Zertal.

« Etude comparative entre la photodégradation d'un polluant organique par exposition à l'irradiation solaire naturelle et artificielle »
2nd International Symposium of Chemistry on the Organic Material and Renewable Energies, may 28-29th **2012, Tebessa**, Algeria.

4. **Zakaria REDOUANE SALAH**, Badis KHENNAOUI, Moulay Abd Errahman MALOUKI and **Abdennour ZERTAL**

“Degradation of ORII by $W_{10}O_{32}^{4-}$ photocatalyst in aqueous solution at 310 nm”
International symposium on Catalysis and Speciality Chemicals IS CSC 23-26 September **2012, Tlemcen**, Algeria.

III. NATIONAL CONFERENCES AND WORKSHOPS

1. *School on Materials, Nanomaterials and Soft matter from 27 to 30 April 2015 in Tunisia.*
2. **Zakaria Redouane Salah** et Badis Khennaoui
« **Water Purification From Azo Dyes By Different Advanced Oxidation Processes** »
Journée Mondiale de l'Environnement: Eau et Environnement, 07 juin 2012, Université Abdelhamid Ibn Badis, **Mostaganem**, Algérie.
3. M. A. Malouki, B. Khennaoui, **Z. Redouane Salah** and C. Richard
« **Photosensitizing properties of protein hydrolysate-based fertilizers** »
Séminaire National: Eau, Environnement et Biodiversité, 9-10 novembre 2011, Université Abbas Laghrour, **khenchela**, Algérie.
4. **Zakaria REDOUANE SALAH** «*Elimination du colorant Orange II par les deux procédés H_2O_2/UV_{254} et $S_2O_8^{2-}/UV_{254}$* »
Journée Mondiale de l'Environnement 2012 'Dégradation de l'Environnement' SKIKDA.
5. "A One day conference on "WATER AND ENERGY" UDES-Bousmail (EPST/CDER)**Tipaza**
6. "Specialized Courses On Membrane Techniques" Hassiba BenBouali University **Chlef**
7. Workshop on "Research Paper Authorship and English Technical Writing"**Constantine**

SKILLS

- **Languages:**
 - ✓ **Arabic:** Mother tongue.
 - ✓ **English:** good in Speaking, Reading and Writing
 - ✓ **French:** good in Speaking, Reading and Writing
- **Computer:**
 - ✓ Chemdraw, Chems sketch, Origine 8, Xalibure, microsoft office

RESEARCH INTERNSHIP

Short-term Research internship in Spain: October 2016

MASTER'S THESIS SUPERVISION

1. Elimination de 2-MBT par adsorption sur des argiles locales naturelles.
2. Elimination d'un polluant organique par procédé photo-Fenton homogène sous irradiation solaire.

TEACHING EXPERIENCES

Undergraduate courses (teaching in French and Arabic languages)

2016-2017:

- Methods of phase separation and chromatography
- Physico-chemical analytical techniques I
- Physico-chemical analytical techniques II
- Equilibrium in solution

2015-2016:

- Physico-chemical analytical techniques II
- Equilibrium in solution
- Quantitative analysis techniques
- Methods of phase separation and chromatography
- English for Chemists (Graduate courses for master's student in Chemistry)

2014-2015:

- Physico-chemical analytical techniques II
- Analytical Chemistry
- General Chemistry

2013-2014:

- General chemistry
- English for Chemists (Graduate Courses for master's student in chemistry)

2012-2013:

- General Chemistry
- Thermodynamics

OTHERS

- ❖ First Aid Certificate.
- ❖ HSE Certificate.

- ❖ Computer Sciences certificate.
- ❖ Sport and general reading.

Summary

The problem of water pollution has been an environmental concern for many years, which lead researchers around the world to looking for effective methods to solve this issue.

The incapability of conventional methods to remove effectively biorecalcitrant and toxic pollutants, have promoted the research of more efficient and ecologically friendly water treatment technologies.

In the same aspect, this thesis is a small contribution to the development of a new advanced oxidation process considered as promising and clean method for the destruction of water pollutants. In this process we investigated the efficiency of untreated local natural clay rich in iron oxides as a cost-free photocatalyst for the degradation of a persistent organic pollutant under simulated sunlight irradiation.

The targeted pollutant was: 2-mercaptobenzothiazole (MBT). The study showed that:

Firstly, the adsorption capacity, kinetics and isotherms models were examined in the dark.

Secondly, experiments of degradation by heterogeneous Fenton process under various operational parameters were investigated.

And then, we focused our research on the photodegradation of MBT by heterogeneous photo-Fenton process using the same natural clay powder (NCP) as photocatalyst and under simulated sunlight irradiation. Experiments were conducted at natural pH with a bath reactor equipped with a medium-pressure Hg lamp emitting mainly at 366 nm. The natural clay was crushed into small homogeneous particles (powder) and then characterized by SEM-EDS, UV-Vis diffuse reflectance spectroscopy, XRF and XRD analysis. The specific BET surface area measured for the clay was $30.22 \text{ m}^2 \cdot \text{g}^{-1}$.

Our main results indicated that, the photodegradation of MBT follows first order (for direct photolysis) or pseudo-first order kinetics (for photocatalysis).

Direct photolysis of MBT showed a negligible effect both upon 254 and 365 nm irradiation, while 42.5% and 62% of MBT was eliminated in 3 h under 310 nm irradiation in the presence of H₂O₂, and under sunlight irradiation (using NCP), respectively. Kinetic runs carried out with 5.0.10⁻⁵M MBT and 0.5g·L⁻¹clay showed higher MBT conversion and photodegradation rate at basic pH and in oxygenated media.

The photodegradation of MBT is mainly attributed to reaction with HO[•], leading to different intermediates that have been identified by HPLC-MS. A reaction mechanism is proposed at the end of our thesis. The highest TOC removals were obtained using UVA at low pHs, in the absence of O₂ with 68% and 65% TOC removal respectively. The presence of oxalic acid and H₂O₂ enhanced significantly MBT photodegradation.

Finally, the obtained results support the use of natural clay rich in iron oxides as a free, clean and efficient photocatalysts for water pollutants abatement.

Keywords: MBT, heterogeneous photo-Fenton process, natural clay powder (NCP), photodegradation, hydroxyl radical, simulated sunlight irradiation.

ملخص

مشكلة تلوث المياه باتت شاغلا بيئيا لسنوات عديدة. فالعديد من الباحثين حول العالم لا زالوا يبحثون عن طرق فعالة لحل هاته المشكلة.

ولأن عدم قدرة الأساليب التقليدية على إزالة الملوثات العضوية والسامة بشكل فعال، قد عزز البحث عن تكنولوجيات جديدة لمعالجة المياه أكثر كفاءة وصديقة للبيئة.

في نفس الاتجاه، هاته الأطروحة تساهم في تطوير عملية أكسدة متقدمة جديدة تعتبر طريقة واعدة ونظيفة لتدمير ملوثات المياه. في هذا الإطار قمنا بالتحقيق في كفاءة طين طبيعي غير معالج غني بعنصر الحديد كمحفز ضوئي غير مكلف لتدهور الملوثات العضوية صعبة الإزالة، وذلك تحت تأثير أشعة اصطناعية مماثلة لأشعة الشمس الطبيعية.

الملوث البيئي المختار لهاته الأطروحة هو: 2-مركابتوبنزوثيازول (مبت) أو (MBT باللغة الأجنبية).

أولاً، تم دراسة قدرة الطين على إمتصاص الملوث في وسط مائي، مع دراسة حركية ونماذج الإمتصاص في غياب الأشعة.

ثانياً، قمنا بالتحقيق في تجارب التدهور من خلال عملية فنتون غير متجانسة تحت تأثير مختلف عوامل البحث المخبرية.

الجزء الأهم من أبحاثنا ركزناه على التحلل والتدمير الضوئي لل مبت (MBT) من خلال عملية فوتو-فنتون غير متجانسة باستخدام الطين الطبيعي سالف الذكر كمحفز ضوئي تحت أشعة الشمس الاصطناعية، أجريت التجارب في درجة الحموضة الطبيعية داخل مفاعل صغير مجهز بمصباح زئبقي متوسط الضغط يصدر إشعاعات ذات طول موجة رئيسية عند 366 نانومتر. قبل ذلك تم سحق الطين الطبيعي إلى ذرات صغيرة متجانسة (مسحوق) ثم تم معرفة مختلف خصائصه بواسطة المسح بالمجهر الإلكتروني (SEM) مع تحليل تشتت الطاقة (EDS)، منتشر الانعكاس الطيفي في المجال المرئي - فوق البنفسجي (UV-Vis DRS)، بالإضافة إلى تحاليل XRF و XRD.

تحليل المساحة السطحية برونور-إيميت-تيلر (BET) للطين أعطى نتيجة 30.22 م² للغرام.

من خلال النتائج المتحصل عليها، وجدنا أن التحلل الضوئي لل MBT يتبع حركية من الدرجة الأولى (بالنسبة للتحلل الضوئي المباشر) أو حركية شبه درجة أولى (بالنسبة للتحليل الضوئي الغير مباشر).

أظهر التحلل الضوئي المباشر لل MBT تأثير ضئيل جدا عند 254 و 365 نانومتر على حد سواء ، في حين تم القضاء على 42.5% من ال مبت خلال 3 ساعات تحت أشعة 310 نانومتر في وجود H₂O₂ و 62% تحت أشعة شبيهة لأشعة الشمس (في وجود الطين الطبيعي) خلال نفس المدة الزمنية.

الدراسة الحركية التي أجريت بوجود تركيز 5.0 - 10⁻⁵ مول.ل لل ميب و 0.5 غرام ل من الطين أظهرت أن أعلى معدل تدهور و تحلل ضوئي لل ميب كان في درجة الحموضة القاعدية وفي وسط مزود بالأكسجين.

التحلل الضوئي لل ميب ينسب أساسا إلى التفاعل مع الجذور الهيدروكسيلية (HO•)، مما أدى إلى ظهور عدة مركبات وسيطة مختلفة تم تحديدها بواسطة تقنية الكروماتوغرافيا السائلة عالية الكفاءة مدمجة بمطيافية الكتلة (HPLC-MS). وبذلك أمكننا إقتراح آلية للتفاعل عند نهاية البحث. أعلى نسبة إزالة لل الكربون العضوي الكلي (TOC) تم الحصول عليها تحت تأثير أشعة مافوق البنفسجية أ (UVA) عند درجات الحموضة المنخفضة، وفي غياب الأكسجين (O₂) بنسبة 68% و 65% على التوالي. إضافة حمض الأوكساليك و H₂O₂ عزز بشكل كبير التحلل الضوئي لل ميب.

النتائج التي تم الحصول عليها في هذه الدراسة تدعم بشكل كبير إستخدام الطين الطبيعية الغنية بأكاسيد الحديد كمحفزات ضوئية غير مكلفة، نظيفة وفعالة للتخفيف من أثر الملوثات المائية أو حتى إزالتها تماما.

الكلمات الدالة: ميب، عملية فوتو فنتون غير متجانسة، مسحوق الطين الطبيعي، تحلل ضوئي، جذر هيدروكسيلي، محاكاة أشعة الشمس، أشعة مافوق بنفسجية أ، آلية التفاعل.

Résumé

Le problème de la pollution de l'eau est une préoccupation environnementale majeure depuis de nombreuses années. Plusieurs chercheurs autour du monde sont toujours à la recherche des méthodes efficaces pour résoudre ce problème.

L'incapacité des méthodes conventionnelles d'éliminer efficacement les polluants biorécalcitrants et toxiques a favorisé la recherche de nouvelles technologies de traitement de l'eau plus efficace et amie de l'environnement.

Cette thèse peut être considérée comme une contribution au développement d'un nouveau procédé d'oxydation avancée. Les résultats montrent que cette méthode est prometteuse et propre pour la destruction des polluants de l'eau. Dans ce processus, nous avons examiné l'efficacité d'une argile naturelle non traitée riche en fer en tant que photocatalyseur gratuit pour la dégradation d'un polluant organique persistant, sous irradiation solaire simulée.

Le polluant ciblé était : le 2-mercaptobenzothiazole (MBT).

Tout d'abord, la capacité d'adsorption, les modèles cinétiques et les isothermes d'adsorption ont été examinés dans l'obscurité.

Ensuite, des expériences de dégradation par le processus de Fenton hétérogène sous l'effet de divers paramètres opérationnels ont été étudiées.

La partie la plus importante de notre recherche a porté sur la photodégradation du MBT par photo-Fenton hétérogène en utilisant l'argile naturelle comme un photocatalyseur sous irradiation solaire simulés. Les expériences ont été menées à pH naturel avec un réacteur de bain équipé d'une lampe Hg à moyenne pression émettant principalement à 366 nm. L'argile naturelle a été broyée en petites particules homogènes (poudre) puis caractérisée par SEM-EDS, spectroscopie d'absorption en réflexion diffuse UV-Vis-DRS, Fluorescence des rayons X et diffraction des rayons X. La surface BET spécifique mesurée pour l'argile était de $30,22 \text{ m}^2 \cdot \text{g}^{-1}$.

Les résultats obtenus ont indiqués que, la photodégradation du MBT suit une cinétique de premier ordre (pour la photolyse directe) ou de pseudo-premier ordre (pour la photocatalyse hétérogène).

La photolyse directe du MBT a montré un effet négligeable lors des irradiations à 254 et 365 nm, tandis que 42,5% et 62% du MBT ont été éliminés en 3 h sous l'irradiation à 310nm en présence de H₂O₂, et sous irradiation solaire simulée (en utilisant la poudre de l'argile naturelle), respectivement.

L'étude cinétiques réalisée avec $5.0 \cdot 10^{-5}$ M MBT et 0,5g.L⁻¹ d'argile a montré une conversion plus élevée du MBT à pH basique en aérobiose.

La photodégradation du MBT est principalement attribuée à la réaction avec les radicaux HO[•] conduisant à différents intermédiaires qui ont été identifiés par HPLC-MS. Un mécanisme de dégradation est proposé à la fin de la thèse. Les mesures de COT ont montrés que la minéralisation la plus élevée a été obtenue en utilisant des UVA d'une part à des faibles valeurs de pH et d'autre part en absence de l'oxygène. Les taux d'abattement étaient 68% et 65% respectivement. La présence d'acide oxalique ou de H₂O₂ a significativement amélioré la photodégradation du MBT.

Les résultats obtenus sont à la faveur de l'utilisation d'argiles naturelles riches en oxydes de fer comme photocatalyseurs gratuits, propres et efficaces pour la dégradation des polluants en milieu aquatique.

Mots clés: MBT, procédé photo-Fenton hétérogène, poudre d'argile naturelle, photodégradation, radical hydroxyle, irradiation solaire simulée.